İ. B. BAL

ATILIM UNIVERSITY 2024

PREPARATION AND PERFORMANCE INVESTIGATION OF HIGH EFFICIENT CATALYST FOR HIGH TEMPERATURE ELECTROCHEMICAL HYDROGEN SEPARATION

THE GRADUATE SCHOOL OF NATURAL AND APPLIED SCIENCES
OF
ATILIM UNIVERSITY

İLAY BİLGE BAL

A MASTER OF SCIENCE THESIS
IN
THE DEPARTMENT OF MECHANICAL ENGINEERING

JUNE 2024

PREPARATION AND PERFORMANCE INVESTIGATION OF HIGH EFFICIENT CATALYST FOR HIGH TEMPERATURE ELECTROCHEMICAL HYDROGEN SEPARATION

A THESIS SUBMITTED TO
THE GRADUATE SCHOOL OF NATURAL AND APPLIED SCIENCES
OF
ATILIM UNIVERSITY

BY

ILAY BILGE BAL

IN PARTIAL FULFILLMENT OF THE REQUIREMENTS
FOR
THE DEGREE OF MASTER OF SCIENCE
IN
THE DEPARTMENT OF MECHANICAL ENGINEERING

JUNE 2024

Approval of the Graduate School of Natural and Applied Sciences, Atilim University.

_____

Prof. Dr. Ender Keskinkılıç
Director

I certify that this thesis satisfies all the requirements as a thesis for the degree of **Master of Science in Mechanical Engineering Department, Atılım University**.

_____

Prof. Dr. Sadık Engin Kılıç
Head of Department

This is to certify that we have read the thesis **PREPARATION AND PERFORMANCE INVESTIGATION OF HIGH EFFICIENT CATALYST FOR HIGH TEMPERATURE ELECTROCHEMICAL HYDROGEN SEPARATION** submitted by İLAY BİLGE BAL and that in our opinion it is fully adequate, in scope and quality, as a thesis for the degree of Master of Science.

_____

Prof. Dr. Yılser Devrim
Supervisor

Examining Committee Members:

Prof. Dr. Can Özgür Çolpan
Mechanical Engineering, Dokuz Eylül University _____

Prof. Dr. Yılser Devrim
Energy Systems Engineering, Atılım University _____

Asst. Prof. Dr. Gizem Nur Bulanık Durmuş
Energy Systems Engineering, Atılım University _____

Date: *11.06.2024*

I hereby declare that all information in this document has been obtained and presented in accordance with academic rules and ethical conduct. I also declare that, as required by these rules and conduct, I have fully cited and referenced all material and results that are not original to this work.

Name, Last Name : İlay Bilge BAL

Signature :

ABSTRACT

PREPARATION AND PERFORMANCE INVESTIGATION OF HIGH EFFICIENT CATALYST FOR HIGH TEMPERATURE ELECTROCHEMICAL HYDROGEN SEPARATION

Bal, İlay Bilge
M.S., Department of Mechanical Engineering
Supervisor: Prof. Dr. Yılser DEVRİM

June 2024, 92 pages

Currently, global hydrogen (H_2) production largely relies on fossil resources. The most widely used method for H_2 production is steam-methane reforming (SMR). However, H_2 produced by this method contains impurities such as carbon monoxide (CO) and carbon dioxide (CO_2). H_2 must be of a certain purity to be utilized as a feedstock in industry or as an energy carrier in fuel cell systems. Therefore, a purification step is inevitable to remove these impurities from H_2.

At this point, electrochemical hydrogen purification (ECHP) systems are a strong alternative to conventional H_2 purification methods with advantages such as simultaneous H_2 purification and compression, no moving parts, low operating and energy costs, and scalability.

Within the scope of this thesis study, a high-temperature electrochemical H_2 purification (HT-ECHP) cell has been developed. One potential issue encountered in ECHP cells is the poisoning of the catalyst layer due to impurities present in the reformate gas. Typically, Pt catalyst is used for hydrogen oxidation reaction (HOR). However, the CO tolerance of Pt catalyst is quite limited, and catalyst poisoning occurs even in the presence of low levels of CO. In this study, graphene nanoplatelet (GNP)

supported platinum (Pt) and bimetallic platinum-ruthenium (PtRu) catalysts were synthesized for investigation of HT-ECHP performances. The catalysts were prepared using a rapid and simple method called microwave-assisted synthesis. The prepared catalysts were combined with phosphoric acid-doped polybenzimidazole (PBI) membrane for HT-ECHP application. The structural and electrochemical properties of the catalysts were investigated by thermogravimetric analysis (TGA), X-ray diffraction (XRD), X-ray photoelectron spectroscopy (XPS), transmission electron microscopy (TEM) and cyclic voltammetry (CV) analyses. The characterization results show that the catalysts provided the required properties for HT-ECHP application. The HT-ECHP performances of Pt/GNP and PtRu/GNP catalysts were examined with a reformate gas mixture containing H_2, CO_2 and CO in the temperature range of 140-180 °C. The results show that the electrochemical H_2 purification performances of the catalysts increase with increasing operating temperature. The highest H_2 purification performance was obtained with PtRu/GNP catalyst. Gas chromatography (GC) results showed that a high H_2 purity of 99.938% was obtained at 160 °C with PtRu/GNP catalyst. The high electrochemical H_2 purification performance of PtRu/GNP catalyst can be attributed to the strong synergistic interactions between Pt and Ru particles decorated on GNP. These results indicate that PtRu/GNP is a promising catalyst for HT-ECHP application.

Keywords: Electrochemical Hydrogen Purification, Bimetallic Catalyst, Graphene Nanoplatelet, PBI Membrane.

ÖZ

YÜKSEK SICAKLIKTA ELEKTROKİMYASAL HİDROJEN AYRIŞTIRMA İÇİN YÜKSEK VERİMLİ KATALİZÖR HAZIRLANMASI VE PERFORMANSININ İNCELENMESİ

Bal, İlay Bilge
Yüksek Lisans, Makine Mühendisliği Bölümü
Tez Yöneticisi : Prof. Dr. Yılser DEVRİM

Haziran 2024, 92 sayfa

Mevcut durumda küresel hidrojen (H_2) üretimi büyük ölçüde fosil kaynaklara dayanmaktadır. H_2 üretiminde en yaygın kullanılan yöntem buhar-metan reformasyonudur. Fakat bu yöntemle üretilen H_2, karbon monoksit (CO) ve karbon dioksit (CO_2) gibi safsızlıklar içermektedir. H_2'nin endüstride hammadde olarak veya yakıt hücresi sistemlerinde enerji taşıyıcısı olarak kullanılabilmesi için belirli bir saflıkta olması gerekir. Dolayısıyla, bu safsızlıkları H_2'den uzaklaştırmak için bir saflaştırma adımı kaçınılmazdır.

Bu noktada, elektrokimyasal hidrojen saflaştırma (ECHP) sistemleri eş zamanlı H_2 saflaştırma ve sıkıştırma yapabilme, hareketli parça içermeme, düşük işletme ve enerji maliyetleri, ölçeklenebilirlik gibi avantajları ile geleneksel H_2 saflaştırma yöntemlerine güçlü bir alternatiftir.

Bu tez çalışması kapsamında yüksek sıcaklık elektrokimyasal H_2 saflaştırma (HT-ECHP) hücresi geliştirilmiştir. ECHP hücrelerinde karşılaşılabilecek olası problemlerden biri katalizör tabakasının reformat gaz içerisinde bulunan safsızlıklar nedeniyle zehirlenmesidir. Literatürde hidrojen oksidasyon reaksiyonu için tipik olarak Pt katalizörü kullanılmaktadır. Fakat, Pt katalizörünün CO toleransı oldukça

sınırlıdır ve düşük miktarda CO varlığında bile katalizör zehirlenmesi meydana gelir. Bu çalışmada, HT-ECHP performansları incelenmek üzere grafen nanoplatelet (GNP) destekli platin (Pt) ve bimetalik platin-rutenyum (PtRu) katalizörleri sentezlenmiştir. Katalizörler, hızlı ve basit bir yöntem olan mikrodalga-destekli sentez yöntemiyle hazırlanmıştır. Hazırlanan katalizörler HT-ECHP uygulaması için fosforik asit katkılı polibenzimidazol (PBI) membran ile birleştirilmiştir. Katalizörlerin yapısal ve elektrokimyasal özellikleri termogravimetrik analiz (TGA), X-ışını kırınımı (XRD), X-ışını fotoelektron spektroskopisi (XPS), geçirimli elektron mikroskopisi (TEM) ve döngüsel voltametri (CV) analizleri ile incelenmiştir. Karakterizasyon sonuçları, katalizörlerin HT-ECHP uygulaması için gerekli özellikleri sağladığını göstermektedir. Pt/GNP ve PtRu/GNP katalizörlerinin HT-ECHP performansları 140-180 °C sıcaklık aralığında H_2, CO_2 ve CO içeren reformat gazı karışımı ile incelenmiştir. Sonuçlar, katalizörlerin elektrokimyasal H_2 saflaştırma performanslarının artan çalışma sıcaklığı ile arttığını göstermektedir. En yüksek H_2 saflaştırma performansı PtRu/GNP katalizörü ile elde edilmiştir. Gaz kromatografisi (GC) sonuçları, PtRu/GNP katalizörü ile 160 °C'de %99.938 yüksek H_2 saflığının elde edildiğini göstermiştir. PtRu/GNP katalizörünün yüksek elektrokimyasal H_2 saflaştırma performansı, GNP üzerine dekore edilmiş Pt ve Ru partikülleri arasındaki güçlü sinerjik etkileşimlere bağlanabilir. Bu sonuçlar, PtRu/GNP'nin HT-ECHP uygulaması için umut verici bir katalizör olduğunu göstermektedir.

Anahtar Kelimeler: Elektrokimyasal Hidrojen Saflaştırma, Bimetalik Katalizör, Grafen Nanoplatelet, PBI Membranı.

To my family

ACKNOWLEDGMENTS

I would like to express my deepest gratitude to my supervisor Prof. Dr. Yılser Devrim for her great guidance, encouragement, support, and patience throughout my study. I am grateful to her for introducing me with hydrogen, including me in her valuable projects, and all the laboratory opportunities she provided me. I felt the privilege of working with her throughout my Master's degree.

I would like to thank Gizem Nur Bulanık Durmuş for her support during my laboratory studies.

I would like to express my special thanks to Hüseyin Devrim and the members of Teksis for sharing their valuable knowledge with me.

I would like to express my sincerest and endless thanks to my family for their unconditional love and support throughout my whole life. This accomplishment would not have been possible without their believe and moral support.

This study was supported by Atılım University Research Support Program (Grant number: ATU-ADP-2021-01).

TABLE OF CONTENTS

LIST OF TABLES

LIST OF FIGURES

LIST OF SYMBOLS/ABBREVIATIONS

H_2	Hydrogen
FCEV	Fuel cell electric vehicle
CNG	Compressed natural gas
SMR	Steam methane reforming
CCUS	Carbon capture, utilization and storage
CO	Carbon monoxide
CO_2	Carbon dioxide
CH_4	Methane
H_2O	Water vapor
N_2	Nitrogen
ISO	International Organization for Standardization
SAE	Society of Automobile Engineers
Ar	Argon
O_2	Oxygen
H_2S	Hydrogen sulphide
HCHO	Formaldehyde
HCOOH	Formic acid
NH_3	Ammonia
PSA	Pressure swing adsorption
TSA	Temperature swing adsorption
S	Sulphur
ECHP	Electrochemical hydrogen purification
HT-ECHP	High-temperature electrochemical hydrogen purification
PEMFC	Proton exchange membrane fuel cell
LP	Low pressure
HP	High pressure
HOR	H_2 oxidation reaction
HER	H_2 evolution reaction

I	Current (A)
F	Faraday's constant (9.648×10^4 C/mol)
E_{Nernst}	Nernst Voltage (V)
E_{cell}	Cell voltage (V)
E_0	Standard potential of a hydrogen reaction
R	Universal gas constant (8.314 J/molK)
T	Temperature (K)
$P_A^{H_2}$	H_2 partial pressure at the anode
$P_C^{H_2}$	H_2 partial pressure at the cathode
i	Current density (A/cm^2)
A	Area (cm^2)
GDL	Gas diffusion layer
GDE	Gas diffusion electrode
CL	Catalyst layer
MEA	Membrane electrode assembly
PFSA	Perfluorosulfonic acid
PTFE	Polytetrafluoroethylene
PBI	Polybenzimidazole
SPEEK	Sulfonated polyether ether ketone
CrPSSA	Cross-linked poly(styrene sulfonic acid)
PEI	Polyethyleneimine
PEO	Polyethylene oxide
PAAM	Polyacrylamide
H_3PO_4	Phosphoric acid
H_2SO_4	Sulfuric acid
$HClO_4$	Perchloric acid
HNO_3	Nitric acid
HCl	Hydrogen chloride
HBr	Hydrogen bromide
$C_2H_5SO_3H$	Methyl methane sulfonate
CH_3SO_3H	Methane sulphonic acid
Ru	Ruthenium

Co	Cobalt
Pd	Palladium
Fe	Iron
Pt	Platinum
PtRu	Platinum-Ruthenium
CNT	Carbon nanotube
CNF	Carbon nanofiber
GNP	Graphene nanoplatelet
EG	Ethylene glycol
IPA	Isoproyl alcohol
TGA	Thermogravimetric analysis
XRD	X-ray diffraction
XPS	X-ray photoelectron spectroscopy
TEM	Transmission electron microscopy
CV	Cyclic voltammetry
GC	Gas chromatography
SAED	Selected area electron diffraction
ECSA	Electrochemical surface area
SSA	Specific surface area

CHAPTER 1

1. INTRODUCTION

1.1. Motivation of the Thesis

The majority of global energy demand is met by fossil sources. The risk of depletion of these resources, and their negative effects on the environment, which become more noticeable with climate change, have led to the search for alternative energy sources. Hydrogen (H_2) is seen as a promising solution to this quest with its high gravimetric energy density and potential for carbon-free production and usage. However, the technical and economic challenges encountered in the purification, pressurization, storage and transportation of H_2 hinder its widespread adoption.

When H_2 is used as an energy carrier in fuel cells, only water is released as a by-product. In this regard, H_2 is seen as a key player in reducing emissions and achieving global climate targets, especially in sectors that are hard to decarbonize, such as transportation and heavy industry. In order for H_2 to be used in fuel cells, it must be of high purity. In addition, the transportation of H_2 via existing natural gas pipelines has recently emerged as an alternative solution in the storage and transportation rings of the H_2 value chain and an important step in the transition to a sustainable energy economy. In this scenario, H_2 will need to be separated from natural gas at the point of use.

Currently, separate systems are used to purify and pressurize H_2, and these systems have high energy consumption or offer low H_2 purity. Offering one-step H_2 purification and compression, high H_2 purity, high efficiency, low maintenance and quiet operation, ECHP systems are a powerful alternative to existing technologies. One of the most critical problems that may cause performance loss in ECHP systems is the poisoning of the catalyst layer by impurities such as CO and CO_2 in the feed gas. Therefore, the development of catalysts with high impurity tolerance, high

electrochemical activity and low cost is crucial to improve the efficiency of ECHP systems and to obtain high purity H_2. Additionally, high operating temperatures in the range of 120-200 ℃ significantly increase the contaminant tolerance of ECHP systems. There are not many studies in the literature on the catalyst development for HT-ECHP systems. Developing highly efficient catalysts is important for this innovative technology to be competitive with existing systems.

1.2. Aim of the Thesis

The aims of the thesis are listed below:

- To develop high-efficient catalysts for HT-ECHP cells. It is aimed to prepare GNP-supported Pt and bimetallic PtRu catalysts with high electrochemical activity and high CO tolerance by microwave-assisted synthesis method.
- To examine the physical and electrochemical properties of the prepared catalysts by several characterization analyses.
- To separate high-purity H_2 from a gas mixture of H_2:CO_2:CO-75:22:3 at different temperatures using the HT-ECHP cell prepared with the synthesized catalysts.
- To investigate the effect of operating temperature varying between 140-180 ℃ on the H_2 purification performance of the prepared catalysts.

1.3. Thesis Outline

In the second chapter, the properties of H_2, H_2 production and purification methods are explained.

In the third section, the ECHP technology is expressed in detail. The working principle of ECHP, cell components, effect of the high operating temperature on ECHP performance is explained. A literature review on ECHP is also given in this section.

The fourth chapter describes the experimental studies conducted. In this section, the materials used in experimental studies, catalyst and MEA preparation procedures, catalyst characterization analyses, and HT-ECHP test station structure are described in detail.

In the fifth chapter, the results of catalyst characterization analyzes and HT-ECHP performance tests are discussed.

In the sixth chapter, a comprehensive summary of the outputs obtained in the thesis study is presented.

CHAPTER 2

2. HYDROGEN ENERGY

2.1. The Hydrogen Energy

Currently, most of the global energy demand is met by fossil fuels, which are unsustainable sources with limited stocks and serious negative impacts on the environment. There is a strong urge to use renewable energy sources to replace fossil fuels to meet future energy needs. Hydrogen (H_2), the most abundant and lightest element on the universe, comes to the forefront as an alternative fuel since it can be produced from domestic sources and used with emission-free energy and as high energy density and clean burning characteristics [1].

H_2 is used as a feedstock in different industries such as refineries, ammonia production for fertilizers, the methanol sector, and the direct reduced iron process for steel production [2]. It is a coolant in turbine generators since it has a tremendous specific heat capacity and thermal conductivity [3]. Also, H_2 provides seasonal energy storage for renewable energy sources such as wind and solar power that fluctuate and vary [4]. H_2 can be used as a clean fuel instead of hydrocarbon-based fuels in the transportation, power generation and manufacturing sectors, reducing the reliance on fossil fuels [5].

H_2 is an energy carrier, not an energy source as a secondary form of energy. Using H_2 as a clean fuel in fuel cell electric vehicles (FCEVs) and combustion engines reduces foreign oil dependency and decreases transportation sector emissions [6]. H_2 has unique combustion properties, such as comprehensive air flammability, limited ignition energy, and a high flame propagation rate that enables prompt ignition [7]. The properties of H_2 compared to compressed natural gas (CNG), gasoline and diesel are given in Table 2.1.

Table 2.1 The properties of hydrogen in comparison with compressed natural gas (CNG), gasoline and diesel [8]

Property	**H_2**	**CNG**	**Gasoline**	**Diesel**
Molecular weight	2.016	16.043	~110	~170
Carbon content (mass%)	0	75	84	86
Lower heating value (MJ/kg)	119.7	45.8	44.8	42.5
Density @1bar, 273K (kg/m^3)	0.089	0.72	730-780	830
Energy content @1bar, 273K (MJ/m^3)	10.7	33.0	33×10^3	35×10^3
Boiling point (K)	20	111	298-488	453-633
Auto-ignition temperature (K)	858	813	~623	~523
Minimum ignition energy in air (mJ)	0.02	0.29	0.24	0.24
Stoichiometric air/fuel mass ratio	34.5	17.2	14.7	14.5
Stoichiometric vol. fraction in air (%)	29.53	9.48	~2	-
Quenching distance (mm)	0.64	2.1	~2	-
Laminar flame speed in air (m/s)	1.85	0.38	0.37-0.43	0.37-0.43
Diffusion coefficient in air (m^2/s)	8.5×10^{-6}	1.9×10^{-6}	-	-
Flammability limits in air (vol. %)	4-76	5.3-15	1-7.6	0.6-5.5
Adiabatic flame temperature (K)	2480	2214	2580	~2300

The report published by the Hydrogen Council [9] envisaged that hydrogen could meet 18% of the total final energy demand in 2050.

2.2. Hydrogen Production

Global H_2 production is primarily based on fossil sources; 76% of the H_2 is produced from natural gas through steam methane reforming (SMR), 22% via coal gasification and only 2% by electrolysis [10]. Although water electrolysis is a carbon-free method that provides high-purity H_2, its share in global hydrogen production is relatively low because of its high cost [11].

H_2 is classified under different colors in the literature according to the primary source and the process used in its production. Although the coloring may differ among the

sources, H_2 is primarily expressed as black, brown, grey, blue, turquoise, and green. Figure 2.1 shows the H_2 production methods according to color.

H_2 is coded with black or brown color when it is produced by gasification process using black coal or brown coal (lignite), respectively [12]. Black and brown H_2 are the most environmentally harmful forms due to high greenhouse gas emissions during the production process [13]. On the other hand, coal gasification is a technologically mature, efficient, large-scale, and economical H_2 production method [14].

Grey H_2 refers to H_2 produced by SMR without carbon capture, utilization and storage (CCUS) technology and accounts for the majority of H_2 produced [15]. SMR is the most widely used technology for large-scale H_2 production and provides H_2 extraction from natural gas with 74-85% conversion efficiency [16]. The SMR process involves the production of syngas containing CO and H_2 by a reaction between methane and steam over a nickel-based catalyst at 850-900 ℃ (Eq. (1)) [16], [17]. Then, water-gas shift (WGS) reaction (Eq. (2)) is conducted as a second step to increase the H_2 product amount by converting CO to CO_2 and H_2 [10], [17].

$$CH_4 + H_2O \rightarrow CO + 3H_2 \quad (1)$$

$$CO + H_2O \rightarrow CO_2 + H_2 \quad (2)$$

While about 6% of the natural gas produced worldwide is used for H_2 production, most of the current H_2 production is carried out by SMR due to the relatively low capital cost of the plant and the ease with which the chemical reaction can be controlled [18].

Blue H_2, which is produced from natural gas similar to grey H_2 but whose production process includes CCUS, is considered as a potential solution in the decarbonization of sectors such as industry and transportation [19]. Captured CO_2 can be stored underground, but there is still a risk of leakage, and uncertainty regarding the influences of long-term storage [20]. Also, the total cost of blue H_2 could be substantially higher than grey H_2, as underground storage may require high capital costs [17]. Furthermore, the overall efficiency of the SMR process may decrease by 5-14% with the integration of CCUS [21]. Another issue to consider in blue H_2

production is water consumption. Large amount of water, even more than in electrolysis in some cases, consumes for blue H_2 production [22]. Although CO_2 emissions for blue H_2 are 9-12% lower than those for grey H_2, it has higher fugitive methane emissions due to the increased utilization of natural gas for carbon capture [23].

Green H_2 is an environmentally friendly form of H_2, produced with zero greenhouse gas emissions through the electrolysis of water using renewable energy sources like wind or solar [24]. Producing green H_2 using renewable energy sources, that vary according to daily and seasonal cycles, enables the energy to be stored as gas form and then converted back into electricity by scalable fuel cell systems. In this respect, green H_2 offers the advantages of storing renewable energy, ensuring stability in the grid, and increasing utilization of renewable energy sources [25]. Green H_2 emits no greenhouse gases during its production, making it a key player for reaching global climate targets and decarbonizing hard-to-abate sectors such as transportation and heavy industry. It also reduces dependence on fossil resources, reducing foreign dependency on energy and ensuring energy security [26]. The cost of H_2 production is highly dependent on the type of electrolyser and energy source [14]. There are four types of electrolyser which are alkaline (ALK), polymer electrolyte membrane (PEM), anion exchange membrane (AEM) and solid oxide electrolysers. Among them, the most mature technologies are PEM and alkaline electrolysers. The cost of PEM electrolysers is 50-60% higher compared to alkaline [27]. Currently, green H_2 is the most expensive option, it will become cost competitive with advanced electrolysis technology, lower renewable energy costs, and improved economies of scale [28].

Turquoise H_2 is produced by pyrolysis of methane, where methane is split into CO_2-free H_2 and solid carbon [29]. Turquoise H_2 is much less energy intensive than SMR and water electrolysis, and it offers the advantage of utilizing existing natural gas infrastructure [30]. Also, the by-product solid carbon can be stored long-term and it can be used as electrode material, or as an additive in concrete, rubber, or asphalt [31].

In addition, H_2 produced through electrolysis process powered by nuclear energy is called pink [32] or purple [33] H_2 by some authors.

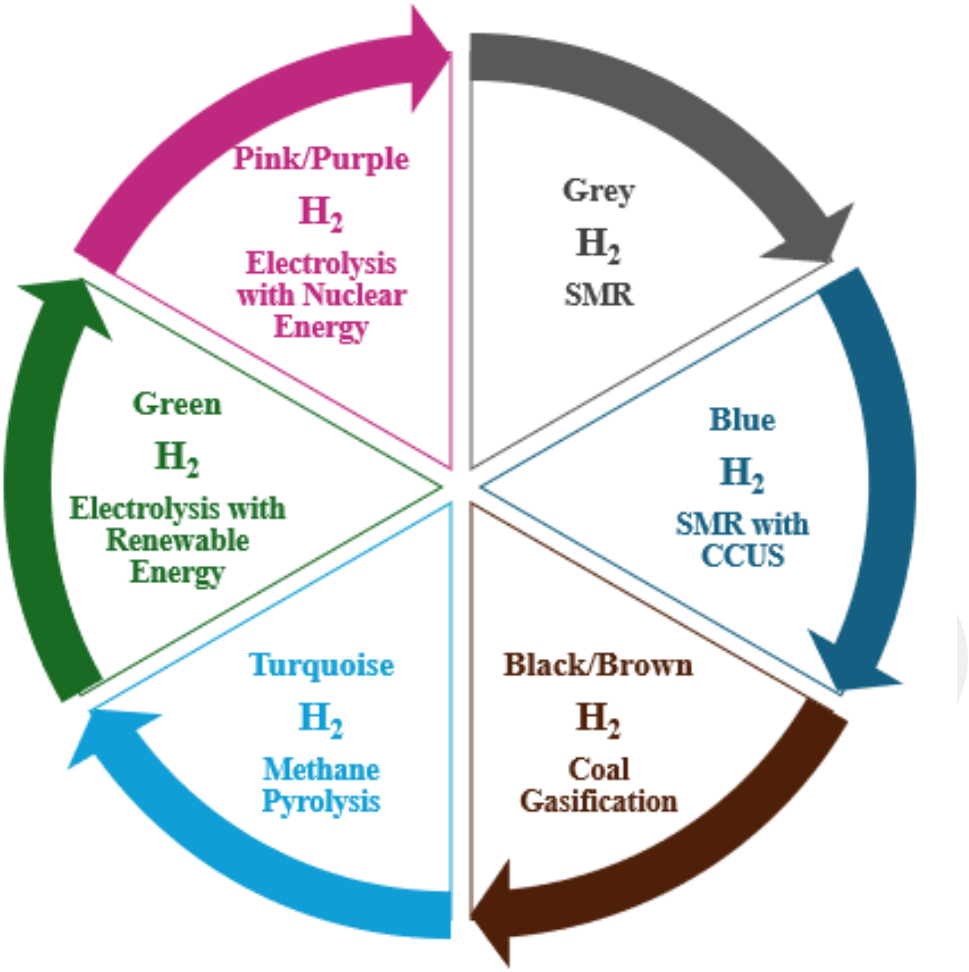

Figure 2.1 H_2 production methods

The H_2 produced by SMR, the most economical and standard method, contains impurities such as carbon monoxide (CO), carbon dioxide (CO_2), methane (CH_4), water vapor (H_2O) and nitrogen (N_2). Hence, a purification step is required to remove these impurities from the H_2 [34].

2.3. Hydrogen Purification Methods

H_2 must be of a certain purity to be used as a feedstock in chemical processes or as an energy carrier in fuel cells, so effective purification of H_2 from contaminants is essential [35]. The lifetime of the fuel cell can be significantly affected by hydrogen purity, and even traces of impurities may cause degradation of the catalyst layer of the fuel cell [36]. The H_2 quality requirements for fuel cells have been determined by the ISO 14687:2019 standard published by the International Organization for

Standardization (ISO) in November 2019 and followed by this standard the SAE J2719-202003 standard issued by the Society of Automobile Engineers (SAE) in March 2020. According to these standards, the H_2 purity requirement is 99.97%, and the allowable CO_2 and CO content is limited to 2 ppm and 0.2 ppm, respectively [37]. The H_2 fuel quality requirements according to ISO 14687:2019 and SAE J2719-202003 standards are in Table 2.2.

Besides, blending hydrogen into existing natural gas pipelines is an attention-grabbing option that enables the economical transportation of H_2 [38]. Blending H_2 into existing pipelines provides large-scale and long-distance H_2 transmission and distribution, saves construction time and investment costs for dedicated H_2 pipelines, and opens all links of the hydrogen value chain [39]. Moreover, there are also other advantages, such as reducing greenhouse gas emissions by mixing renewable H_2 with natural gas, encouraging the use of systems that require pure H_2 in end-use by starting from a mixture and reducing storage costs by blending H_2 into natural gas pipelines instead of dedicated H_2 storage systems [40]. In this case, for applications requiring pure H_2 or deficient amounts of H_2, the hydrogen mixed with natural gas must be separated near or at the end-use point [41]. The hydrogen purification methods are pressure swing adsorption (PSA), cryogenic separation, membrane separation, metal hydrides and electrochemical hydrogen purification [42].

Table 2.2 The H_2 fuel quality requirements according to ISO 14687:2019 and SAE J2719-202003 standards [37]

Component	**Concentration**
H_2 purity	99.97 %
Total non-hydrogen gases	300 ppm
H_2O	5 ppm
Non-methane hydrocarbon (by C_1)	2 ppm
Methane	100 ppm
O_2	5 ppm
He	300 ppm
N_2	300 ppm
Ar	300 ppm
CO_2	2 ppm
CO	0.2 ppm
Total sulfide (by H_2S)	0.004 ppm
HCHO	0.2 ppm
HCOOH	0.2 ppm
NH_3	0.1 ppm
Total halide (by halide ion)	0.05 ppm
The concentration of max particulate matter	1 mg/kg

2.3.1. Pressure Swing Adsorption (PSA)

Pressure swing adsorption (PSA) is the commonly used method worldwide for H_2 purification, which provides 98-99.999 mol% H_2 purity with 70-90% H_2 recovery at

the feed gas pressure from a gas mixture containing 60-90 mol% H_2. In the PSA process, the refinery off-gas from varied sources and the SMR off-gas processed in a water-gas shift reactor are generally used as feed gas [43]. The working concept of the PSA process is as follows: When the feed gas containing H_2 comes into contact with the solid in a packed column of the adsorbent, the impurities in the feed gas are selectively adsorbed at a relatively high pressure on the microporous and mesoporous solid adsorbent. Then, the adsorbed contaminants are desorbed from the solid to recharge the adsorbent. Desorption can be achieved by purging by flowing some purified H_2 gas over the adsorbent at a lower pressure or depressurization by reducing the column pressure [44]. Alternatingly, temperature swing adsorption (TSA), in which desorption is achieved by increasing the adsorbent temperature, can be used to remove small amounts of contaminants. Different PSA process designs are used from single column up to 16 large multiple parallel columns, with flows between 30-400,000 Nm^3/h. [45]. The PSA process generally has a multi-column system design operating under a cyclic steady state. It includes adsorption, desorption, and multiple complementary steps designed to enhance the H_2 purity and recovery and achieve optimum separation performance [46]. Activated carbons, zeolites, activated aluminas and silica gels are commonly used adsorbents. Activated carbons are favorable in removing hydrocarbons and CO_2 due to their low adsorption enthalpies and high capacities. At the same time, they are not very effective in removing N_2 and CO because of their large pore diameter and non-polar structure. On the other hand, zeolites show high selectivity to polar adsorbates. Still, their regeneration after CO_2 adsorption is challenging due to the strong interaction strength between the charged zeolite pore surface and the CO_2 molecules. Therefore, the adsorption columns often comprise two or more adsorbent layers, each targeting certain impurities to improve separation efficiency [47]. Fuderer and Rudelstorfer, in the U.S. Patent 3,986,849 [48] disclosed the Polybed process design, which contains ten adsorbent beds, each involving activated carbon at the feed end and calcium zeolite A molecular sieve at the product discharge end. They reported that 99.999% H_2 purity could be obtained with 86% recovery from the feed gas containing in mol basis 77.1% H_2, 22.5% CO_2, 0.35% CO and 0.013% CH_4. Majlan and colleagues [49] stated that 99.999% H_2 purity is obtained and the concentrations of CO_2 and CO in the $H_2/CO_2/CO$ mixture are reduced

from 5% to 7.0 ppm and 4000 ppm to 1.4 ppm, respectively, using the compact PSA system comprise four adsorption beds contains activated carbon as the adsorbent. Moreover, recently, metal-organic frameworks (MOFs) have been considered as an alternative to traditional adsorbents for the PSA process [50], [51], [52]. In the PSA systems, the energy consumption is high and the H_2 purity is inversely scaled to the gas recovery. While it is an ideal method for large-scale industrial plants, it is not optimal for small units, such as in the hydrogen refueling stations required for the FCEVs [53].

2.3.2. Membrane-Based Separation

The membrane is a selective barrier allowing certain compounds in the feed stream to pass while retaining others. Hydrogen separation membranes provide purification by allowing only H_2 to pass to the other side of the membrane from the H_2-containing feed gas mixture containing side [54]. The driving force in the membrane-based separation is the gradient in pressure, concentration, electrical potential, or temperature between the two sides of the membrane [55]. Various transport mechanisms exist for membrane-based separation, which are prevalent examples of Knudsen diffusion, Poiseuille flow, capillary condensation, molecular sieving, solution diffusion, surface diffusion and facilitated transport. The dominant mechanisms for hydrogen purification membranes are solution diffusion and molecular sieving [56]. Permeability and selectivity are the main parameters that are performance indicators of a membrane. Permeability expresses the tendency of compound flux to pass through the membrane and using materials with higher permeability results in improved productivity. "Selectivity" refers to the ability of a membrane to separate gases. Higher-purity hydrogen can be produced with higher selectivity materials, which may result in lower productivity. Temperature, humidity, gas compositions, pressure and other factors affect the permeability and selectivity [57]. H_2 separation membranes can be classified into four as porous, polymeric, dense-metal and proton-conducting membranes [58]. The H_2 separation membranes classification scheme is given in Figure 2.2.

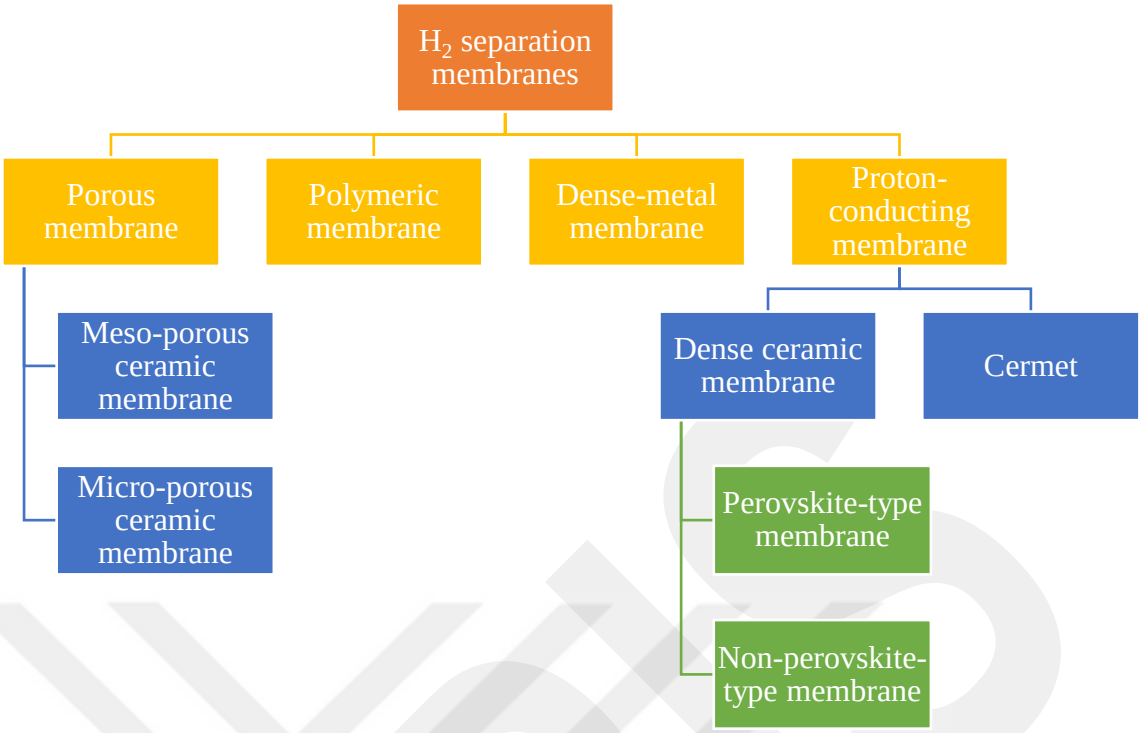

Figure 2.2 The H_2 separation membranes classification scheme [58]

In contrast with PSA systems, membrane separation is a suitable method for small-scale applications. In addition, this technology is the preferable option for vibrating, shock-exposed and mobile applications where PSA adsorbent beds may be damaged. The membrane-based separation process is easily controllable [59]. Furthermore, membrane-based separation consumes less energy than continuous operation [60]. On the other hand, this method has a lower feed flow rate, produces medium purity H_2 in the range of 90-95%, and a lower recovery rate of 85-90% [61].

2.3.3. Cryogenic Distillation

In the cryogenic distillation method, which is a very energy-intensive process since it takes place at low temperatures, separation is based on the varying boiling points of the constituents in the feed gas mixture. Since H_2 has the lowest boiling point of -252.9 °C, it remains in the gas phase, while the contaminant gases in the feed mixture condense to create a liquid phase [62]. Refineries and petrochemicals by-products are used as feed gas sources in cryogenic distillation. The purity of the obtained H_2 is limited to 90-98%, with a 96% recovery rate [63]. The H_2 purity depends on the feed

gas composition, the applied temperature and pressure [64]. In this method, no chemicals are used and any secondary pollutants are not released. Hence it is environmentally clean [65]. Cryogenic distillation provides the opportunity for the liquid storage of H_2; on the other hand, it has the disadvantages of requiring pre-treatment of the feed gas and high cooling costs [66]. As with PSA, this technology is an adequate solution for large-scale industrial applications. However, it is not a suitable method to purify small amounts of H_2 at refueling stations for FCEVs [64].

2.3.4. Metal Hydrides

Metal hydrides, extensively used for storage, can also be utilized for H_2 purification from gas mixtures. Presently, metal hydrides for H_2 purification are predominantly employed within the automotive sector with severe operational restrictions. This technology offers merits, including ease and safe operation, low energy consumption, and fast H_2 extraction rate [64]. This technique relies on the ability of the metal hydrides to absorb H_2 selectively. The H_2-containing gas mixture is introduced into a metal hydride reactor, and the metal hydride is formed by selective absorption of H_2 by the alloy bed. The heat released during this reaction is transferred to the coolant liquid. After the H_2 breakthrough, the absorption is terminated, and then the extraction of purified H_2 can be conducted by desorption. The outlet H_2 pressure can be arranged by heating the circulating liquid [67]. While pressurization or cooling is required for the metal hydride formation reaction, desorption occurs under decompression or heating. This technique has a limited H_2 recovery ratio of 75-95%, and the feed gas content and impurities' composition primarily affect the resulting H_2. When the H_2 content in the feed gas surpasses 50-60%, the metal hydride method can produce high-purity H_2. Even when the H_2 content exceeds 15%, H_2 separation through metal hydride remains viable [68]. Metal hydride exhibits sensitivity to certain reactive gases, notably CO, and contains sulfur (S) elements. Even a minor presence of impurities can significantly diminish the reversible H_2 adsorption and desorption ability after just a few cycles [69]. Some contaminants like CO and H_2S have a poisoning impact; CO_2 may pollute the metal hydrides, while inert gases such as N_2 cause the slowing down of the H_2 sorption reaction [70]. Metal hydride reactor design is crucial in practice for the effective purification and recovery of H_2. Unlike batch

reactors employed for H_2 storage, flowthrough reactors are favored for H_2 purification and recovery since they offer brief impurity residence time and low working pressure [69]. The heat and mass transfer requirements should be carefully considered when designing a metal hydride reactor. H_2 separation relies on numerous factors, such as the pressure and temperature of the hydride bed, reaction kinetics, cycle time, and enthalpy. To address the challenge of reaction kinetics, introducing amorphous Ni-Li-B catalysts enhances the reaction kinetics of aluminum-based alloys [65].

2.3.5. Electrochemical Hydrogen Purification (ECHP)

The electrochemical H_2 purification method is a novel and promising approach for H_2 purification [42]. The ECHP technology is explained in detail in Chapter 3.

CHAPTER 3

3. ELECTROCHEMICAL HYDROGEN PURIFICATION (ECHP)

Fishel et al. [71] stated that the approach of utilizing electrochemical reactions in combination with polymer-based proton exchange membranes for the purification, separation, and compression of H_2 emerged as an unexpected consequence of endeavors to develop solutions for power generation for spacecraft and satellites in the USA in the 1950s. The development of membrane-based fuel cell technology by General Electric in the 1960s and 1970s led to applications in H_2 and other alkali ion-intensive processes like water electrolysis, chlor-alkali membrane process, oxygen concentrators, and electrochemical H_2 pumping.

A single ECHP cell, which has a pretty similar structure to the proton exchange membrane fuel cell (PEMFC), consists of a proton conductive membrane in the middle and catalyst layers, gas diffusion layers (GDLs), bipolar plates, current distribution plates and end plates on both sides, respectively [72].

ECHP presents advantages of elevated H_2 purity and recovery rate, fewer maintenance demands, low energy cost, and operation at low temperatures compared to traditional H_2 purification techniques. Foremost, H_2 compression, besides purification, can be achieved in one step in a single system [53]. ECHP systems can be scaled up to more considerable demands even though they are more suited for small-scale applications, and their integration into existing processes is easier since they have less footprint [73].

3.1. Working Principle of ECHP

The working principle of ECHP is illustrated in Figure 3.1. The H_2-containing gas mixture is fed from the anode side of the ECHP cell. When H_2 in the gas mixture comes into contact with the anode catalyst layer, the H_2 oxidation reaction (Eq. (3)) takes place and H_2 is split into protons and electrons. An external DC power source is

connected to the cell by current distribution plates for the H_2 oxidation reaction. While protons transport to the cathode side through the membrane, electrons pass to the cathode via the external circuit. Here, protons and electrons are recombined by H_2 evolution reaction (Eq. (4)), and purified H_2 is obtained. On the other hand, the selectively permeable membrane acts as a barrier against impurity gases in the gas mixture, and these impurities remaining on the anode side are removed from the cell via the anode outlet. The electrochemical reactions that occur during ECHP operation are given below:

$$Anode: H_2\ (LP) \rightarrow 2H^+ + 2e^-\ (H_2\ oxidation\ reaction, HOR) \quad (3)$$

$$Cathode: 2H^+ + 2e^- \rightarrow H_2\ (HP)\ (H_2\ evolution\ reaction, HER) \quad (4)$$

$$Overall\ cell\ reaction: H_2\ (LP) \rightarrow H_2\ (HP) \quad (5)$$

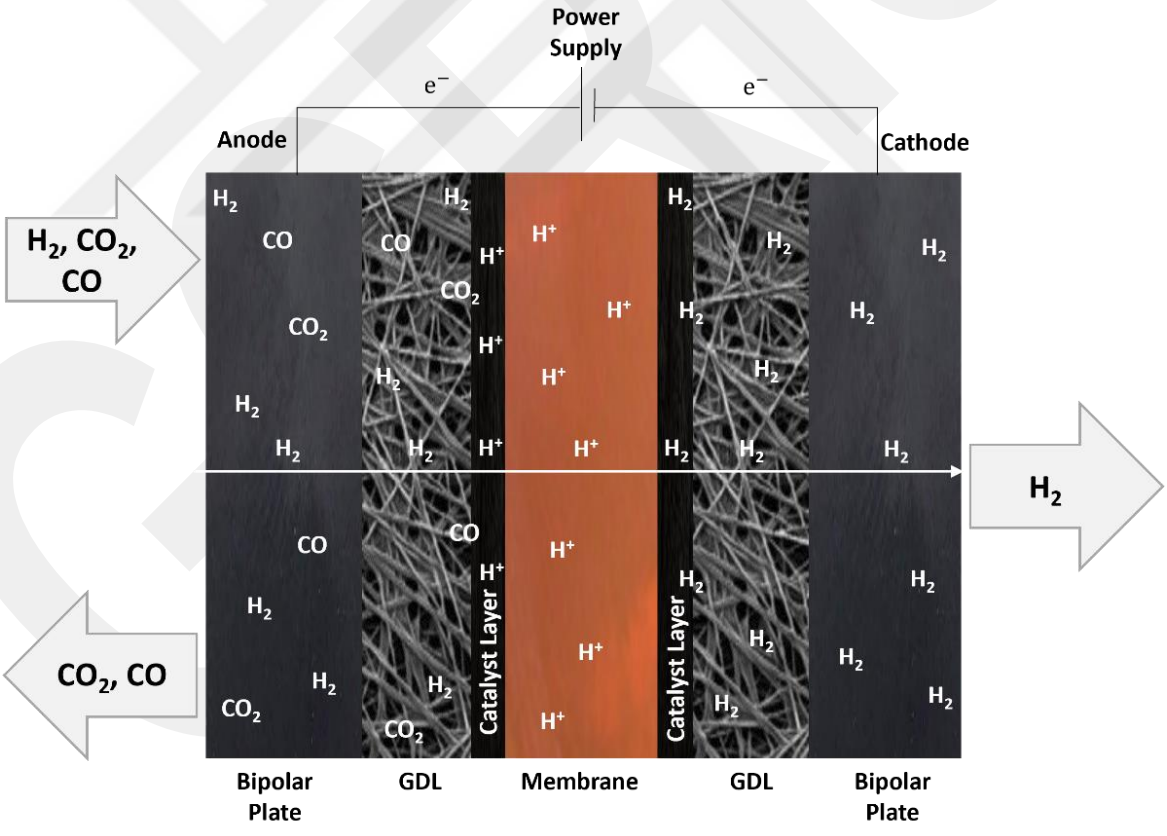

Figure 3.1 Working principle of the electrochemical H_2 purification

The rate of H_2 separation can be controlled by varying the current supplied to the cell [74]. As the provided current increases, the rate of transition of protons from the anode to the cathode side increases, and it can be explained by Faraday's law (Eq. (6)) [75].

$$\frac{dn}{dt} = \frac{I}{2F} \tag{6}$$

where n is the inlet H_2 flow (mol), I is the current (A), and F is the Faraday's constant (9.648×10^4 C/mol).

Besides purification, simultaneous H_2 compression can also be performed with an ECHP cell without an extra system. The purified H_2 in the cathode side can be compressed by regulating the cathode outlet with a back pressure valve [76]. The required theoretical cell voltage is specified by the Nernst equation (Eq. (7)) [77].

$$E_{Nernst} = E_0 + \frac{RT}{2F}\ln\left(\frac{{P_C}^{H_2}}{{P_A}^{H_2}}\right) \tag{7}$$

where E_0 is the standard cell potential, which is assumed as 0 for electrochemical compression, R is the universal gas constant (8.314 J/molK), T is the temperature in Kelvin, and ${P_A}^{H_2}$ and ${P_C}^{H_2}$ are H_2 partial pressures at the anode and cathode sides, respectively.

When the ECHP cell is operated just for purification purposes without compression, the anode and cathode total pressure are equal, while the H_2 partial pressure on the cathode side, ${P_C}^{H_2}$, is greater than the H_2 partial pressure at the anode, ${P_A}^{H_2}$. When compression is performed, the total pressure at the cathode side is more significant than at the anode side [78].

In practical applications, the operating voltage of the cell is higher than the theoretical value due to voltage losses, which are ohmic overpotential due to the conductivity of the membrane, activation overpotential associated with the catalyst activity and mass-transfer overpotential [77]. The ohmic overpotential can be determined by Eq. (8).

$$\Delta E_{Ohmic} = iR_{Ohmic} = i\frac{t_m}{\sigma} \tag{8}$$

where i is the current density (A/cm^2), R_{ohmic} is the ohmic resistance of the cell that includes membrane resistance, electrode resistance, resistance of the cell hardware [71] and contact resistance between the components [79], t_m is the thickness of the membrane (cm), and σ is the ionic conductivity of the cell (S/cm). It is seen from Eq. (8) that the membrane thickness and the ionic conductivity have a direct influence on the ohmic losses.

Activation polarization is the overpotential that must be overcome for an electrochemical reaction. The activation overpotentials for the anode and cathode electrodes can be described by the Tafel equation (Eq.(9)-Eq.(10)) [80].

$$E_{Activation,Anode} = \frac{RT}{2\alpha_a F}\ln(\frac{i}{i_{0,a}}) \quad (9)$$

$$E_{Activation,Cathode} = \frac{RT}{2\alpha_c F}\ln(\frac{i}{i_{0,c}}) \quad (10)$$

$$\Delta E_{Activation} = E_{Activation,Anode} + E_{Activation,Cathode} \quad (11)$$

where α denotes the charge transfer coefficient and is accepted as equal to 0.5 for both the anode and cathode electrodes [80], $i_{0,a}$ and $i_{0,c}$ are the exchange current density (A/cm^2) at the anode and cathode, respectively. While HOR at the anode is dominated by the Volmer-Tafel mechanism, HER at the cathode is dominated by the Volmer-Heyrovsky mechanism. Since the HER rate is slower than the HOR rate, the overpotential caused by HER on the cathode side is higher than the anode overpotential [76], but in general, the reaction kinetics of H_2 electrodes are fast [80] and the activation overpotentials are relatively small [81].

Mass transport limitations, which are more dominant at higher flows, caused by decreasing H_2 mole fraction obstruct the transportation of the reactant gas to the anode catalyst through GDL, causing voltage increase [82]. Mass transfer overvoltages can be estimated by assessing each species' concentration at the reaction sites by Fick's Law of diffusion, and after that, using the Nernst equation to define the diffusion overvoltage at the anode and cathode electrodes (Eq.(12)-Eq.(13)) [83]:

$$E_{Mass\ Transport,Anode} = \frac{RT}{2F} \ln \frac{C_a}{C_{a,0}} \quad (12)$$

$$E_{Mass\ Transport,Cathode} = \frac{RT}{2F} \ln \frac{C_c}{C_{c,0}} \quad (13)$$

where C_a and C_c are the concentration of H_2 in mol/m^3, $C_{a,0}$ and $Cc_{,0}$ are "0" conditions that is reference working conditions in mol/m^3 for the anode and cathode sides, respectively.

Suppose the ECHP cell is used for compression. In that case, pressure on the cathode side increases while the anode side remains at atmospheric pressure, and the resulting pressure difference between the two sides may cause the back diffusion of H_2 through the membrane to the anode [84]. The cell voltage must be greater than the Nernst voltage to overcome all these irreversibilities (Eq. (14)):

$$E_{Cell} = E_{Nernst} + \Delta E_{Ohmic} + \Delta E_{Activation} + \Delta E_{Mass\ Transport} + \Delta E_{Back\ Diffusion} \quad (14)$$

3.2. Components of an ECHP Cell

Similar to the PEMFC structure, a single ECHP cell consists of a proton conductive membrane in the middle and catalyst layers, gas diffusion layers, gaskets, bipolar plates, current distribution plates and end plates on both sides, respectively. Catalyst layers promote the electrochemical reaction kinetics, while GDLs support the catalyst particles and uniformly ensure reactant distribution into the active area. Bipolar plates provide mechanical support to the cell and ensure uniform transport and distribution of reactants to the electrode surface through gas flow channels. Gas leakage is prevented by using gaskets, end plates hold the cell components together by providing mechanical strength [77], [85]. The ideal operating performance of the ECHP cell is only possible by optimizing its core components, membrane, and catalysts [86].

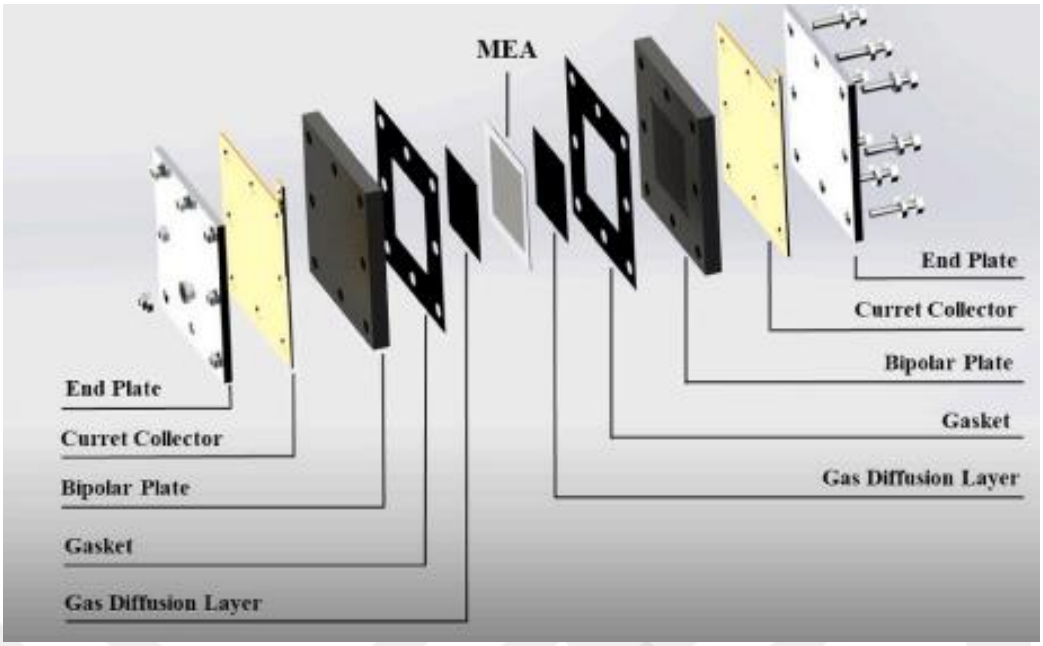

Figure 3.2 Components of the ECHP cell [42]

3.2.1. ECHP Membranes

A proton exchange membrane should exhibit high proton conductivity, low permeability to gas, electrical insulation, high mechanical strength both in dry and humidified conditions, limited water transport through electro-osmosis and diffusion, cost-effectiveness, and the ability to be fabricated into membrane electrode assemblies (MEAs) [87]. The most commonly used membranes for low-temperature applications below 100 ℃ are perfluorosulfonic acid (PFSA) membranes i.e., Nafion™ while acid-loaded polybenzimidazole (PBI) membranes are used for high-temperature operation [85]. In an ECHP cell, the purity of the produced H_2 depends on membrane permeability, gas feed, and membrane integrity [88].

3.2.1.1. Low-Temperature ECHP Membranes

The most common example of PFSA membranes used in low-temperature applications is Nafion™ developed by DuPont, which has a perfluorinated structure in which ether-linked side chains terminate the sulfonate cation exchange site and terminal sulfonic acid end groups [3]. Typical operating temperatures of these types of membranes are in the range of 50-80 ℃. Since the proton conductivity of PFSA membranes is highly

dependent on the water content of the membrane, the feed gas must be humidified and the working temperature must be kept below 100 ℃ to prevent the membrane from drying out [89]. Insufficient water content causes decreased membrane conductivity and, thus, increased ohmic losses. Also, the physical degradation of the membrane is facilitated when the water content is insufficient. On the other hand, excessive water content blocks the diffusion pores, resulting in mass transfer losses [90]. Anantaraman et al. [91] experimentally measured the conductivity of the Nafion™ 117 membrane as a function of relative humidity and reported that the proton conductivity decreases from 6.61×10^{-2} $S.cm^{-1}$ to 1.40×10^{-4} $S.cm^{-1}$ when the relative humidity reduced from 100% to 34%.

Lee et al. [92] investigated the electrochemical H_2 separation using the Nafion™ 115 membrane at low temperatures. They stated that the current efficiency is improved with working pressure and temperature since the reactivity of proton transfer in the Nafion™ membrane, H_2 dissociation and H_2 partial pressure increases as the pressure and temperature. Casati et al. [93] studied the H_2 separation performance of an ECHP cell with Nafion™ 117 membrane in galvanostatic and tensiostatic operation mod. They remarked that under the tensiostatic operating condition, the reaction kinetics are self-controlled based on the hydration degree of the membrane. In contrast, in the galvanostatic mode, where the process kinetics are fixed, the cell shows unstable behavior since the membrane water content is uncontrollable. They also reported that the MEA resistance is decisive on the surface area of the membrane, and the crossover and the H_2 purity cause H_2 losses. Nordio et al. [94] analyzed the electrochemical H_2 separation using Nafion™ 212 membrane and indicated that temperature positively impacts H_2 separation by enhancing membrane conductivity and reducing ohmic resistance.

Although Nafion™ is extensively used due to its high proton conductivity, good chemical stability, and mechanical strength, it has a limited operating temperature range and high cost [95]. Sulfonated poly ether ether ketone (SPEEK), a polyaromatic hydrocarbon membrane with low permeability and robust chemical and thermal stability, is emerging as a cost-effective substitute for Nafion™. The SPEEK membrane's proton conductivity depends on the sulfonation degree. An elevated

sulfonation degree can enhance the proton conductivity, while excessive sulfonation significantly diminishes membrane stability [96]. Both Nafion™ and SPEEK membranes contain hydrophilic regions dispersed within a hydrophobic continuous matrix, and the proton conduction in these membranes occurs through hydrophilic domains arising from sulfonic acid groups. Hydrophilic domains swell and bind with water absorption, forming the percolation paths necessary for proton conduction. Nafion™ has better proton conductivity for lower sulfonation degree and increasing the sulfonation degree of SPEEK membrane to achieve competitive proton conductivity with Nafion™ causes its mechanical strength to decrease and become water-soluble [97].

Studies have been carried out on improving the membrane properties by additional components and developing Nafion™ or SPEEK-based hybrid/composite membranes. Wu et al. [98] evaluated the H_2 separation from the H_2/CO_2 mixture with the semi-interpenetrating polymer network (sIPN) membrane prepared by incorporating the cross-linked poly(styrene sulfonic acid) (CrPSSA) into SPEEK. They reported that the SPEEK/CrPSSA sIPN membrane has better proton conductivity compared to the pristine SPEEK and that the energy efficiency of the SPEEK/CrPSSA membrane-based cell is 30%, slightly below that of the Nafion™ -based cell, which has 40%. Rico-Zavala et al. [99] observed that the proton conductivity of the SPEEK-based membranes modified with Halloysite nanotubes and phosphotungstic acid-impregnated Halloysite nanotubes enhanced by 42% and 88%, respectively, compared to unmodified one.

The water required to ensure proton conduction in these membranes can cause flooding by blocking the flow channels and electrodes, resulting in decreased performance. Thus, precise water management is essential for low-temperature cells. Another challenge faced by low-temperature cells is the low tolerance of electrodes to contaminants such as CO, which can cause severe degradation. Membranes designed to operate at elevated temperatures can be employed to overcome these challenges [71].

3.2.1.2. High-Temperature ECHP Membranes

Operating at high temperatures allows simpler system design by eliminating water management, offering enhanced catalyst tolerance to impurities and improving reaction kinetics. The critical element in electrochemical cells that enable operation at higher temperatures is membrane [100].

One of the approaches for developing proton-conducting membranes for high-temperature applications is acid-base complexation. Polymers bearing primary groups such as alcohol, ether, imine, imide, or amide function as a proton acceptor and react with strong acids [101]. Polymers have been studied in the literature include polyethyleneimine (PEI) [102], polyethylene oxide (PEO) [103], polyacrylamide (PAAM) [104] and polybenzimidazole (PBI) [105]. PBI offers easy fabricability with its strong chemical resistance and exceptional textile fiber characteristics. It has a high glass-transition temperature and remains mechanically stable under high temperatures [106].

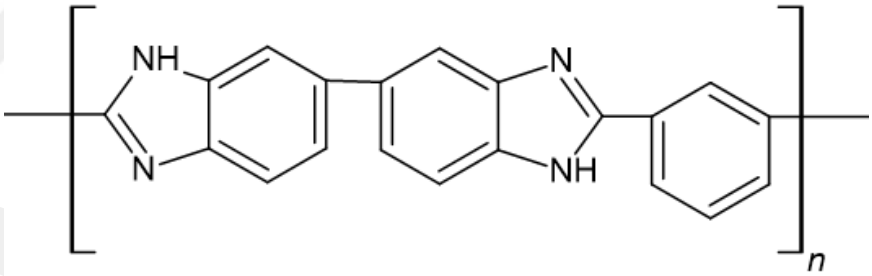

Figure 3.3 Chemical structure of PBI

Several inorganic acids including H_3PO_4 (Phosphoric acid, PA), H_2SO_4 (Sulfuric acid), $HClO_4$ (Perchloric acid), HNO_3 (Nitric acid), HCl (Hydrogen chloride), HBr (Hydrogen bromide) and organic acids such as $C_2H_5SO_3H$ (Methyl Methane sulfonate) and CH_3SO_3H (Methane sulphonic acid) have been researched to be doped in PBI membranes. Among them, amphoteric acids, such as H_3PO_4, act as proton donors and acceptors and thus provide proton transfer alongside the anionic chain. H_3PO_4, which stands out with its high proton conductivity and excellent thermal stability even at elevated temperatures, strongly interacts with PBI [107]. The pioneering study on the

use of H_3PO_4-doped PBI as a polymer electrolyte membrane was done by Wainright et al. [108]. Some authors have claimed that the only membrane that matches the U.S. Department of Energy (DOE)'s high-temperature membrane criteria is H_3PO_4-doped PBI [100]. Proton conductivity of H_3PO_4-doped PBI membranes is directly related to the acid doping level and increasing H_3PO_4 doping leads to the formation of more dynamic H_2 bond networks that promote proton transfer, while high levels of doping cause diminished interaction among PBI chains, resulting in weakening of mechanical properties [109].

Using an acid-doped PBI membrane-based high-temperature electrochemical cell for H_2 purification is proposed in the U.S. patent application 2003/0196893A1 [110]. Perry et al. [88] used an H_3PO_4-doped PBI membrane for high-temperature electrochemical hydrogen separation at 160 °C. They stated that the membrane exhibits long-term durability of up to 4000 h, which can be attributed to the ability of PBI membranes to retain adequate amounts of phosphoric acid under both humidified and non-humidified operating conditions over prolonged durations. Huang et al. [111] prepared three different phosphoric acid-doped PBI membranes, which are para-PBI, m/p-PBI, and meta-PBI, with the poly (phosphoric acid) (PPA) sol-gel process to investigate the high-temperature electrochemical H_2 separation performances and also included the conventionally impregnated meta-PBI membrane in their study for comparison. The team reported that the rank of proton conductivity of these membranes from high to low is as para-PBI, m/p-PBI, meta-PBI, and conventional meta-PBI.

Polymer blend membranes and organic-inorganic composite membranes are the other membrane types studied for high-temperature applications [112]. Polymer-blend membranes researched in the literature include PBI/polyether blend [113], Nafion™/poly(1-vinyl-1,2,4-triazole) blend [114], PPO/poly (styrene-b-vinylbenzylphosphonic acid) blend [115], while Nafion™/Teflon/$Zr(HPO_4)_2$ composite [116], sulfonated poly(ether sulfone) (SPES)/boron phosphate (BPO_4) composite [117], Nafion™/TiO_2 composite [118] are the organic-inorganic composite membrane examples.

Ceramic proton conducting membranes with typically high operating temperatures of 800-900 ℃ can also be used as solid electrolytes for ECHP. Ceramic membranes for H_2 separation should have high chemical stability in reducing and hydrothermal environments and a combination of protonic and electronic conductivity [119]. Sakai et al. [120] confirmed using $La_{0.9}Ba_{0.1}YbO_{3-\alpha}$ (LBYb-91) that LBYb-91 exhibits high chemical resistance to H_2O and CO_2. They reported a cell voltage of 0.7 V at 40 mA/cm^2, 800 ℃, and concluded that the membrane is a promising material for electrochemical H_2 separation.

PBI membranes find extensive application owing to their excellent resistance to high temperatures, elevated proton conductivity, zero electron osmotic draw, minimal gas permeability and lower cost, while the phosphoric acid doping enhances proton conductivity and improves thermal and mechanical stability [121].

3.2.2. Catalyst Layer (CL)

The competitiveness of ECHP cells, which are power-consuming systems, with current technologies is only possible if they operate with low cell voltage at high current densities and achieving such performance necessitates the optimization of the core components of the cell, membrane and electrocatalysts [86]. The catalyst layer activity significantly impacts the efficiency of the ECHP [122]. Given that the H_2-containing gas mixture is fed to the system from the anode side, it is crucial for the anode catalyst layer, in particular, to exhibit a high tolerance to impurities and promote a rapid HOR to attain the desired performance in ECHP. Due to the structural similarities between ECHP and PEMFC, impurities in the reformate gas cause similar impacts in both systems. Pt, a frequently employed catalyst for HOR in the literature, exhibits limited tolerance to CO, a commonly found component in reformate gases. CO molecules adsorb strongly onto Pt, blocking the active catalytic sites and resulting in diminished cell performance, even a trace amount of CO can lead to catalyst poisoning [123]. Gardner et al. [124] studied ECHP using H_2/CO_2 and $H_2/CO_2/CO$ feed gases. They observed significant catalyst poisoning and a 300 mV rise in the anode potential in the presence of 1000 ppm CO in the feed gas. The team suggested that increasing the anode potential to approximately 700 mV vs. RHE enables the

removal of absorbed CO on the active catalyst sites through its oxidation to CO_2 by reacting with hydroxyl species formed on the Pt surface. Kim et al. [125] synthesized the Ir/C catalyst and examined the performance of separating H_2 from the H_2/CO_2 mixture, stating that Ir/C has higher CO_2 tolerance and better catalytic activity for hydrogen oxidation than the conventional Pt/C catalyst. They reported a lower cell voltage of 0.18 V at 0.8 A/cm^2 for Ir/C while the required cell voltage is 0.20 V at the same current density for Pt/C. Wu et al. [126] compared the ECHP performances of Nafion™-115-based catalyst-coated membranes (CCM) prepared with Pt/C and Pd/C catalysts using CO_2/H_2 reformate gas mixtures. They stated that MEA prepared with Pd/C catalyst showed higher resistance due to the stronger adsorption of CO_2 into the Pd compared to Pt. Kim et al. [127] investigated how the amount of Pt loading influences the high-temperature ECHP performance. Their experiments, conducted at 160 °C with the gas mixture of 20% H_2/80% CO_2 without humidification, revealed a 72% increase in cell voltage when the Pt loading of the anode side was reduced from 1.1 mg/cm^2 to 0.2 mg/cm^2. They concluded that while the HOR in the anode is a determinant in cell performance, the Pt loading at the cathode does not have a significant effect.

3.2.2.1. Bimetallic Catalysts

Besides CO and CO_2, reformate gas may contain some gases that can have serious effects on the catalyst such as hydrogen sulphide (H_2S) and ammonia (NH_3), as well as inert gases such as CH_4 and N_2, which acts as H_2 diluents without causing irreversible damage on the catalyst [128]. The catalyst materials must be tailored to tolerate these impurities to ensure high efficiency in ECHP operation. The electrocatalytic activity and CO tolerance can be improved by modifying the morphology and structure of the catalyst [86]. The use of a second metal such as Ruthenium (Ru), Cobalt (Co), Palladium (Pd), and Iron (Fe) along with Pt as an anode catalyst for HOR has been recognized as a promising approach not only to achieve improved performance and improved CO tolerance but also for cost reduction in PEMFC [129]. The second metal enables the formation of hydroxyl species (M-OH), which needed for the oxidation of adsorbed CO to CO_2, at lower potentials than pure Pt, thus regenerating active Pt sites and enabling H_2 oxidation reaction [130]. Among

the various bimetallic catalysts, PtRu stands out as the most promising candidate for improved CO tolerance [131], [132]. The high activity of PtRu catalyst towards CO oxidation can be attributed to that Ru is a Pt-group metal that has similar properties; adsorbs CO and has quasi-reversible OH_{ads} states for CO oxidation in the low potential region. In addition, Pt d-band electron vacancies increase in the Ru presence, and the bonds between Pt and CO weaken as the electron density available for the Pt-CO bond formation reduces [129]. While numerous researchers in the literature have explored the performance of various bimetallic catalysts in PEMFC, few studies have focused on using bimetallic catalysts for ECHP. Ibeh et al. [133], as a result of their research on electrochemical H_2 separation using Pt and PtRu as the anode catalysts with various concentrations of H_2/CH_4 mixtures in the temperature range of 20-70 °C, reported that methane has an inert gas effect under these operating conditions and does not cause degradation of the anode catalyst. Tokarev et al. [134] conducted a modeling study of CO adsorption on different bimetallic PtRu surfaces for the electrochemical H_2 separation and compression. Jackson and colleagues [135] used H_2/20 ppm CO feed gas to compare the CO tolerance of Pt/C, PtRu/C and PtNi/C catalysts and observed that the PtNi/C exhibits the lowest tolerance to CO while the best performance is obtained with PtRu/C. Aykut et al. [136] synthesized Pt/C, Pd/C, and PtPd/C catalysts to assess their applicability for electrochemical H_2 purification and compression and stated that the PtPd/C bimetallic catalyst exhibited better catalytic activity. Vermaak et al. [137], studied the high-temperature electrochemical H_2 separation from various gas mixtures using bimetallic PtCo/C as the anode catalyst, reported that the presence of CO_2 in the feed gas seriously affects the catalyst even at high temperatures, causing catalyst deactivation and thus a decrease in cell performance.

3.2.2.2. Catalyst Support Materials

Support materials play a crucial role in improving catalyst utilization and reducing the amount of metal loading through enabling even distribution of metal nanoparticles, as well as contribute to promoting durability and prolonging the cell's lifespan by mitigating catalyst poisoning. The support material effectively determines the performance, lifetime and cost of the catalyst layer and the complete cell [138]. Properties such as high electrical conductivity, broad surface area, a porous structure to optimize triple-phase boundaries (TPB) and good interaction with the catalyst metal

are taken into account when selecting the support material. Corrosion of the catalyst support, a common problem in PEM fuel cells and electrolyzers, is disregarded for the ECHP cell since the required voltage for the oxidation and reduction reactions is zero by definition and caused only by minimal overvoltages [77]. Many materials such as carbon black, carbon nanotubes (CNTs), carbon nanofibers (CNFs), carbides and conductive or semiconductive oxides are used as support materials [139]. Another support material that has garnered attention is graphene nanoplatelet (GNP), which is composed of multiple layers of graphene sheets and stand out with its exceptional mechanical, thermal and electrical characteristics. GNP exhibits the favored properties of both single-layer graphene and graphitic carbon has a large surface area, good mechanical strength, excellent conductivity, and high stability. Moreover, since it can be derived directly from graphite, it offers a lower cost than other carbon-based nanomaterials [140]. Xia et al. [141] reported that the Pt/GNP catalyst displayed superior durability, catalytic activity, and CO tolerance compared to commercial Pt/C. Gonzalez-Hernandez et al. [142] examined the performance of PtRu/N-GNP, PtRuMo/N-GNP, and PtRu/C as the anode catalysts in PEMFC. Their findings indicated that N-GNP-supported catalysts demonstrated decreased metal loss, enhanced stability and better CO tolerance compared to PtRu/C.

3.2.3. Gas Diffusion Layer (GDL)

Gas diffusion layers are porous structures placed between the catalyst layer and bipolar plate in both the anode and cathode compartments and are critically important to the ECHP performance. The preferable characteristics for a GDL include efficient gas diffusion coupled with optimal bending stiffness, suitable surface contact angle, appropriate porosity, air permeability, electrical conductivity, water vapor diffusion, a surface morphology free of cracks, robust mechanical integrity, improved resistance to oxidation and high durability across diverse working conditions [143]. The function of GDL in an electrochemical cell is to supply reactant gases to the CL, support the CL, provide the electron and heat conduction within the cell and facilitate water management [144]. Carbon-based products such as carbon paper, carbon cloth and carbon felt are extensively used as GDL because of their stability in acidic environments, high reactant gas permeability, good electronic conductivity, and

elasticity under compression, while metallic GDLs like metal mesh and metal foam have also been studied due to their high mechanical strength and good stability across a broad potential range [145]. Electrodes are formed by applying a catalyst layer on GDL, and polytetrafluoroethylene (PTFE) is widely used to bind the catalyst particles and enhance the hydrophobicity of the electrodes to prevent water flooding [146]. Toghyani et al. [147] investigated the effect of GDL porosity and thickness on the H_2 compression performance of an electrochemical cell. They noticed that GDL porosity does not seriously affect the polarization curve, while increasing GDL thickness from 0.2 to 0.5 mm causes more overall voltage and thus reduces cell performance. Lee and Huang [148] applied a hydrophobic coating made of Nafion™ and oxidized carbon nanotubes (O-CNT) mixture to the porous GDL to examine its effect on anode flooding in an electrochemical cell used for H_2 compression. They reported that the coating enhances water management performance by making GDL hydrophobic. The team applied silver particles as a binding and roughening agent and heptadecafluoro-1-decanethiol (HDFT) as a hydrophobic surface modifier on porous metallic GDL in another study [149], indicated that the coated metallic GDL renders very hydrophobic and shows significantly improved water management performance.

3.2.4. Sealing Gaskets

Leakage during operation is a critical concern. It reduces the electrochemical performance and lifespan of the cell and poses a severe safety risk. Sealing gaskets ensure that the reactant and coolant stay in designated areas and play a vital role in ensuring stability and durability [150]. The sealing materials must have excellent chemical and heat resistance, high mechanical strength and bear a high level of compression [151]. The stack is sealed by compressing the gaskets during assembly. The contact stress significantly affects the sealing performance. Rubbers, with their notable elastic properties, are considered hopeful sealing materials [152]. Silicone rubber, ethylene propylene diene terpolymer (EPDM) and fluoroelastomer copolymer (FKM) are commonly used for sealing [151]. Kapton, a polyimide film produced by DuPont, can also be used as a gasket. It has outstanding electrical, physical, and mechanical characteristics across various temperatures [153]. It is relatively cheap and easily shaped, so it is used in various fields, from electrical insulation to vacuum

experiments [154]. Perry et al. [88] used Kapton framed electrodes hot pressed onto PBI films in their electrochemical H_2 pumping study.

3.2.5. Bipolar Plates

The functions of bipolar plates in an electrochemical cell are to supply gases to the electrodes through flow channels, provide heat and water management, separate the individual cells that compose the stack, connect the cathode side of one cell to the anode side of the adjacent cell, provide mechanical support to the MEA. The bipolar plate should have excellent electrical conductivity, high mechanical strength, good gas impermeability and low cost to provide these functions [155]. The criteria a material must meet to be used in bipolar plate manufacturing are determined by the DOE and are given in Table 3.1 [156].

Bipolar plates greatly influence the stack volume, weight (80% of the total weight), and cost (45% of the stack cost); hence, they must be lightweight, cheap, and easily fabricated. Non-porous graphite, non-coated and coated metals and polymer composites are bipolar plate materials [157]. Graphite is the most commonly used bipolar plate material due to its high conductivity and corrosion resistance. However, it requires machining to form flow channels and its thickness cannot be reduced due to its brittleness and poor mechanical strength, which leads to thicker plates with bulkiness [158]. Metals are considered alternative plate materials because of their high electrical conductivity, good mechanical strength, and low gas permeability. In addition, metals stand out with the advantages of being easily manufactured at low cost and flow channels can be readily formed on thin metals by pressing method [159]. Stainless steel, aluminum, nickel, and titanium are the metals studied as bipolar plate materials. Metal plates have low corrosion resistance, to prevent this, they can be coated with protective layers [157]. Another bipolar plate material is polymer composites, a lighter and lower-cost option than graphite and metallic plates. Bipolar plates containing flow channels can be manufactured by injection or compression molding, reducing machining costs [160].

Table 3.1 Technical requirements for bipolar plate materials [156]

Property	**Value**
Tensile strength (MPa)	>41
Flexural strength (MPa)	>59
Electrical conductivity (S $cm^{-1)}$	>100
Corrosion rate (μA cm^{-2})	<1
Contact resistance (mΩ cm^2)	<20
Hydrogen permeability (cm^3 (cm^2 $s)^{-1}$)	$<2.10^{-6}$
Mass (kg/kW)	<1
Density (g cm^{-3})	<5
Thermal conductivity (W (m $K)^{-1}$)	>10
Impact resistance (J m^{-1})	>40,5

Flow channels are machined onto the bipolar plate surface to provide even gas distribution across the MEA active area. The design of the flow channels must ensure both appropriate rib thickness to maintain electrical conductivity and sufficient channel width for gas flow, along with effective water management. Serpentine, parallel, parallel serpentine, interdigitated, spiral and porous mesh flow channel geometries are commonly used [161], as shown in Figure 3.4. Casati et al. [93] compared two different flow channel designs, one with 21 parallel channels and the other with a single zigzag channel and reported that the flow channel geometry has no impact on the H_2 purification and compression performance.

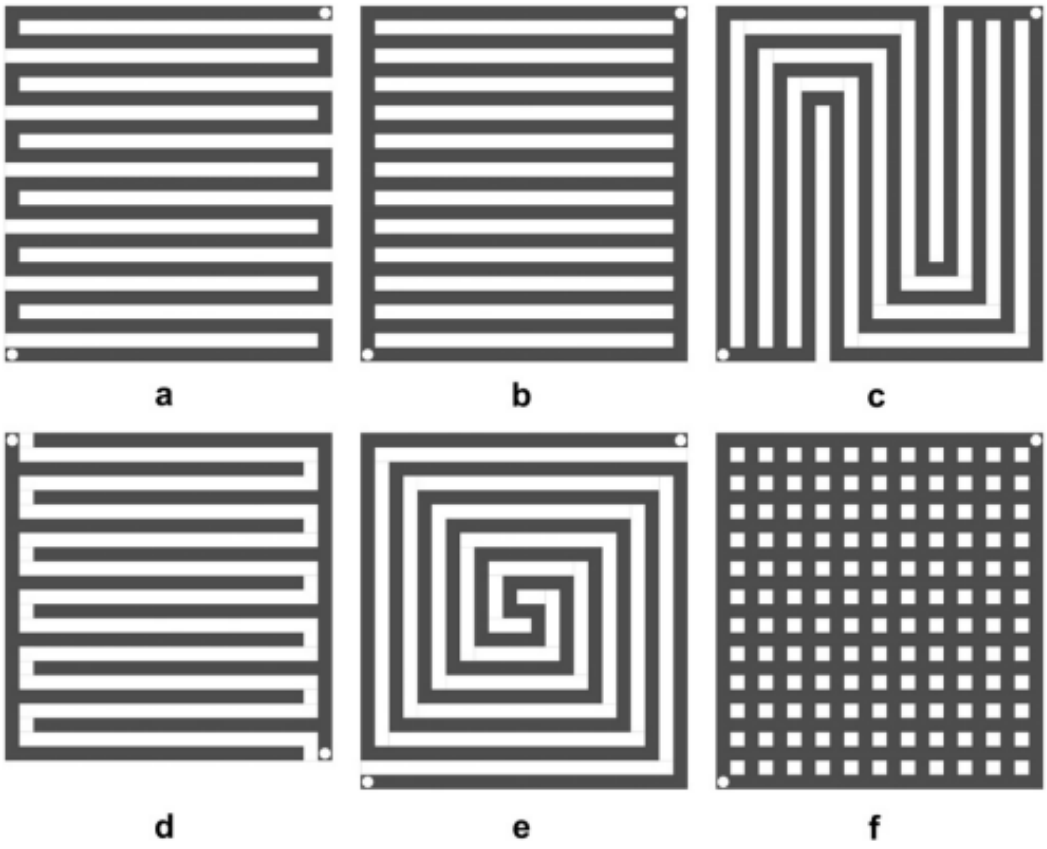

Figure 3.4 Bipolar plate flow channel geometries a) serpentine, b) parallel, c) parallel serpentine, d) interdigitated, e) spiral, and f) porous mesh [161]

3.2.6. Current Distribution Plates

Current distribution plates, located between the bipolar plate and end plate on both sides of the cell, transfer the current from the external circuit to the cell. The external DC power source is connected to the cell via the tabs of the current distribution plates. They are generally made of copper and titanium, which have good electrical conductivity. Tabbed end plates can also be used as current distribution plates in specific performances.

3.2.7. End Plates

End plates are clamping parts placed at either end of the cell, holding the individual components together and providing mechanical support. The cell assembly is fastened with bolts inserted through holes drilled in the edges of the end plates. The main functions of the end plates are to assemble other components (MEA, GDL, gasket,

bipolar plate and current distribution plate) into cell/stack, provide pathways for gases and coolant, and maintain effective sealing at various interfaces [162]. Ensuring proper and uniform pressure distribution is critical to cell performance during assembly. Optimum assembly pressure should decrease the contact resistance between the cell components and minimize the ohmic losses. Insufficient or uneven assembly pressure can lead to leakage and excessive contact resistance. Conversely, overpressure can damage the porous structure and block the gas diffusion channels [163]. Also, the geometry of the end plate and, the number of bolts used for tightening and their location on the plate significantly affect the contact pressure and its distribution [164]. End plate materials should have low density and high Young's modulus. Aluminum, steel, and various composite materials are used as end plates [165].

3.3. Effect of High Operating Temperature on ECHP Performance

Operating at elevated temperatures within the range of 120-200 ℃ is one of the most effective methods for enhancing ECHP cells' resistance against impurities found in reformate gas. Working at such high temperatures offers substantially increased catalyst tolerance to impurities, as well as faster reaction kinetics [111]. At low temperatures ranging from 20 to 80 ℃, CO content in reformate gas as low as 20 ppm causes poisoning in the catalyst and performance degradation, while CO tolerance level can exceed 3% when operating at high temperatures [166]. In addition, in low-temperature cells, the Nafion™ membrane must be hydrated to maintain high proton conductivity, and advanced water management must be provided in these systems to ensure proper humidification [167]. If water management is not adequately maintained, flooding can occur, and the active area decreases and reduces the cell performance due to the collection of water in the gas flow channels and electrodes. Working at high temperatures eliminates this precise water management requirement, simplifying operation. PBI membranes are used in high-temperature cells since their improved thermal stability and chemical resistance [71]. Chen et al. [168] examined the effects of the various reformate gases containing H_2, N_2 and CO on the PA-doped PBI membrane-based high-temperature PEMFC. They reported that raised operating temperature suppressed the Pt-CO bonding reaction, increasing CO tolerance. Perry et al. [88] studied high-temperature ECHP at 160 ℃ and stated that the cell exhibited

high efficiency and low power demand by achieving almost Faradic flows and that the PBI membrane demonstrated prolonged durability under these operating conditions. Vermaak et al. [137] studied the high temperature-ECHP performance in the range of 100-160 ℃ with various gas mixtures. They reported that the overall cell performance enhanced with improving mass transfer rate and decreasing ohmic resistance with increasing temperature. Huang et al. [111] studied the high temperature-ECHP performance of four different PA-doped PBI membranes using two different reformate gases. They observed that temperature increase had a positive effect on the CO tolerance of the catalyst due to the accelerated CO desorption rate with increasing operating temperature and reported that all membranes showed improved performance as temperature raised from 160 to 200 ℃. Maxwell et al. [169] conducted a high-temperature electrochemical H_2 separation experiment with a humidified 4:1 CO_2/H_2 gas mixture and indicated that the reaction kinetics slowed with increasing temperature from 120 ℃ to 180 ℃. They attributed this to the fact that as a result of the feed relative humidity being fixed during the study, the scaled relative humidity essentially decreased with increasing temperature, resulting in a decrease in proton conductivity.

3.4. Literature Review on ECHP

The ECHP cell concept, to the best of the author's knowledge, was first mentioned in the patent application numbered US3489670A by Maget in 1964 [170]. The patent describes a method of employing a fuel cell apparatus for gas purification by supplying electrical energy to the electrodes, resulting in gas dissociation near one electrode. Using an ion exchange membrane, the ionic product is directed across the electrolyte to the opposite electrode, where it recombines into a molecular product. This process allows the regeneration of a pure gas at the second electrode when an impure gas is supplied to the first electrode. It has been stated that H_2 and O_2 mixed with other gases can be purified with this technique. Sedlak et al. [171] studied H_2 purification and compression with a cell with 46.6 cm^2 active area and <4 mg/cm^2 Pt catalyst loading using H_2/N_2 gas mixture at 25 ℃. They indicated that N_2 can be effectively removed from H_2 using the ECHP system with high efficiency and low cell voltage. Lee et al. [92] examined the effects of operating temperature and feed pressure on ECHP performance. As a result of their experiments performed within the 30-70 ℃ and 1-3

atm feed pressure range, they stated that increasing temperature enhances the H_2 purity, whereas an increase in feed gas pressure improves the produced H_2 yield but leads to decreasing H_2 purity due to an increase in the permeation flux of contaminants like N_2 and CO_2. They reported that 99.76% H_2 purity was achieved from $H_2/N_2/CO_2$ gas mixture containing 30% H_2 in a two-stage process at 900 mA/cm^2 under 70 ℃ and 1 atm feed pressure working conditions. Onda et al. [78] conducted electrochemical H_2 separation and compression tests and then analyzed the test results with the simulation model they developed. The team reported that the test data were in good agreement with the simulation results and stated that in the separation studies carried out with H_2 feed concentration as low as 1% under atmospheric pressure and compression studies up to 1 MPa cathode pressure, the open circuit voltage closely matched the Nernst potential and H_2 can be separated and pressurized with almost 100% current efficiency. Perry et al. [88] investigated the high-temperature electrochemical H_2 separation at 160 ℃ with the non-humidified premixed natural gas containing 35.8% H_2, 11.9% CO_2, 1906 ppm CO and N_2 balance. They reported that the CO and CO_2 compositions are reduced to 11 ppm and 0.37% at 0.4 A/cm^2 current density and 13 ppm and 0.19% at 0.8 A/cm^2, respectively. Doucet et al. [172] studied electrochemical H_2 separation from hydrogen/ethylene mixtures using a cell with an active area of 25 cm^2 and Pt loading of 1 mg/cm^2 at both electrodes. They stated that experimental and mathematical modeling results show that most of the H_2 reacts with ethylene on the Pt catalyst to form ethane and that using alternative catalysts or streams containing small amounts of alkenes may lead to improved process efficiency. Onda et al. [173] reported that H_2 can be separated and recovered at almost 100% due to their experiments with gases containing N_2 or CO_2 with H_2 concentrations ranging from 1-99.99%. Thomassen et al. [174] investigated the performance of a PBI membrane-based high-temperature ECHP cell at 160 ℃ using 40% H_2 in N_2, 44% H_2/21% CO_2/100 ppm CO/N_2 balance and 74.7% H_2/ 23.5% CO_2/1.36% CO/0.36% CH_4 reformate gases. The team found that reformate gas containing 100ppm CO had a similar effect with N_2 containing 40% H_2, indicating that at low level CO only acts as a diluent. On the other hand, they reported that when a reformate gas with 1.36% CO was fed, a significant rise in cell voltage occurred at high current densities and that increasing the CO concentration in the feed had a detrimental effect on cell

performance. Nguyen et al. [122] investigated the electrode activity and cell conductivity of 7 cm^2 ECHP cell MEA prepared with Nafion™-117 membrane, 0.7 mg/cm^2 Pt loaded anode electrode and 1.0 mg/cm^2 Pt loaded cathode electrode using electrochemical impedance spectroscopy (EIS). They reported that the catalyst activity improved while the membrane resistance decreased as the temperature increased. The optimum performance was obtained when the feed gas humidifier and cell temperature were close to each other and around 70 °C. Bouwman [175] stated that almost pure H_2 containing only 188 ppm CO_2 and 14 ppm CO from a gas mixture containing 70.05% H_2, 19.97% CO_2, 7.48% CO, and 2.50% CH_4 with the ECHP method. Huang et al. [176] observed that the energy efficiency of non-fluorinated sulfonated poly (phthalazinone ether sulfone ketone) (SPPESK) membrane-based ECHP was approximately 20% lower compared to Nafion/PTFE-based ECHP. Ru et al. [177] examined the effects of electric current, feed flow rate, and temperature on the ECHP performance to determine the optimum operating conditions. They reported that as the applied current was increased in the range of 0-2.5 A at the same temperature, both the H_2 recovery rate, since the number of protons passing through the membrane was directly proportional to the applied current, and the H_2 purity increased. Moreover, when they compared the H_2 purity against the applied current at 25 °C and 50 °C operating temperatures, they observed that the H_2 purity increased with temperature. On the other hand, as a result of tests performed with flow rates varying between 90–300 mL/min, they stated that higher feed flow rates caused an increase in CO_2 concentration and lower H_2 purity, attributed to insufficient electrical power supply. Nordio et al. [94] investigated the performance of ECHP through both experimental and modeling approaches. They reported that they achieved high purity of H_2 from H_2/N_2 and H_2/CH_4 mixtures and more than 98% H_2 purity from He/H_2 mixtures. Additionally, comparing the energy consumption of the ECHP system with the PSA unit, it was noted that the PSA method is more appropriate for high H_2 concentrations and large-scale processes. In contrast, ECHP is more suitable for small-scale operations and lower H_2 concentrations. Huang et al. [111] examined the ECHP performances of four different types of PBI membranes in the temperature range of 160-200 °C with a gas mixture containing 30% H_2, 67% N_2, and 3% CO. Their results showed that high H_2 purity ranging from 99.6% to 99.96% with below 0.4% N_2 and

CO at ppm levels with all types of PBI membranes, depending on the applied current. They further noted that higher current densities led to increased H_2 flux on the cathode, diluting the contaminants and producing better H_2 purity. Additionally, the study found no significant correlation between the PBI membrane type and the achieved H_2 purity. Vermaak et al. [137] studied high-temperature ECHP within th100-160 ℃ temperature using H_2/CH_4, H_2/CO_2, and H_2/NH_3 mixtures. They obtained >99.9% H_2 purity from mixtures, 98-99.5% H_2 purity from 10% H_2/CO_2 mixture and 96-99.5% H_2 purity from 50% H_2/CO_2 mixture. Durmuş et al. [178] studied high-temperature ECHP within 140-160 ℃ with various gas mixtures containing H_2, CO_2 and CO and announced that they purified the reformate gas mixture containing 72% H_2, 26% CO_2 and 2% CO to 99.999% H_2 at 160 ℃. Venugopalan et al. [179] presented that they achieved H_2 purity of 99.36%-99.78% at a current density of 0.25 A/cm² and 99.65%-99.85% at a current density of 1 A/cm² through high-temperature ECHP at 200 ℃ using various gas mixtures containing H_2, CO_2, CO, CH_4, and N_2. Some of the studies on ECHP presented in the literature are summarized in Table 3.2.

Table 3.2 Summary of some ECHP studies from the literature

Membrane	**Catalyst**	**Operating Temperature (℃)**	**Anode Gas Composition**	**H_2 Purity (%)**	**Ref.**
Nafion™ 115	Pt	30-70	$H_2/N_2/CO_2$	99.76	[92]
Nafion™ 115	Pt-Ru	20	H_2/CO_2 & $H_2/CO_2/CO$	N/A	[124]
Nafion™ 117	Pt	25-70	H_2/N_2	N/A	[93]
PA-doped PBI	Pt	120-160	$H_2/CO_2/CO/N_2$	N/A	[88]
Nafion™ 115	Pt/C	25	H_2/ethylene	N/A	[172]
PBI	N/A	160-200	H_2/N_2 & $H_2/CO_2/CO/N_2$ & H_2/ $CO_2/CO/CH_4$	N/A	[174]
Nafion™ 117	Pt/C	N/A	H_2/N_2	N/A	[180]
Nafion™ 117	Pt /Vulcan XC-72	23-70	H_2/N_2	N/A	[122]
PA-doped PBI	Pt/C	160	H_2/CO_2	N/A	[127]
SPEEK/ CrPSSA sIPN	Pt/C	80	H_2/CO_2	N/A	[98]
TPS®-based PEM	Pt-Co/C	120-160	H_2/CO_2 & H_2/CO_2	99.44-99.6 & 99.29-99.39	[137]
PA-doped PBI	Pt/C	160	$H_2/CO_2/CO$	99.999	[178]
QPPSf- PBI H_3PO_4	Pt/C	200	$H_2/CO/N_2$	99.85	[179]
N/A	Pt	25	H_2/N_2	99.8-99.99	[171]
N/A	Pt & Pt-Ru	20-70	H_2/CH_4	N/A	[133]
para-PBI & m/p-PBI & meta-PBI	Pt	160-200	$H_2/N_2/CO$	99.6-99.96	[111]

CHAPTER 4

4. EXPERIMENTAL STUDIES

While GNP-supported Pt and PtRu catalysts show promise for PEMFCs, their electrochemical H_2 separation performance under high-temperature ECHP conditions remains mostly unexplored. Furthermore, despite the widespread use of acid-loaded PBI membranes in high-temperature PEMFC applications, there is limited research on their application in HT-ECHP. To the best of the author's knowledge, there is no existing study in the literature in which PA-doped PBI membrane and GNP-supported Pt and PtRu catalysts are used together for HT-ECHP purpose, and it has been investigated for the first time within the scope of this thesis study. Pt/GNP and PtRu/GNP catalysts were prepared by microwave-assisted synthesis method, and their physical characterizations were carried out by XRD, TGA, XPS and TEM analyses, confirming successful synthesis. The electro-catalytic properties of the catalysts were examined by CV analysis and HT-ECHP experiments with the reformate gas mixture containing 75% H_2, 22% CO_2 and 3% CO within the temperature range of 140-180 °C.

4.1. Materials

The metal precursors chloroplatinic acid hexahydrate ($H_2PtCl_6.6H_2O$) and ruthenium (III) chloride ($RuCl_3.xH_2O$) were purchased from Sigma-Aldrich (USA). Graphene Nanoplatelet (GNP) support material was supplied from Nanografi (Turkiye). Ethylene glycol (99%, EG, $HOCH_2CH_2OH$), isopropyl alcohol (IPA, $CH_3CH(OH)CH_3$), sodium hydroxide (NaOH), nitric acid (HNO_3, 65%), perchloric acid ($HClO_4$, 70-72%), phosphoric acid (H_3PO_4, 85%) and acetone (C_3H_6O) were also purchased from Sigma-Aldrich. The commercial 40 wt% Pt on carbon support (Tanaka, Japan) was utilized as the cathode catalyst. Polytetrafluoroethylene solution (PTFE, 60 wt% dispersion in H_2O, Sigma-Aldrich) and gas diffusion layer (GDL,

Freudenberg, Germany) were used in the electrode preparation. H_3PO_4-doped PBI membranes, prepared during another study conducted by our research group [178], were used to prepare MEA. H_2, CO_2, CO and N_2 gases were supplied from Linde (Türkiye).

4.2. Catalyst Preparation

Selecting the proper method for catalyst synthesis is crucial to achieving the desired stability and performance by controlling the metal nanoparticle size and distribution [181]. In this study, anode catalysts Pt/GNP and PtRu/GNP were prepared using microwave-assisted rapid and facile synthesis by the previously described procedure [182]. Microwave irradiation offers shorter crystallization times and more even nucleation by providing more uniform heat transfer than conventional heating in which temperature gradients occur [183]. Firstly, 100 mg GNP was dispersed in 48 ml EG and 12 ml IPA mixture with an ultrasonic bath for 60 min. EG is a reducing agent that converts metal ions into metal or alloy nanoparticles, a capping agent, and a solvent. Glycolate anions are generated, which function as stabilizers for metal nanoparticles, during the oxidation of EG [184]. Moreover, EG also serves as a microwave additive due to its high dielectric constant, and it heats up rapidly under microwave irradiation [185]. Then, an adequate amount of $H_2PtCl_6.6H_2O$ and $RuCl_3.xH_2O$ metal salts were added into the solution to achieve 30% metal loading and ultrasonically mixed for 10 min. For the PtRu/GNP catalyst, the atomic ratio between Pt and Ru is 0.5:0.5. The pH of the solution was then increased above 12 by adding 1 M NaOH in the EG solution. After that, the resultant mixture was placed into the household microwave oven (Samsung, 800 W) and synthesis was carried out at 600 W for 1 min. The solution waited for cooling after the synthesis step and the pH was adjusted to around 2 by adding 0.2 M HNO_3. The final solution was centrifuged, washed with acetone and DI water to remove impurities, and dry in an oven at 100 ℃ overnight. The catalyst preparation process is illustrated in Figure 4.1.

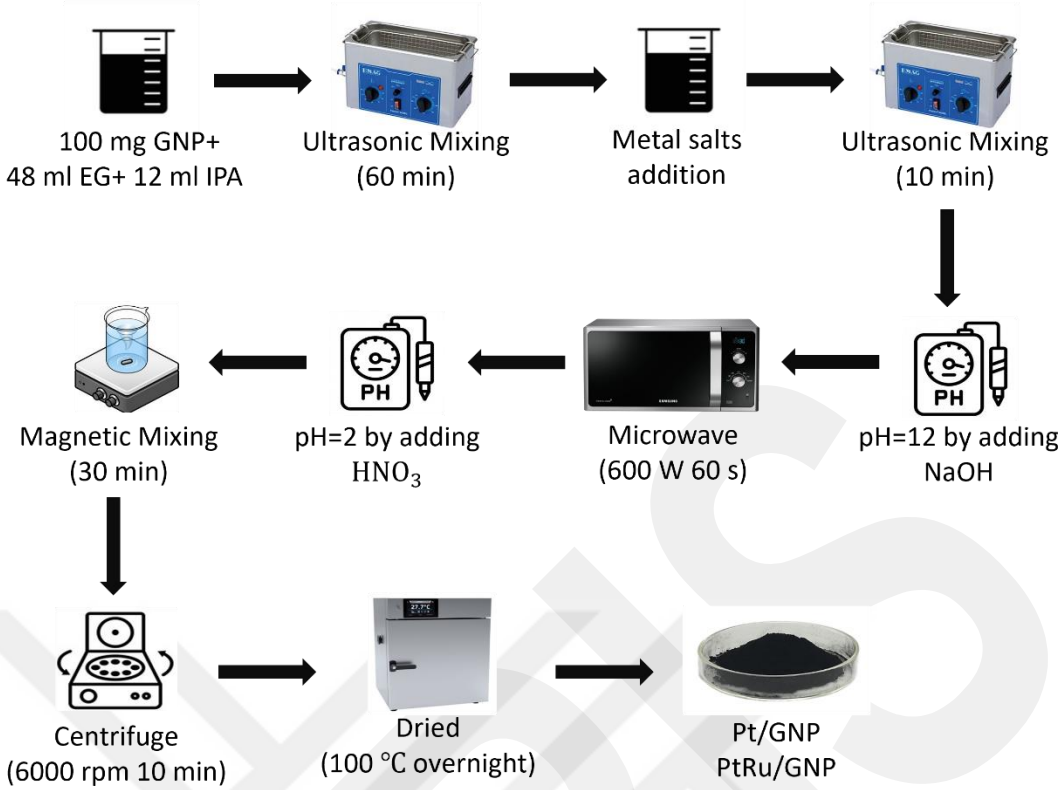

Figure 4.1 Catalyst synthesis steps

4.3. Catalyst Characterization

Thermogravimetric analysis (TGA) was performed to observe the catalysts' thermal behavior and determine the metal loading on the GNP support material. TGA analyses were executed using Perkin Elmer Pyris 1 Thermal Analyser in the 25-900 ℃ temperature range at a heating rate of 10 ℃/min in an air atmosphere. X-ray diffraction (XRD) examined the catalysts' crystalline structures. Measurements were executed on a Rigaku Ultima-IV diffractometer using Cu K_α (λ= 1.5406 Å) radiation source in the range of $10° \leq 2\theta \leq 90°$. X-ray photoelectron spectroscopy (XPS) was carried out to examine the chemical states of Pt and Ru. The distribution of the metal nanoparticles on the GNP support material was investigated by the JEOL 2100 JEM high-resolution transmission electron microscopy (HR-TEM). The average particle size of the catalysts was determined from the TEM images using the ImageJ software program. Electrochemical characterization was performed using a three-electrode system (Wonatech ZIVE SP2 electrochemical workstation). A glassy carbon (GC) disk electrode (3 mm diameter) was used as the working electrode, Ag/AgCl filled with

saturated KCl solution as the reference electrode and Pt wire as the counter electrode. The catalyst ink prepared using a certain amount of catalyst, IPA, DI water and ionomer solution was mixed ultrasonically, and then dropped onto the carefully polished GC electrode, and dried at room temperature overnight. CV tests were performed in 0.1 M $HClO_4$ electrolyte solution for 1000 cycles at 25 ℃ with a scan rate of 100 mV/s between -0.25 V and 1.2 V. Before the tests, the electrolyte solution was purged with N_2 for 30 min to remove any contaminant.

4.4. Membrane Preparation

H_3PO_4-doped PBI membranes were prepared by the solution casting method as reported previously [178]. First, PBI polymer (5 wt.%) was dissolved in DMAc solution at atmospheric pressure, and the homogeneous solution was cast onto the glass surface. The cast glass' surface was dried at 80 ℃ in a ventilated oven for 12 hours. Then, PBI membranes were kept in H_3PO_4 for acid doping. After 1 week, the membranes were taken from the acid solution, excess acid was removed with blotting paper from the surface, and the membranes were kept in an airtight container until the tests. The acid doping level of the PBI membranes was determine as 12 using the Eq. (15):

$$Acid\ doping = \frac{W_{PA}}{W_{dry}} \times \frac{MW\ of\ PBI\ repeat\ unit}{MW\ of\ H_3PO_4} \quad (15)$$

where W_{PA} is the weight of the H_3PO_4-doped membrane, W_{dry} is the weight of the dry membrane, and MW indicates molecular weight in g/mol [111].

Proton conductivity of H_3PO_4-doped PBI membranes was examined by conductivity tests performed in the longitudinal direction without humidification, by a four-probe analysis with WonATech, Korea impedance analyzer. The proton conductivity was calculated as 0.083 S/cm at 160 ℃ using Eq. (16):

$$\sigma = \frac{L}{r \times w \times t} \quad (16)$$

where σ is the proton conductivity (S/cm), L is the space between two probes of the conductivity cell (cm), r is the membrane resistance (Ω), w is the membrane width (cm), and t is the membrane thickness (cm).

4.5. MEA Preparation

The gas diffusion electrodes (GDEs) with a 25 cm^2 active area were fabricated by applying catalyst inks onto commercial GDLs using the spraying method. The catalyst ink consists of a catalyst, PTFE (15% by weight, on a dry basis), and DI water: IPA (1:7). The catalyst ink was ultrasonically mixed for 30 minutes before the coating. The synthesized Pt/GNP and PtRu/GNP catalysts were used as the anode catalysts, while commercial Pt/C was used as a cathode catalyst. The catalyst loading for both the anode and cathode GDEs was 1.5 mg/cm^2.

MEAs were assembled by attaching the anode and cathode GDEs to both sides of the H_3PO_4-doped PBI membrane by hot pressing at 172 N/cm^2 and 150 °C for 15 min. The prepared MEAs were covered with a double-layer Kapton frame to ensure sealing. MEA preparation is illustrated in Figure 4.2.

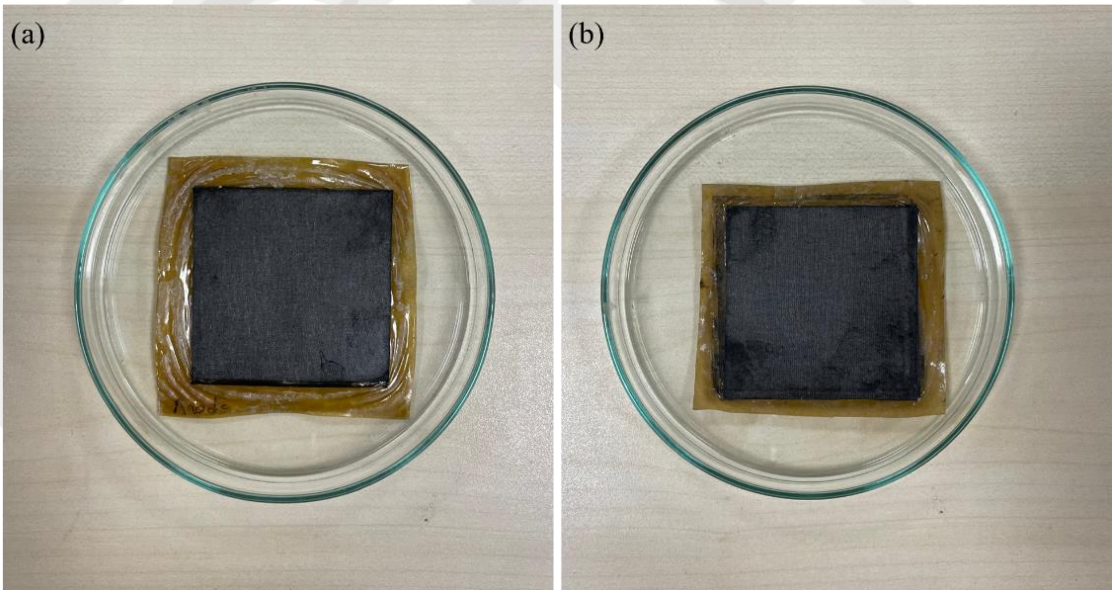

Figure 4.2 Prepared MEAs with a) Pt/GNP catalyst and b) PtRu/GNP catalyst

4.6. HT-ECHP Test System

The MEAs prepared were integrated into the HT-ECHP test cell to evaluate the H_2 purification performance of Pt/GNP and PtRu/GNP catalysts. The HT-ECHP test cell was constructed using graphite bipolar plates, gold current collector plates, and stainless-steel end plates. Firstly, the cathode bipolar plate was settled on the end plate. Then, a double layer of Kapton-framed MEA was placed on the bipolar plate. After the anode bipolar plate was also placed on the MEA, the single-cell structure was completed by closing it with the anode end plate. A torque wrench tightened the test cell to ensure an even pressure distribution. HT-ECHP test cell preparation is shown in Figure 4.3.

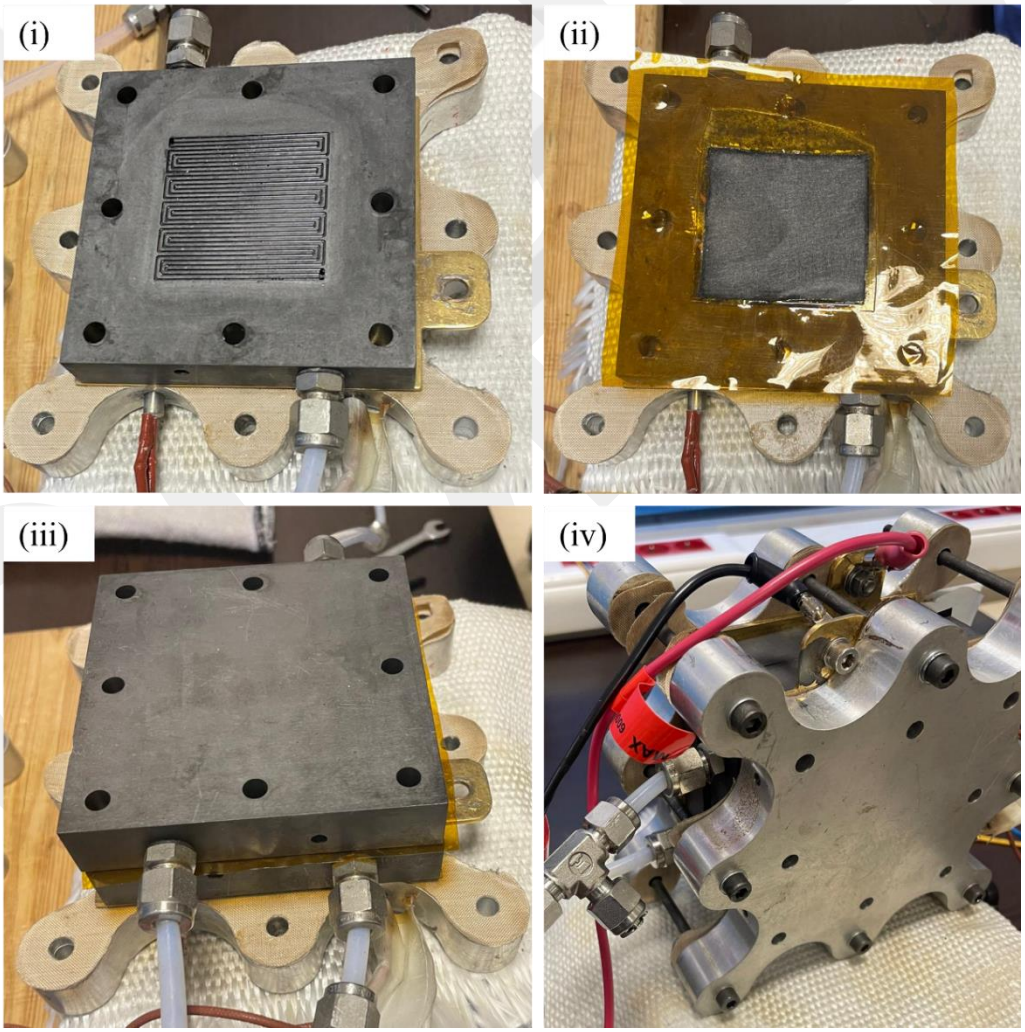

Figure 4.3 HT-ECHP test cell preparation

Firstly, the HT-ECHP experiments were performed using pure H_2, followed by H_2:CO_2:CO-75:22:3 reformate gas at 140-180 °C. The operating temperature of the test cell was adjusted using a heating rod on both the anode and cathode sides and measured with connected thermocouples. The gas mixtures were adjusted with mass flow controllers to the desired rates. Gases stored in high-pressure gas cylinders were supplied to the test station with Teflon tubes and fed into the cell by a heated line to raise the gas temperature to the cell operating temperature. Mass flow controllers (MFC, Aalborg) were used to regulate the volumetric flow rates of the gas streams.

Figure 4.4 Images of the HT-ECHP test station

The test station was purged with N_2 before the experiments. The pure H_2 and reformate gas mixture were fed into the cell from the anode inlet without humidification, and the stream from the cathode outlet was fed into the gas chromatography (GC) instrument (Shimadzu Co., Nexis GC-203) using an automated gas sample valve to monitor the purification rate. Argon (Ar) was used as the carrier gas. Before the experiments, the GC system's thermal conductivity detector (TCD) equipment was calibrated using gas mixtures containing known concentrations of H_2, N_2, CO_2, CO, NH_3, and CH_4. All the performance tests were conducted under atmospheric conditions.

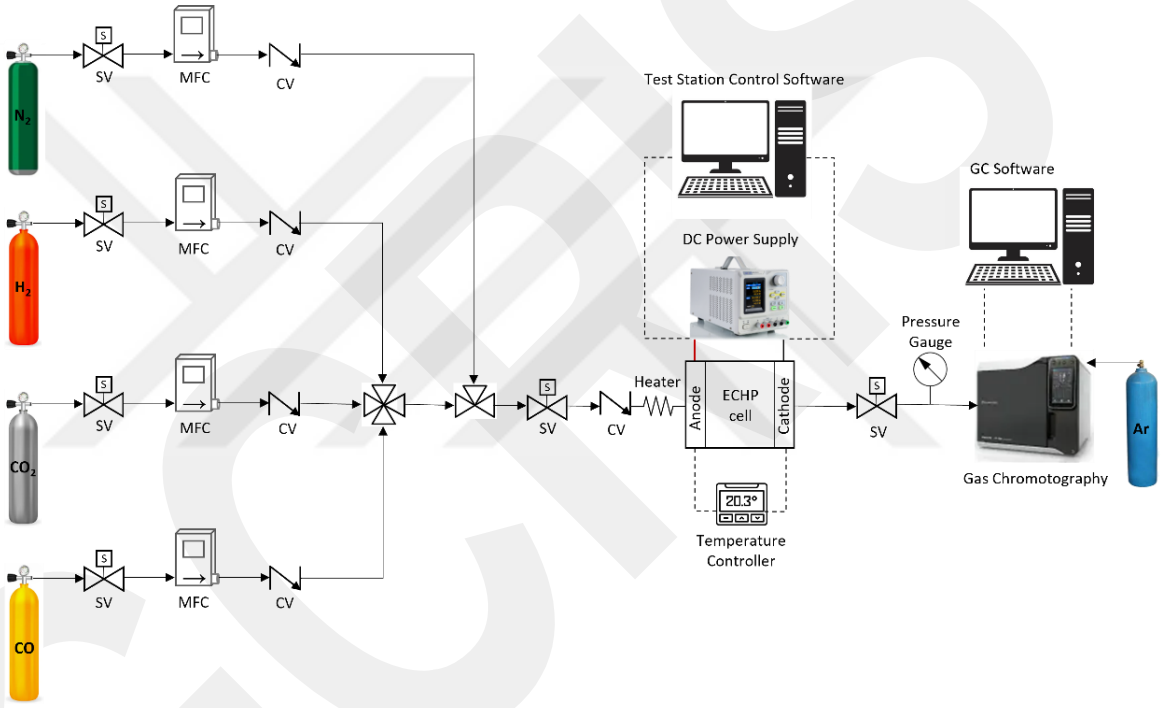

Figure 4.5 HT-ECHP test station diagram

CHAPTER 5

5. RESULTS AND DISCUSSION

5.1. Physico-chemical Characterization Results

The thermal behavior of the Pt/GNP and PtRu/GNP catalysts is depicted in Figure 5.1. It was observed that there are three distinct weight loss regions in the TGA curve of Pt/GNP catalyst.

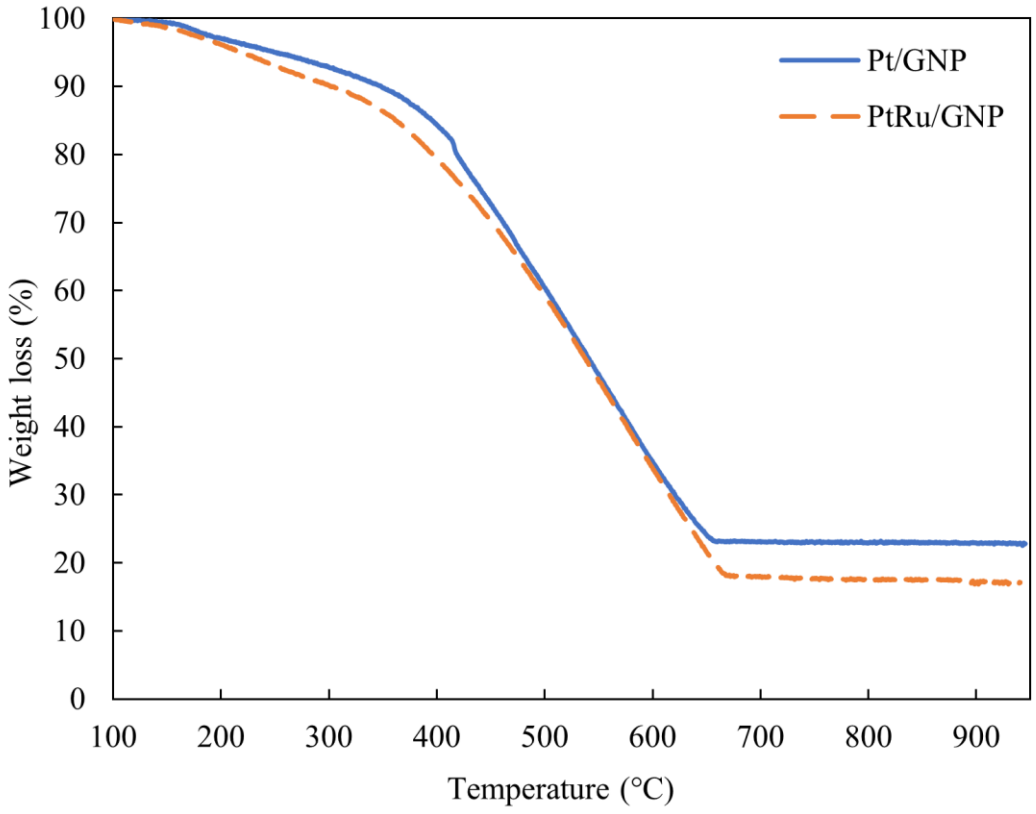

Figure 5.1 TGA curves of the Pt/GNP and PtRu/GNP catalysts

Removing the volatile content can cause the first weight loss of up to approximately 200 ℃. The second weight loss region between ~200 and ~420 ℃ can be explained by the initial degradation step, while the final stage from ~420 to ~650 ℃ can be

attributed to the primary decomposition of the GNP support. For the PtRu/GNP catalyst, two weight loss regions were determined. The first loss region, up to about 320 ℃, can be attributed to the elimination of volatile materials, while the second one, up to ~670 ℃ can be related to the thermal decomposition of the carbon-based support material. It is also identified from the TGA results that the metal loading on the GNP support is 22.85% and 17.11% for Pt/GNP and PtRu/GNP, respectively [182].

Figure 5.2 presents the XRD patterns of the catalysts. The diffraction peaks observed at 2θ values around 26.5° correspond to the (002) plane of the hexagonal graphitic structure of the GNP. Peaks at approximately 54° and 78° can be indexed as C(004) and C(110) reflections of graphite [186], [187], respectively, indicating the high crystallinity carbon structure of the support material [188], [189].

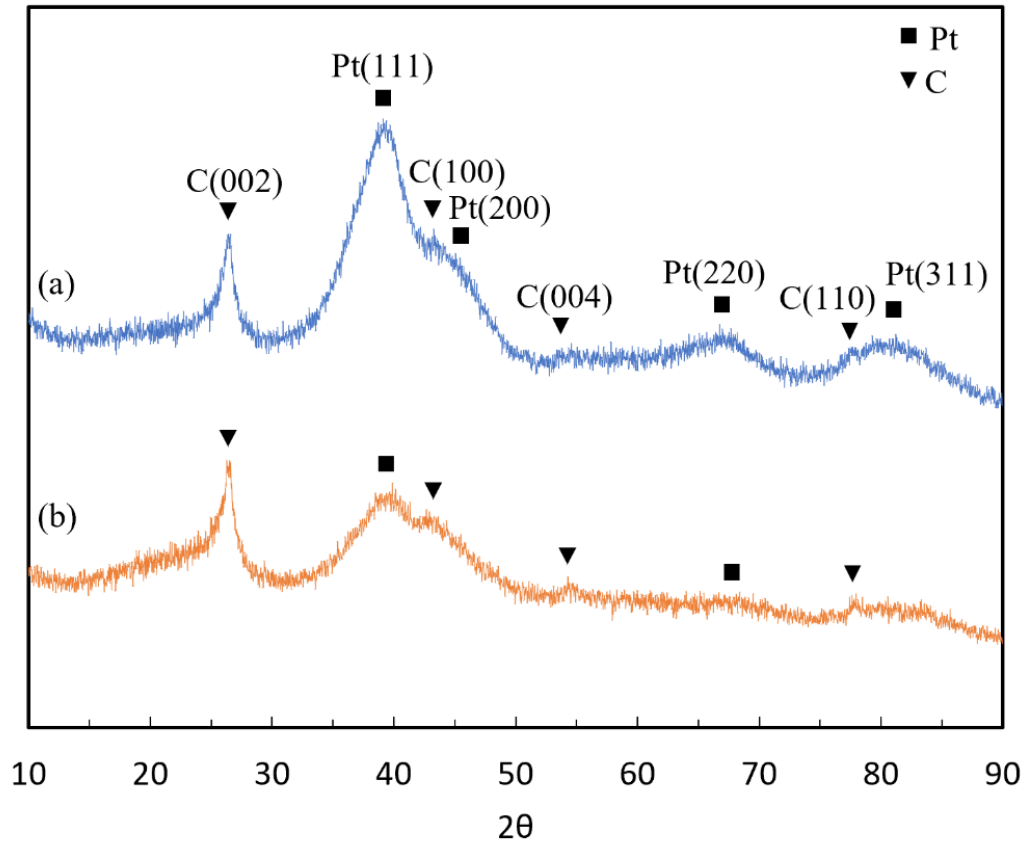

Figure 5.2 XRD patterns of the a) Pt/GNP and b) PtRu/GNP catalysts

In the diffractogram of the Pt/GNP, the characteristic diffraction peaks of the crystalline Pt that appeared at 2θ values of 39.2°, 67.4°, 80.7° correspond to the (111),

(220) and (311) planes of the face-centered cubic (fcc) lattice structure. Around 2θ=44°, the reflections of C(100) and Pt(200) overlapped.

The characteristic diffraction peak for Ru was not detected in the diffractogram of the PtRu/GNP catalyst. Several groups have reported similar results for bimetallic PtRu catalysts [190], [191], [192]. Ru and its oxides probably exist on the PtRu alloy particle surface, even if there is no peak related to pure Ru and RuO_2 in the XRD spectrum of PtRu/GNP [193]. While no peak corresponding to metallic Ru appeared, the Pt(111) peak shifted slightly to a higher 2θ value in the XRD pattern of PtRu/GNP than that of Pt/GNP. This shift is caused by the incorporation of smaller-sized Ru atoms into the Pt lattice structure, revealing the formation of an alloy between Pt and Ru metals [194], [195]. Other characteristic peaks of Pt were not distinctly visible in the diffractogram of the PtRu/GNP due to the catalyst's amorphous nature or the broadening of peaks caused by the tiny size of the PtRu nanoparticles [196]. The average crystallite size of the catalysts was calculated from XRD using the Scherrer equation [188] (Eq. (17)), based on the highest diffraction peaks Pt (111) [197].

$$d = \frac{0.89 \times \lambda}{B2\theta \times \cos\theta} \tag{17}$$

where d is the crystallite size (nm), λ is the wavelength of X-ray used in diffraction (0.154 nm), B2θ is the full width at half maximum (FWHM) of the peak (radians), and θ is the angle at the maximum of the peak (radians). The average crystallite sizes were determined as 1.68 nm for Pt/GNP and 1.67 nm for PtRu/GNP [182]. It is important to note that the calculated sizes may be inaccurate and provide only an estimation because the Pt (111) peaks of the synthesized catalysts overlapped with others.

The XPS spectra of the Pt 4f, C 1s, and Ru 3d regions for the Pt/GNP and PtRu/GNP catalysts are depicted in Figure 5.3. The deconvoluted Pt 4f spectra of both catalysts show two pairs of doublets corresponding to the Pt $4f_{5/2}$ and Pt $4f_{7/2}$ peaks, as given in Figure 5.3a.

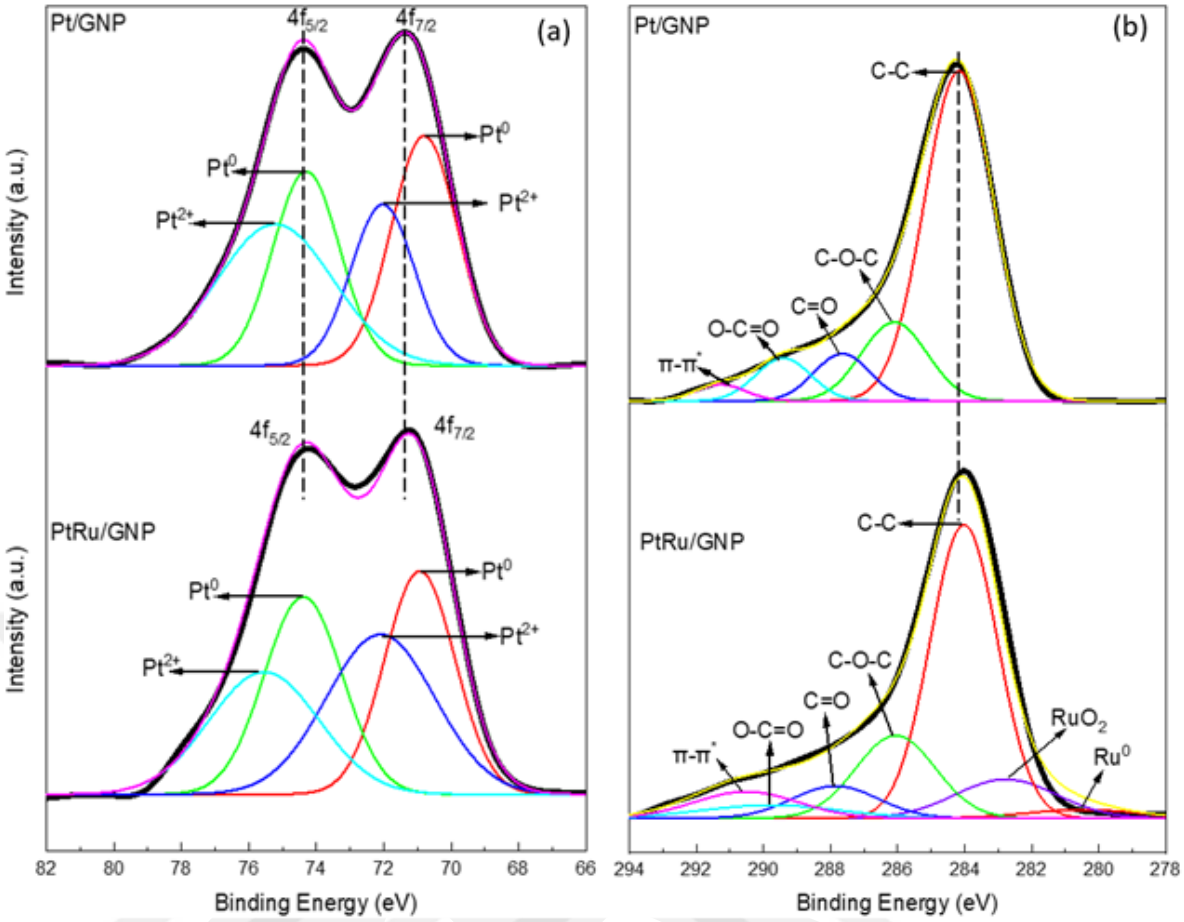

Figure 5.3 XPS spectra of Pt/GNP and PtRu/GNP catalysts (a) Pt 4f and (b) C 1s and Ru 3d

The doublets with the highest intensity at 74.3 eV ($4f_{5/2}$) and 70.8 eV ($4f_{7/2}$) for Pt/GNP, and 74.4 eV ($4f_{5/2}$) and 70.9 eV ($4f_{7/2}$) for PtRu/GNP are attributed to metallic Pt (Pt^0). The weaker doublets at 75.2 eV ($4f_{5/2}$) and 72.0 eV ($4f_{7/2}$) for Pt/GNP, and at 75.6 eV ($4f_{5/2}$) and 72.1 eV ($4f_{7/2}$) for PtRu/GNP could be ascribed to the Pt^{2+} oxidation state on PtO or $Pt(OH)_2$ [198]. It is observed that the Pt $4f_{5/2}$ and Pt $4f_{7/2}$ peaks of both catalysts shifted to lower values compared to the standard $4f_{5/2}$ and $4f_{7/2}$ binding energy (74.53 eV and 71.2 eV) for the Pt^0 state [199]. This shift is a consequence of electron transfer from the carbon support to the Pt nanoparticles [200]. Additionally, a slight shift in the Pt 4f peaks of the PtRu/GNP compared to that of Pt/GNP was observed, which may be caused by the modifications in the electronic nature of Pt induced by adding Ru atoms. The acid-base properties of the carbon support might be influenced by the Ru presence, leading to a strong support material-metal interaction that affects

the electronic structure of the Pt sites [201]. The dominant species observed in the Pt 4f spectra of the catalysts appear to be the zero-valent metallic form, revealing Pt nanoparticles are effectively reduced by the microwave synthesis method and thus will have better electrochemical performance [202].

For PtRu/GNP, the oxidation state of Ru was analyzed from the Ru 3d spectrum (Figure 5.3b) since the Ru 3p signals were weak, it made analysis difficult. The C 1s peak of the carbon support obscured the Ru $3d_{3/2}$ signal. The deconvoluted Ru $3d_{5/2}$ signal shows two peaks at 280.5 eV and 282.7 eV, corresponding to Ru^0 and RuO_2, respectively. Since Ru is unstable and ready to oxidize when exposed to air, the presence of Ru oxides is expected [203]. In the C 1s spectrum of the PtRu/GNP, the peaks located at 284.1 eV, 286.1 eV, 287.9 eV, 289.8 eV and 290.5 eV are corresponding to the C-C, C-O-C, C=O, O-C=O and π-π*, respectively. Similarly, the deconvolution of the C 1s XPS spectra of the Pt/GNP reveals peaks at 284.2 eV (C–C), 286.1 eV (C–O-C), 287.7 eV (C=O), 289.4 eV (O–C=O), and 291.3 eV (π-π*), corresponding to similar carbon functionalities [204].

TEM analysis was performed to examine the morphology in more detail and confirm the particle size of the synthesized catalysts. TEM images and particle size distribution histograms of Pt/GNP and PtRu/GNP catalysts are given in Figure 5.4. Some nanoparticle agglomerations were identified on the support material from TEM images, possibly due to non-uniform heating in the microwave and poor mixing of the support material and the metal precursors [205]. TEM images of both catalysts also show almost spherical particles. The average diameters are estimated to be 3.06 nm and 2.62 nm for the Pt and PtRu nanoparticles, respectively. As seen in Figure 5.4a, the selected area electron diffraction (SAED) diagram shows that the Pt particles have an fcc structure with four rings, corresponding to (111), (200), (220), and (311) crystal planes, likewise the XRD results. Despite that the (220) and (311) planes were not visible in the XRD pattern of the PtRu/GNP catalyst, the four-ring fcc structure was observed in the SAED diagram (Figure 5.4b). The SAED pattern of the PtRu/GNP shows that well-ordered Pt-Ru nanoclusters are present on the GNP [206].

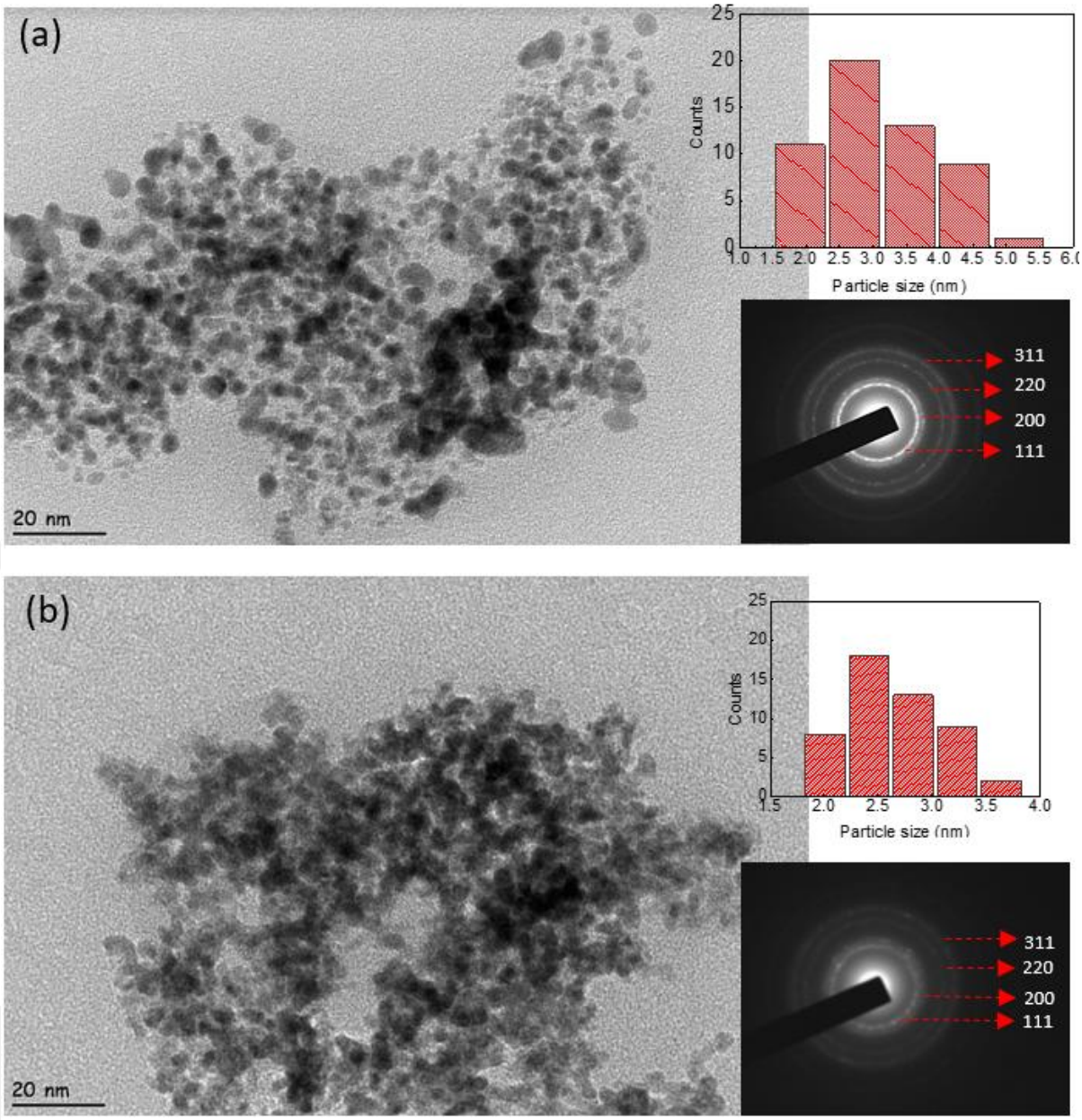

Figure 5.4 TEM images, particle size distribution histograms and SAED patterns of of a) Pt/GNP and b) PtRu/GNP catalysts

CV tests were conducted to investigate the electrochemical stability and the ECSA of the Pt/GNP and PtRu/GNP catalysts. The cyclic voltammograms of the catalysts in 0.1 M $HClO_4$ solution is shown in Figure 5.5. The ECSA of the catalysts were calculated before and after degradation CV tests by Eq. (18) given below:

$$ECSA\ \left(\frac{m^2}{g_{metal}}\right) = \frac{Q_H(\frac{\mu C}{cm^2})}{K(\frac{\mu C}{cm^2})\times L(\frac{g_{metal}}{m^2})} \quad (18)$$

where Q_H is the charge of H_2 adsorption/desorption ($\mu C/cm^2$), K is the reference charge constant value as 210 $\mu C/cm^2$ for Pt [207], and L is the metal loading (g/m^2). ECSA refers to the active catalytic sites where electrochemical reactions occur; hence, the higher the ECSA, the higher the catalytic activity [208].

The specific surface area (SSA) of the Pt/GNP and PtRu/GNP catalysts was calculated by Eq. (19) [209], assuming the particles have a spherical shape.

$$SSA = \frac{6000}{\rho_{Pt-Ru}\times d} \quad (19)$$

where SSA is the specific surface area (m^2/g), $\rho_{Pt\text{-}Ru}$ is density (g/cm^3), and d is the particle size determined from XRD (nm). The density of the PtRu was determined by using Eq. (20) [209]:

$$\rho_{Pt-Ru} = \rho_{Pt}X_{Pt} + \rho_{Ru}X_{Ru} \quad (20)$$

where ρ_{Pt} is the Pt density (21.4 g/cm^3), ρ_{Ru} is the Ru density (12.2 g/cm^3), X_{Pt} and X_{Ru} are molar fractions of Pt and Ru in bimetallic catalyst without carbon support (Pt:Ru atomic ratio is 0.5:0.5 for PtRu/GNP). The initial and final ECSA values, ECSA loss percent, and SSA values of the Pt/GNP and PtRu/GNP catalysts are presented in Table 5.1.

Table 5.1 The initial and final ECSA, ECSA loss and SSA of the Pt/GNP and PtRu/GNP catalysts

Catalyst	**Initial ECSA (m^2/g)**	**Final ECSA (m^2/g)**	**ECSA Loss (%)**	**SSA (m^2/g)**
Pt/GNP	50.06	28.94	42.19	166.89
PtRu/GNP	20.54	5.23	74.55	213.86

The Pt/GNP catalyst has 50.06 m^2/g and 28.94 m^2/g initial and final ECSA, respectively, while PtRu/GNP has 20.54 m^2/g initial ECSA and 5.23 m^2/g final ECSA

[182]. It is seen that the Pt/GNP has a larger ECSA compared to PtRu/GNP as well as lower ECSA loss after the 1000th cycle, indicating better catalyst stability. It has been recorded in the literature that smaller particles typically exhibit higher ECSA [205].

Smaller particles have a larger ratio of surface atoms to total atoms per unit mass, providing a more significant active catalytic site [210]. Very close values were found when the crystal sizes of Pt/GNP and PtRu/GNP catalysts were calculated according to XRD results. On the other hand, the mean diameters were calculated as 3.06 nm for Pt nanoparticles and 2.62 nm for PtRu nanoparticles, based on TEM analysis results [182]. According to these results, the PtRu/GNP with smaller crystallite size has lower ECSA than Pt/GNP, which seems inconsistent with this statement. Although the Pt/GNP catalyst has a higher particle size, the higher ECSA value compared to PtRu/GNP may be related to the metal content of the catalysts. Metal loading of Pt/GNP and PtRu/GNP catalysts was determined as 23% and 17%, respectively. Higher catalyst loading was necessary to provide the required metal loading for ECSA analysis because of the lower metal content of the PtRu/GNP catalyst [211]. Furthermore, the characterization of catalysts containing Ru by the H_2 adsorption and stripping is unfavorable since the Ru and H_2 oxidation currents overlap. Besides, because of the absorption into the oxide lattice and dissolution of atomic hydrogen into the metallic Ru, multiple monolayers of hydrogen can be formed on a Ru surface [212] and have caused an underestimation of the ECSA of PtRu/GNP [213]. Moreover, the diluting effect of Ru can diminish the H_2 adsorption activity of Pt by altering its electronic structure through the electronic ligand effect, which can also be reflected in the slightly smaller Pt crystallite size determined by XRD [214].

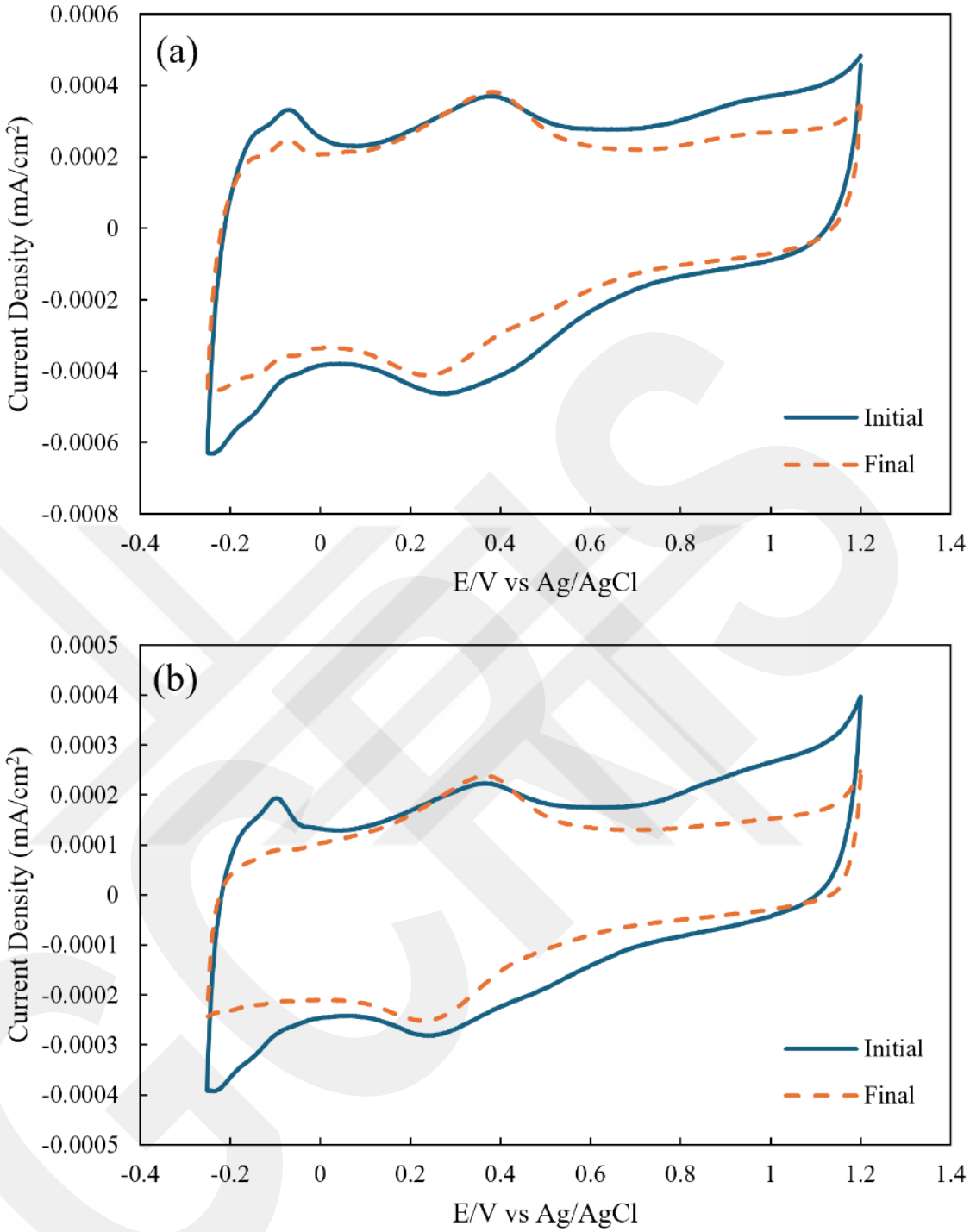

Figure 5.5 CV curves of a) Pt/GNP and b) PtRu/GNP with 100 mV/s between -0.25-1.2 V in 0.1 M $HClO_4$ solution at 25 C for the 100th and 1000th cycles

5.2. HT-ECHP Performance Tests Results

The HT-ECHP experiments were executed using pure H_2 and H_2:CO_2:CO-75:22:3 reformate gas between 140-180 ℃. All the experiments were conducted under atmospheric pressure with a gas flow rate of 0.25 slpm. The gas flow rate was determined considering the best results were obtained at 0.25 slpm in a previous study [178] in our research group. The limiting voltage was kept at 1 and 1.4 V for pure H_2 and reformate gas experiments. The polarization curves were recorded with a step change of 0.1 A starting from 0 A/cm^2. Firstly, pure H_2 experiments were conducted to make a comparison. The V-I curves at 140 ℃, 150 ℃, 160 ℃, 170 ℃ and 180 ℃ operating temperatures of the Pt/GNP and PtRu/GNP catalysts for pure H_2 are given in Figure 5.6.a and b, respectively. As shown in Figure 5.6, the required cell voltage for the same current density is lower for PtRu/GNP catalyst than for Pt/GNP at all operating temperatures, indicating that PtRu/GNP performs better with lower power consumption. The required cell voltages were measured as 0.489 V (140 ℃), 0.530 V (150 ℃), 0.671 V (160 ℃), 0.761 V (170 ℃), and 0.979 V (180 ℃) for Pt/GNP, while 0.354 V (140 ℃), 0.382 V (150 ℃), 0.464 V (160 ℃), 0.518 V (170 ℃), and 0.590 V (180 ℃) for PtRu/GNP catalyst for the current density of 0.2 A/cm^2. Also, cell performance was decreased for both catalysts as the operating temperature was raised from 140 ℃ to 180 ℃. The maximum current densities of 0.416 A/cm^2 for Pt/GNP and 0.564 A/cm^2 for PtRu/GNP were achieved at 140 ℃ [182]. Lobato et al. [215] indicated that the self-dehydration of H_3PO_4 to $H_4P_2O_7$ (pyrophosphoric acid) (Eq. (21)), which is less conductive is accelerated at high temperatures above 130-140 ℃, and elevated operating temperatures promote the catalyst particles agglomeration in the long term, resulting in reduced ECSA.

$$2H_3PO_4 \rightarrow H_4P_2O_7 + H_2O \quad (21)$$

So, the reduced cell performance as the temperature increased from 140 ℃ to 180 ℃ can be explained by the increase in membrane resistance caused by the reduced proton conductivity in PBI due to the formation of pyrophosphoric acid [216].

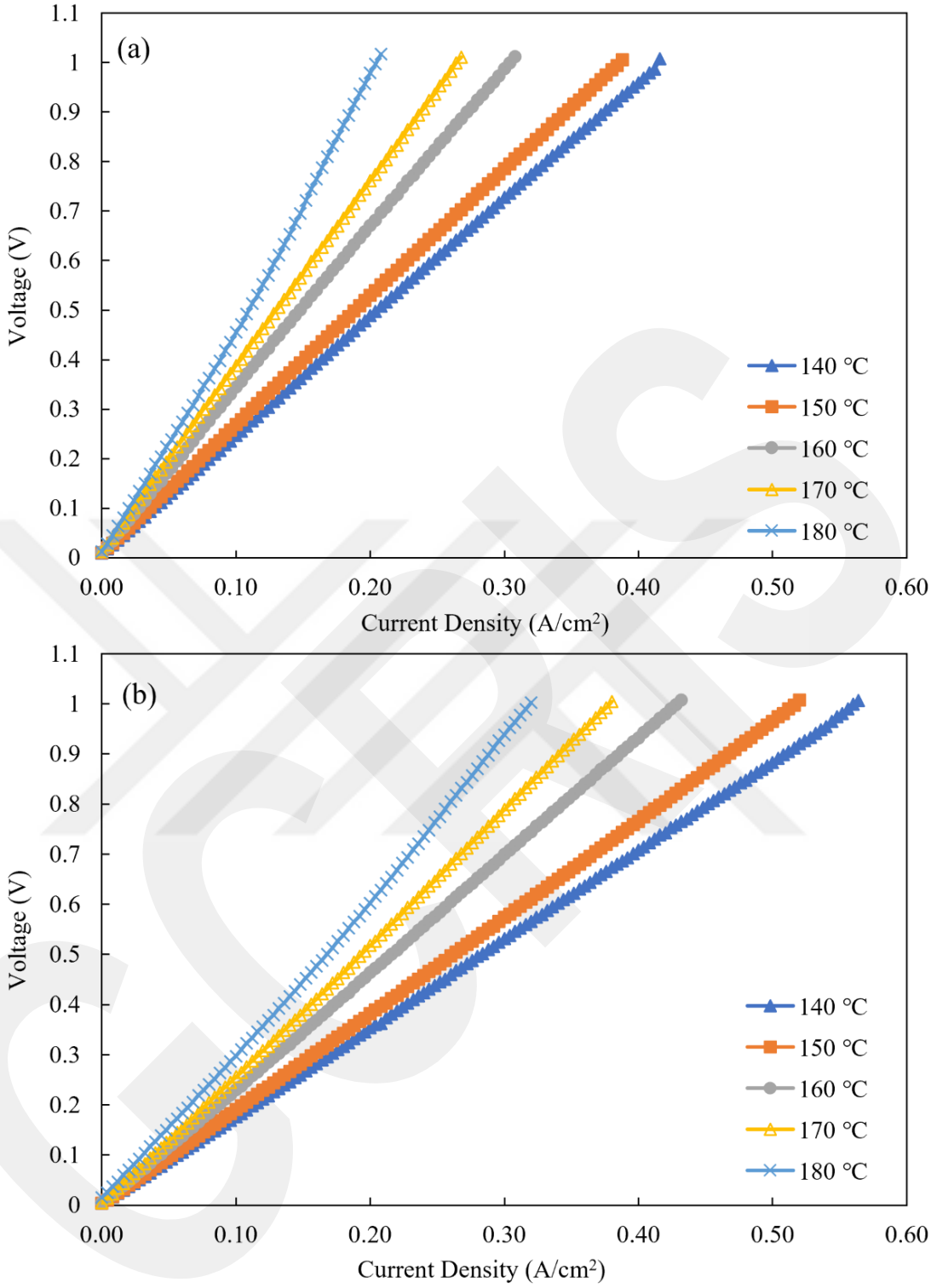

Figure 5.6 HT-ECHP polarization curves of a) Pt/GNP, b) PtRu/GNP for pure H_2 at various operating temperatures

The HT-ECHP polarization curves at 140-180 ℃ of the Pt/GNP and PtRu/GNP catalysts for H_2:CO_2:CO-75:22:3 reformate gas are shown in Figure 5.7a and b, respectively.

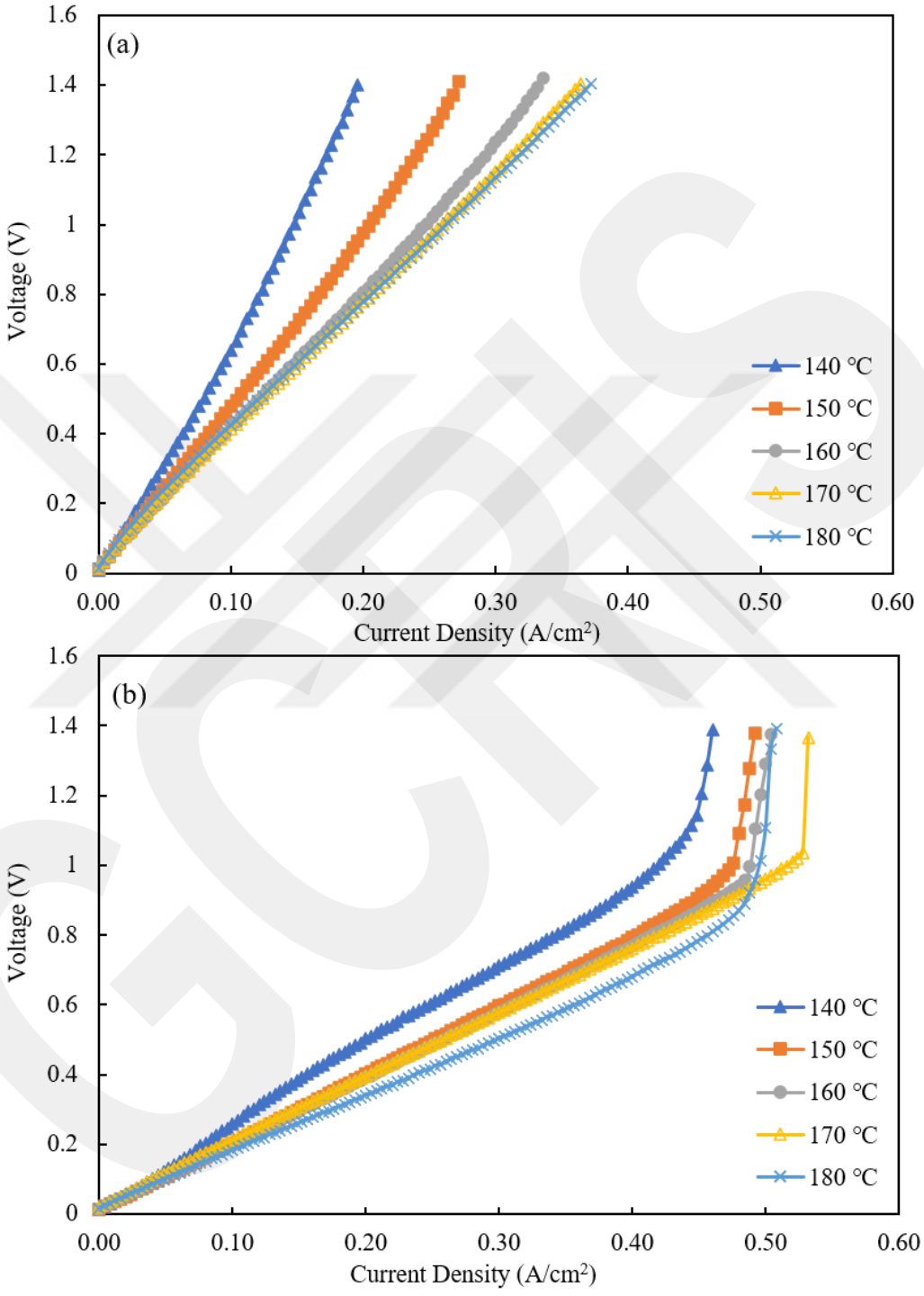

Figure 5.7 HT-ECHP polarization curves of a) Pt/GNP, b) PtRu/GNP for reformate gas at various operating temperatures

Unlike pure H_2 experiments, the open circuit voltage (OCV) for purifying H_2 from the reformate gas is higher than zero due to the difference in H_2 partial pressures on the anode and cathode sides [127]. The linear shape of the Pt/GNP catalyst's V-I curves indicates that ohmic losses dominate the electrochemical H_2 purification over the entire current density range, and the membrane resistance plays a decisive role in cell performance [92]. The polarization curves of PtRu/GNP catalyst also exhibited linearity up to higher current density values, but their final portion showed a curved shape. This suggests that mass transport losses predominate in this region, since the reactant gas cannot rapidly arrive at the anode catalyst [84]. More H_2 is extracted from the anode as the current density increases. When the current density reaches a sufficiently high level, i.e., the limiting current density, an almost vertical rise in the cell voltage occurs, indicating that the H_2 in the anode supply is largely depleted [172].

Table 5.2 Comparison of current density values of the Pt/GNP, PtRu/GNP at 0.6 V from 140 to 180 ℃ [182]

Catalyst	**Current Density (A/cm^2)**				
	140 ℃	**150 ℃**	**160 ℃**	**170 ℃**	**180 ℃**
Pt/GNP	0.096	0.124	0.148	0.150	0.152
PtRu/GNP	0.245	0.302	0.310	0.312	0.356

It is seen from the V-I curves that the H_2 purification performance of the PtRu/GNP bimetallic catalyst is superior to that of the Pt/GNP catalyst. The obtained current density values at 0.6 V cell voltage for both catalysts are given in Table 5.2. When the results were compared, it was observed that higher current density values were achieved with the PtRu/GNP bimetallic catalyst compared to Pt/GNP at an operating voltage of 0.6 V, which refers to higher performance with lower power requirement. The better performance of the PtRu/GNP can be explained by having more free active sites for H_2 adsorption in the presence of CO [217]. The improved CO tolerance of PtRu bimetallic catalyst has been associated with two main phenomena in the literature. The first is the "bifunctional mechanism", which describes the promoted CO oxidation at lower potentials than for Pt through Ru-OH species. The other is the

"ligand effect", which refers that the existence of the second metal Ru changes the electronic nature of Pt, leading to a weaker Pt-CO bond [218], [219], [220]. The bifunctional mechanism is based on the fact that OH adsorption on the Pt surface occurs at higher overpotentials, so when a second transition metal such as Ru is present in the catalyst, OH_{ad} will first form on the second metal. The formed Ru-OH reacts with the CO adsorbed on Pt (Eq. (22)) and provides its removal from the surface and increases the active sites for HOR [221].

$$Ru - OH + Pt - CO \rightarrow Pt + CO_2 + Ru + H^+ + e^- \quad (22)$$

Moreover, introducing the second element, Ru leads to a change in the electronic structure of the surface Pt atoms, as evidenced by XPS results. This change weakens the interaction between Pt and CO, resulting in more active sites for HOR [123]. As a result of the electron lack in the Pt 5d-band of the PtRu catalyst caused by these electronic modifications, the Pt-CO bond weakens and the CO surface coverage decreases. These electronic changes can also influence the CO oxidation rate [221]. In addition, improved CO tolerance is also attributed to the 'detoxification mechanism' in the literature, which is described as the formation of lower CO coverage due to the weakening of the Pt-CO bond strength in the presence of Ru, similar to the ligand effect. However, it has been stated that CO tolerance in the detoxification mechanism is achieved by reducing bond strength and CO coverage, but not related to CO oxidation [222], [223].

When the effect of operating temperature on the ECHP performances of the catalysts was examined, it was observed that the gradually raised temperature between 140-180 °C leads to enhanced cell performance for both Pt/GNP and PtRu/GNP, as can be seen in Figure 5.7a and b. The increased operating temperature results in an improvement in catalyst activity and promotes electrochemical reactions [224]. Furthermore, elevated operating temperatures offer improved CO tolerance. CO adsorption occurs not only on the bare Pt surfaces (Eq. (23)) but also on the Pt-H sites (Eq. (24) and (25)) generated during the dissociation phase of the HOR [225]:

$$CO + Pt \rightarrow Pt - CO_{ads} \quad (23)$$

$$H_2 + 2Pt \rightarrow 2Pt - H_{ads} \quad (24)$$

$$2CO + 2Pt - H_{ads} \rightarrow 2Pt - CO_{ads} + H_2 \quad (25)$$

Since the adsorption of CO on the Pt surface is exothermic, it takes place more strongly at lower temperatures. Consequently, at elevated temperatures, the CO coverage is significantly reduced [226]. On the other hand, it is observed that there is more space between the V-I curves of two consecutive temperature values up to 160 ℃, while above 160 ℃, this space began to close for both catalysts. It can be interpreted that temperature's effect on cell performance is more pronounced at lower temperatures [227]. The V-I curves of Pt/GNP at 170 ℃ and 180 ℃ have almost overlapped. Also, for PtRu/GNP catalyst, the limiting current density at 180 ℃ is lower than that of 170 ℃. It may arise from the CO formation by the reverse water-gas shift (RWGS) reaction (Eq. (26)) with increasing temperature. The RWGS endothermic reactions were favored at higher temperatures [228]. It is reported by Li et al. [229] that CO formation could occur up to 1% as a result of RWGS reaction between 125-200 ℃ operating temperature. Catalyst inhibition can occur even when no voltage is applied to the cell due to the RWGS reaction. Moreover, CO may also be formed by the electrochemical reduction of CO_2 (Eq. (27)) when voltage is applied, but its contribution is negligible compared to the RWGS reaction [228].

$$CO_2 + 2Pt - H_{ads} \rightarrow Pt - CO_{ads} + H_2O + Pt \quad (26)$$

$$CO_2 + 2H^+ + 2e^- + Pt \rightarrow Pt - CO_{ads} + H_2O \quad (27)$$

The cathode outlet of the ECHP cell was connected to an online GC device to monitor the purity level of product H_2. The two GC analysis repetitions show the experiments' admirable reproducibility (±0.001). The purification results are given in Table 5.3.

Table 5.3 H_2 purification results of Pt/GNP and PtRu/GNP catalysts

Catalyst	H_2 Purity (%)				
	140 °C	150 °C	160 °C	170 °C	180 °C
Pt/GNP	98.362	99.821	99.822	99.539	99.832
PtRu/GNP	99.436	99.853	99.938	99.726	99.896

Higher H_2 purity was achieved with PtRu/GNP bimetallic catalyst at all temperatures. The highest H_2 purity levels obtained with Pt/GNP and PtRu/GNP catalysts are 99.832% at 180 °C and 99.938% at 160 °C, respectively. As a result of the experiments, a direct relation between operating temperature and H_2 purity was not determined; similar results were reported in the literature [137].

The separation efficiency of the ECHP system was calculated according to Equation (28) [230]:

$$\varepsilon = \frac{I}{2F\dot{n}} \tag{28}$$

where I is the current (A), F is the Faraday's constant and ṅ is the molar flow rate of the H_2 at the anode inlet (mol/s). The separation efficiency represents the portion of H_2 feeding the anode that exits through the cathode. The separation efficiency of the Pt/GNP and PtRu/GNP were displayed in Figure 5.8a and b, respectively. It is seen that the separation efficiency for both catalysts increases with the increasing operating temperature. The highest separation efficiency obtained for Pt/GNP was 57% at 180 °C, while for PtRu/GNP, it was 80% at 170 °C.

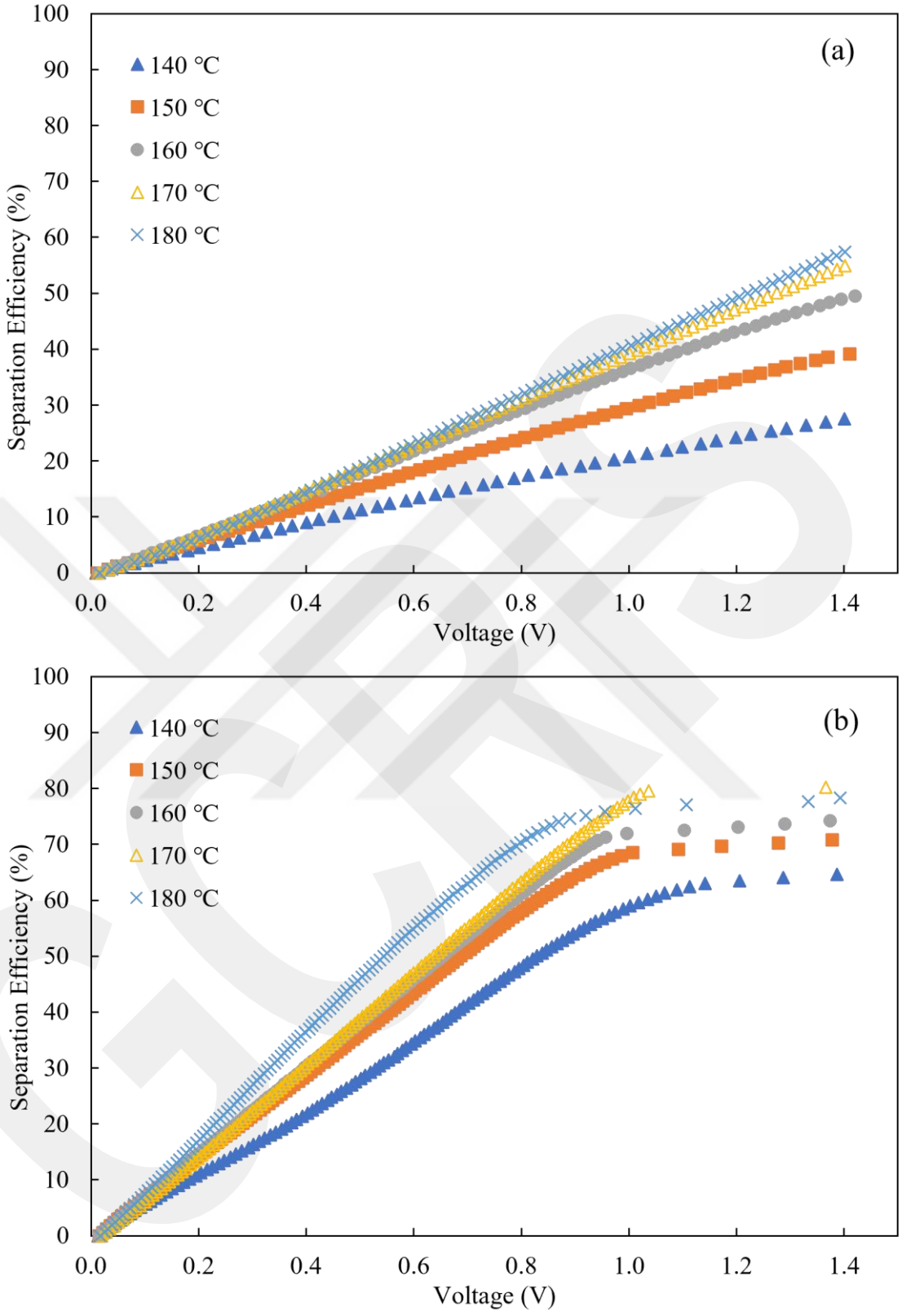

Figure 5.8 The separation efficiency of a) Pt/GNP, and b) PtRu/GNP catalyst

CHAPTER 6

6. CONCLUSION

Within the scope of this thesis, H_2 purification studies were successfully carried out with high-temperature ECHP single cells prepared using Pt/GNP and bimetallic PtRu/GNP catalysts and PA-doped PBI membrane. In this study, GNP-supported Pt and PtRu catalysts were prepared using microwave-assisted synthesis method and physical characterisation analyses revealed that the catalysts were successfully synthesised. The electro-catalytic properties of the Pt/GNP and PtRu/GNP catalysts were examined firstly by CV analysis and then HT-ECHP experiments were carried out with pure H_2 and reformate gas mixture of H_2:CO_2:CO-75:22:3 at the temperature range of 140-180 ℃. The results obtained in this thesis study are listed below:

- As a result of HT-ECHP experiments with pure H_2, it was observed that PtRu/GNP reached a certain current density with a lower voltage requirement than Pt/GNP, indicating that PtRu/GNP has better catalytic activity. Additionally, as the operating temperature increased from 140 ℃ to 180 ℃, it was determined that the cell performance decreased for both catalysts since the resistance of the PBI membrane increased as a result of the accelerated self-dehydration of H_3PO_4 to the less conductive $H_4P_2O_7$ at elevated temperatures.
- The HT-ECHP experiments conducted with H_2:CO_2:CO-75:22:3 reformate gas showed that the PtRu/GNP bimetallic catalyst demonstrated higher H_2 purification performance than the Pt/GNP catalyst at all temperatures. The superior performance of the PtRu/GNP catalyst can be explained by its higher CO tolerance arising from several factors induced by the addition of the secondary metal Ru, including facilitated CO oxidation, weakened Pt-CO bond strength, and reduced CO surface coverage.
- Moreover, in reformate gas experiments, the cell performance for both Pt/GNP and PtRu/GNP enhanced with the increased operating temperature from 140 ℃ to 180

℃, since the increased reaction kinetics and improved CO tolerance as the increasing temperature. On the other hand, it has been observed that the effect of increasing operating temperature on cell performance diminished at temperatures above 160 ℃. It can be explained by the CO formation as a result of the RWGS reaction, which is an endothermic process, with increasing temperature.

- From the reformate gas mixture containing 75% H_2, 22% CO_2 and 3% CO, high-purity H_2 was achieved in the range of 98.362-99.832% with Pt/GNP catalyst and 99.436-99.938% with PtRu/GNP catalyst. The highest H_2 purity at all temperatures was achieved with PtRu/GNP bimetallic catalyst.

The results obtained in this thesis study show that HT-ECHP systems, which can provide simultaneous H_2 purification and compression, have no moving parts and are scalable, are a strong alternative to traditional H_2 purification methods for obtaining high-purity H_2. In addition, PtRu/GNP bimetallic catalyst is a suitable candidate for HT-ECHP cells to obtain high-purity H_2 with improved cell performance.

REFERENCES

[1] A. Pareek, R. Dom, J. Gupta, J. Chandran, V. Adepu, and P. H. Borse, "Insights into renewable hydrogen energy: Recent advances and prospects," *Mater Sci Energy Technol*, vol. 3, pp. 319–327, Jan. 2020.

[2] M. I. Khan and S. G. Al-Ghamdi, "Hydrogen economy for sustainable development in GCC countries: A SWOT analysis considering current situation, challenges, and prospects," *Int J Hydrogen Energy*, vol. 48, no. 28, pp. 10315–10344, Apr. 2023.

[3] G. Venugopalan, "High Temperature Polymer Electrolytes for Hydrogen Fuel Cells and Electrochemical Pumps," LSU Doctoral Dissertations, 2021.

[4] O. J. Guerra, J. Zhang, J. Eichman, P. Denholm, J. Kurtz, and B. M. Hodge, "The value of seasonal energy storage technologies for the integration of wind and solar power," *Energy Environ Sci*, vol. 13, no. 7, pp. 1909–1922, Jul. 2020.

[5] F. Razi and I. Dincer, "Renewable energy development and hydrogen economy in MENA region: A review," *Renewable and Sustainable Energy Reviews*, vol. 168, Oct. 2022.

[6] M. Balat, "Potential importance of hydrogen as a future solution to environmental and transportation problems," *Int J Hydrogen Energy*, vol. 33, no. 15, pp. 4013–4029, Aug. 2008.

[7] B. L. Salvi and K. A. Subramanian, "Sustainable development of road transportation sector using hydrogen energy system," *Renewable and Sustainable Energy Reviews*, vol. 51, pp. 1132–1155, Jul. 30, 2015.

[8] H. L. Yip *et al.*, "A review of hydrogen direct injection for internal combustion engines: Towards carbon-free combustion," *Applied Sciences (Switzerland)*, vol. 9, no. 22, Nov. 2019.

[9] "A sustainable pathway for the global energy transition." [Online]. Available: www.hydrogencouncil.com.

[10] Office of Fossil Energy, U.S. Department of Energy, "HYDROGEN STRATEGY Enabling A Low-Carbon Economy," Washington, DC, 2020. [Online]. Available: https://www.energy.gov/sites/prod/files/2020/07/f76/USDOE_FE_Hydrogen_Strategy_July2020.pdf

[11] G. Bernardo, T. Araújo, T. da Silva Lopes, J. Sousa, and A. Mendes, "Recent advances in membrane technologies for hydrogen purification," *Int J Hydrogen Energy*, vol. 45, no. 12, pp. 7313–7338, Mar. 2020.

[12] J. Dodgshun, "Hydrogen: Clearing Up the Colours." Accessed: May 19, 2024. [Online]. Available: https://www.enapter.com/blog/hydrogen-clearing-up-the-colours/

[13] "The Colors of Hydrogen." Accessed: May 19, 2024. [Online]. Available: https://www.h2greensteel.com/articles/the-colors-of-hydrogen

[14] J. Huang, P. Balcombe, and Z. Feng, "Technical and economic analysis of different colours of producing hydrogen in China," *Fuel*, vol. 337, Apr. 2023.

[15] J. Incer-Valverde, A. Korayem, G. Tsatsaronis, and T. Morosuk, "'Colors' of hydrogen: Definitions and carbon intensity," *Energy Conversion and Management*, vol. 291, Sep. 01, 2023.

[16] P. Nikolaidis and A. Poullikkas, "A comparative overview of hydrogen production processes," *Renewable and Sustainable Energy Reviews*, vol. 67, pp. 597–611, Jan. 01, 2017.

[17] A. Ajanovic, M. Sayer, and R. Haas, "The economics and the environmental benignity of different colors of hydrogen," *Int J Hydrogen Energy*, vol. 47, no. 57, pp. 24136–24154, Jul. 2022.

[18] M. Newborough and G. Cooley, "Developments in the global hydrogen market: The spectrum of hydrogen colours," *Fuel Cells Bulletin*, vol. 2020, no. 11, pp. 16–22, 2020.

[19] S. Cloete, O. Ruhnau, J. H. Cloete, and L. Hirth, “Blue hydrogen and industrial base products: The future of fossil fuel exporters in a net-zero world,” *J Clean Prod*, vol. 363, Aug. 2022.

[20] I. Marouani *et al.*, “Integration of Renewable-Energy-Based Green Hydrogen into the Energy Future,” *Processes*, vol. 11, no. 9, Sep. 2023.

[21] Royal Society (Great Britain), “Options for producing low-carbon hydrogen at scale: Policy briefing.” Accessed: May 20, 2024. [Online]. Available: https://royalsociety.org/~/media/policy/projects/hydrogen-production/energy-briefing-green-hydrogen.pdf

[22] M. Noussan, P. P. Raimondi, R. Scita, and M. Hafner, “The role of green and blue hydrogen in the energy transition—a technological and geopolitical perspective,” *Sustainability (Switzerland)*, vol. 13, no. 1, pp. 1–26, Jan. 01, 2021.

[23] R. W. Howarth and M. Z. Jacobson, “How green is blue hydrogen?,” *Energy Sci Eng*, vol. 9, no. 10, pp. 1676–1687, Oct. 2021.

[24] Q. Hassan, S. Algburi, A. Z. Sameen, H. M. Salman, and M. Jaszczur, “Green hydrogen: A pathway to a sustainable energy future,” *Int J Hydrogen Energy*, vol. 50, pp. 310–333, Jan. 2024.

[25] J. Park, S. Kang, S. Kim, H. Kim, H. S. Cho, and J. H. Lee, “Enhancing the economic viability and reliability of renewables based electricity supply through Power-to-Gas-to-Power with green hydrogen,” *Energy Convers Manag*, vol. 310, Jun. 2024.

[26] A. Islam *et al.*, “Accelerating the green hydrogen revolution: A comprehensive analysis of technological advancements and policy interventions,” *International Journal of Hydrogen Energy*, vol. 67, pp. 458–486, May 20, 2024.

[27] IRENA, “Green Hydrogen Cost Reduction: Scaling up Electrolysers to Meet the 1.5ºC Climate Goal,” International Renewable Energy Agency, Abu Dhabi, 2020. [Online]. Available: https://www.irena.org/-/media/Files/IRENA/Agency/Publication/2020/Dec/IRENA_Green_hydrogen_cost_2020.pdf

[28] Y. Anouti, S. Elborai, R. Kombargi, and R. Hage, "The dawn of green hydrogen: Maintaining the GCC's edge in a decarbonized world." Accessed: May 20, 2024. [Online]. Available: https://www.strategyand.pwc.com/m1/en/reports/2020/the-dawn-of-green-hydrogen/the-dawn-of-green-hydrogen.pdf

[29] F. Angikath *et al.*, "Technoeconomic assessment of hydrogen production from natural gas pyrolysis in molten bubble column reactors," *Int J Hydrogen Energy*, vol. 49, pp. 246–262, Jan. 2024.

[30] J. Diab, L. Fulcheri, V. Hessel, V. Rohani, and M. Frenklach, "Why turquoise hydrogen will Be a game changer for the energy transition," *Int J Hydrogen Energy*, vol. 47, no. 61, pp. 25831–25848, Jul. 2022.

[31] H. Alhamed *et al.*, "From methane to hydrogen: A comprehensive review to assess the efficiency and potential of turquoise hydrogen technologies," *International Journal of Hydrogen Energy*, vol. 68, pp. 635–662, May 28, 2024.

[32] B. Shirizadeh and P. Quirion, "Long-term optimization of the hydrogen-electricity nexus in France: Green, blue, or pink hydrogen?," *Energy Policy*, vol. 181, Oct. 2023.

[33] F. M. Dorn, "Towards a multi-color hydrogen production network? Competing imaginaries of development in northern Patagonia, Argentina," *Energy Res Soc Sci*, vol. 110, Apr. 2024.

[34] F. V. S. Lopes, C. A. Grande, and A. E. Rodrigues, "Activated carbon for hydrogen purification by pressure swing adsorption: Multicomponent breakthrough curves and PSA performance," *Chem Eng Sci*, vol. 66, no. 3, pp. 303–317, Feb. 2011.

[35] L. Shao, B. T. Low, T. S. Chung, and A. R. Greenberg, "Polymeric membranes for the hydrogen economy: Contemporary approaches and prospects for the future," *Journal of Membrane Science*, vol. 327, no. 1–2. pp. 18–31, Feb. 05, 2009.

[36] A. Murugan and A. S. Brown, "Review of purity analysis methods for performing quality assurance of fuel cell hydrogen," *International Journal of Hydrogen Energy*, vol. 40, no. 11, pp. 4219–4233, Mar. 22, 2015.

[37] Z. Du *et al.*, "A review of hydrogen purification technologies for fuel cell vehicles," *Catalysts*, vol. 11, no. 3, pp. 1–19, Mar. 01, 2021.

[38] J. B. Cristello, J. M. Yang, R. Hugo, Y. Lee, and S. S. Park, "Feasibility analysis of blending hydrogen into natural gas networks," *Int J Hydrogen Energy*, vol. 48, pp. 17605-17629, May 2023.

[39] X. Wu, H. Zhang, M. Yang, W. Jia, Y. Qiu, and L. Lan, "From the perspective of new technology of blending hydrogen into natural gas pipelines transmission: Mechanism, experimental study, and suggestions for further work of hydrogen embrittlement in high-strength pipeline steels," *International Journal of Hydrogen Energy*, vol. 47, no. 12, pp. 8071–8090, Feb. 08, 2022.

[40] A. M. Jaffe et al., "The Potential to Build Current Natural Gas Infrastructure to Accommodate the Future Conversion to Near-Zero Transportation Technology," Institute of Transportation Studies, University of California, Davis (Research Report UCD-ITS-RR-17-04), 2017.

[41] K. Topolski *et al.*, "Hydrogen Blending into Natural Gas Pipeline Infrastructure: Review of the State of Technology," 2022. [Online]. Available: www.nrel.gov/publications.

[42] G. N. B. Durmus, C. O. Colpan, and Y. Devrim, "A review on the development of the electrochemical hydrogen compressors," *Journal of Power Sources*, vol. 494, May 15, 2021.

[43] S. Sircar and T. C. Golden, "Purification of hydrogen by pressure swing adsorption," *Sep Sci Technol*, vol. 35, no. 5, pp. 667–687, 2000.

[44] S. Sircar and T. C. Golden, "Pressure Swing Adsorption Technology for Hydrogen Production," in *Hydrogen and Syngas Production and Purification Technologies*, K. Liu, C. Song, and V. Subramani, Eds., pp. 414–450, 2010.

[45] C. A. Grande, "PSA Technology for H2 Separation," in *Hydrogen Science and Engineering: Materials, Processes, Systems and Technology*, D. Stolten and B. Emonts, Eds., pp. 491–508, 2016.

[46] S. Sircar, “Pressure swing adsorption,” *Industrial and Engineering Chemistry Research*, vol. 41, no. 6, pp. 1389–1392, Mar. 20, 2002.

[47] A. M. Banu, D. Friedrich, S. Brandani, and T. Düren, “A multiscale study of MOFs as adsorbents in H2 PSA purification,” *Ind Eng Chem Res*, vol. 52, no. 29, pp. 9946–9957, Jul. 2013.

[48] A. Fuderer and E. Rudelstorfer, “Selective adsorption process,” US3986849A, 1976

[49] E. H. Majlan *et al.*, “Hydrogen purification using compact pressure swing adsorption system for fuel cell,” *Int J Hydrogen Energy*, vol. 34, no. 6, pp. 2771–2777, Mar. 2009.

[50] J.-R. Li, J. Sculley, and H.-C. Zhou, “Metal-organic frameworks for separations,” *Chemical Reviews*, vol. 112, no. 2. pp. 869–932, Feb. 08, 2012.

[51] J. A. Delgado, V. I. Águeda, M. A. Uguina, P. Brea, and C. A. Grande, “Comparison and evaluation of agglomerated MOFs in biohydrogen purification by means of pressure swing adsorption (PSA),” *Chemical Engineering Journal*, vol. 326, pp. 117–129, 2017.

[52] B. Silva *et al.*, “H2 purification by pressure swing adsorption using CuBTC,” *Sep Purif Technol*, vol. 118, pp. 744–756, 2013.

[53] M. Rhandi, M. Trégaro, F. Druart, J. Deseure, and M. Chatenet, “Electrochemical hydrogen compression and purification versus competing technologies: Part I. Pros and cons,” *Chinese Journal of Catalysis*, vol. 41, pp. 756-769, 2020.

[54] Z. Tao, L. Yan, J. Qiao, B. Wang, L. Zhang, and J. Zhang, “A review of advanced proton-conducting materials for hydrogen separation,” *Progress in Materials Science*, vol. 74, pp. 1–50, Apr. 29, 2015.

[55] L. Vermaak, H. W. J. P. Neomagus, and D. G. Bessarabov, “Recent advances in membrane-based electrochemical hydrogen separation: A review,” *Membranes (Basel)*, vol. 11, no. 2, pp. 1–32, Feb. 2021.

[56] P. Li *et al.*, “Recent developments in membranes for efficient hydrogen purification,” *Journal of Membrane Science*, vol. 495, pp. 130–168, Dec. 01, 2015.

[57] D. Mao, J. M. Griffin, R. Dawson, A. Fairhurst, and N. Bimbo, “Metal organic frameworks for hydrogen purification,” *Int J Hydrogen Energy*, vol. 46, no. 45, pp. 23380–23405, Jul. 2021.

[58] M. R. Rahimpour, F. Samimi, A. Babapoor, T. Tohidian, and S. Mohebi, “Palladium membranes applications in reaction systems for hydrogen separation and purification: A review,” *Chemical Engineering and Processing: Process Intensification*, vol. 121, pp. 24–49, 2017.

[59] D. Edlund, “Hydrogen Membrane Technologies and Application in Fuel Processing,” in *Hydrogen and Syngas Production and Purification Technologies*, K. Liu, C. Song, and V. Subramani, Eds., pp. 357–384, 2010.

[60] S. Adhikari and S. Fernando, “Hydrogen membrane separation techniques,” *Industrial and Engineering Chemistry Research*, vol. 45, no. 3. pp. 875–881, Feb. 01, 2006.

[61] C. Y. Chuah, X. Jiang, K. Goh, and R. Wang, “Recent progress in mixed-matrix membranes for hydrogen separation,” *Membranes*, vol. 11, no. 9, 2021.

[62] N. A. Al-Mufachi, N. V. Rees, and R. Steinberger-Wilkens, “Hydrogen selective membranes: A review of palladium-based dense metal membranes,” *Renewable and Sustainable Energy Reviews*, vol. 47, pp. 540–551, 2015.

[63] M. Aasadnia, M. Mehrpooya, and B. Ghorbani, “A novel integrated structure for hydrogen purification using the cryogenic method,” *J Clean Prod*, vol. 278, Jan. 2021.

[64] A. Lider *et al.*, “Materials and techniques for hydrogen separation from methane-containing gas mixtures,” *International Journal of Hydrogen Energy*, Aug. 26, 2023.

[65] M. Amin *et al.*, “Issues and challenges in hydrogen separation technologies,” *Energy Reports*, vol. 9, pp. 894–911, Dec. 01, 2023.

[66] B. E. Lebrouhi, J. J. Djoupo, B. Lamrani, K. Benabdelaziz, and T. Kousksou, "Global hydrogen development - A technological and geopolitical overview," *International Journal of Hydrogen Energy*, vol. 47, no. 11, pp. 7016–7048, Feb. 05, 2022.

[67] D. Dunikov *et al.*, "Biohydrogen purification using metal hydride technologies," *Int J Hydrogen Energy*, vol. 41, no. 46, pp. 21787–21794, Dec. 2016.

[68] X. Y. Chen, L. X. Wei, L. Deng, F. S. Yang, and Z. X. Zhang, "A review on the metal hydride based hydrogen purification and separation technology," in *Applied Mechanics and Materials*, pp. 3027–3036, 2014.

[69] L. Guo *et al.*, "Efficient hydrogen recovery and purification from industrial waste hydrogen to high-purity hydrogen based on metal hydride powder," *Chemical Engineering Journal*, vol. 455, Jan. 2023.

[70] D. Dunikov, V. Borzenko, and S. Malyshenko, "Influence of impurities on hydrogen absorption in a metal hydride reactor," in *International Journal of Hydrogen Energy*, pp. 13843–13848, Sep. 2012.

[71] K. Fishel, G. Qian, G. Eisman, and B. C. Benicewicz, "Electrochemical hydrogen pumping," in *High Temperature Polymer Electrolyte Membrane Fuel Cells: Approaches, Status, and Perspectives*, pp. 527–540, 2016.

[72] G. N. Bulanık Durmuş, E. O. Eren, Y. Devrim, C. O. Colpan, and N. Özkan, "High-temperature electrochemical hydrogen separation from reformate gases using PBI/MOF composite membrane," *Int J Hydrogen Energy*, vol. 48, no. 60, pp. 23044–23054, Jul. 2023.

[73] L. Schorer, S. Schmitz, and A. Weber, "Membrane based purification of hydrogen system (MEMPHYS)," *Int J Hydrogen Energy*, vol. 44, no. 25, pp. 12708–12714, May 2019.

[74] T. Sakai *et al.*, "High performance of electroless-plated platinum electrode for electrochemical hydrogen pumps using strontium-zirconate-based proton conductors," *Electrochim Acta*, vol. 53, no. 28, pp. 8172–8177, Nov. 2008.

[75] G. Sdanghi, G. Maranzana, A. Celzard, and V. Fierro, “Review of the current technologies and performances of hydrogen compression for stationary and automotive applications,” *Renewable and Sustainable Energy Reviews*, vol. 102, pp. 150–170, Mar. 01, 2019.

[76] Y. M. Hao, H. Nakajima, A. Inada, K. Sasaki, and K. Ito, “Overpotentials and reaction mechanism in electrochemical hydrogen pumps,” *Electrochim Acta*, vol. 301, pp. 274–283, Apr. 2019.

[77] J. Zou *et al.*, “Electrochemical Compression Technologies for High-Pressure Hydrogen: Current Status, Challenges and Perspective,” *Electrochemical Energy Reviews*, vol. 3, no. 4, pp. 690–729, Dec. 01, 2020.

[78] K. Onda, K. Ichihara, M. Nagahama, Y. Minamoto, and T. Araki, “Separation and compression characteristics of hydrogen by use of proton exchange membrane,” *J Power Sources*, vol. 164, no. 1, pp. 1–8, Jan. 2007.

[79] J. Zou *et al.*, “Insights into electrochemical hydrogen compressor operating parameters and membrane electrode assembly degradation mechanisms,” *J Power Sources*, vol. 484, Feb. 2021.

[80] N. V. Dale, M. D. Mann, H. Salehfar, A. M. Dhirde, and T. Han, “Modeling and analysis of electrochemical hydrogen compression,” in Proc. NHA Annual Hydrogen Conference, Sacramento, CA, USA, 2008.

[81] F. Barbir and H. Görgün, “Electrochemical hydrogen pump for recirculation of hydrogen in a fuel cell stack,” *J Appl Electrochem*, vol. 37, no. 3, pp. 359–365, Mar. 2007.

[82] W. Wiebe, T. v. Unwerth, and S. Schmitz, “Using of an Electrochemical Compressor for Hydrogen Recirculation in Fuel Cell Vehicles,” *Fuel Cells*, vol. 20, no. 3, pp. 362–369, Jun. 2020.

[83] F. Marangio, M. Santarelli, M. Pagani, and M. Calì Quaglia, “Direct High Pressure Hydrogen Production: a Laboratory Scale PEM Electrolyser Prototype.,” *ECS Trans*, vol. 17, no. 1, pp. 555–567, May 2009.

[84] A. Chouhan, B. Bahar, and A. K. Prasad, “Effect of back-diffusion on the performance of an electrochemical hydrogen compressor,” *Int J Hydrogen Energy*, vol. 45, no. 19, pp. 10991–10999, Apr. 2020.

[85] D. Marciuš, A. Kovač, and M. Firak, “Electrochemical hydrogen compressor: Recent progress and challenges,” *Int J Hydrogen Energy*, vol. 47, no. 57, pp. 24179–24193, Jul. 2022.

[86] M. Trégaro, M. Rhandi, F. Druart, J. Deseure, and M. Chatenet, “Electrochemical hydrogen compression and purification versus competing technologies: Part II. Challenges in electrocatalysis,” *Chinese Journal of Catalysis*, vol. 41, pp. 770-782, 2020.

[87] M. A. Hickner, H. Ghassemi, Y. S. Kim, B. R. Einsla, and J. E. McGrath, “Alternative polymer systems for proton exchange membranes (PEMs),” *Chem Rev*, vol. 104, no. 10, pp. 4587–4611, Oct. 2004.

[88] K. A. Perry, G. A. Eisman, and B. C. Benicewicz, “Electrochemical hydrogen pumping using a high-temperature polybenzimidazole (PBI) membrane,” *J Power Sources*, vol. 177, no. 2, pp. 478–484, Mar. 2008.

[89] S. Yu, “NOVEL POLYBENZIMIDAZOLE DERIVATIVES FOR HIGH TEMPERATURE PEM FUEL CELLS,” 2006. Accessed: Dec. 12, 2023. [Online]. Available: https://hdl.handle.net/20.500.13015/3783

[90] S. D. Knights, K. M. Colbow, J. St-Pierre, and D. P. Wilkinson, “Aging mechanisms and lifetime of PEFC and DMFC,” in *Journal of Power Sources*, pp. 127–134, Mar. 2004.

[91] A. V. Anantaraman and C. L. Gardner, “Studies on ion-exchange membranes. Part 1. Effect of humidity on the conductivity of Nafion®,” *Journal of Electroanalytical Chemistry*, vol. 414, pp. 115–120, 1996.

[92] H. K. Lee, H. Y. Choi, K. H. Choi, J. H. Park, and T. H. Lee, “Hydrogen separation using electrochemical method,” *J Power Sources*, vol. 132, no. 1–2, pp. 92–98, May 2004.

[93] C. Casati, P. Longhi, L. Zanderighi, and F. Bianchi, “Some fundamental aspects in electrochemical hydrogen purification/compression,” *J Power Sources*, vol. 180, no. 1, pp. 103–113, May 2008.

[94] M. Nordio *et al.*, “Experimental and modelling study of an electrochemical hydrogen compressor,” *Chemical Engineering Journal*, vol. 369, pp. 432–442, Aug. 2019.

[95] A. M. Attaran, M. Javanbakht, K. Hooshyari, and M. Enhessari, “New proton conducting nanocomposite membranes based on poly vinyl alcohol/poly vinyl pyrrolidone/BaZrO3for proton exchange membrane fuel cells,” *Solid State Ion*, vol. 269, pp. 98–105, 2015.

[96] P. Knauth, H. Hou, E. Bloch, E. Sgreccia, and M. L. Di Vona, “Thermogravimetric analysis of SPEEK membranes: Thermal stability, degree of sulfonation and cross-linking reaction,” *J Anal Appl Pyrolysis*, vol. 92, no. 2, pp. 361–365, 2011.

[97] X. Wu, X. Wang, G. He, and J. Benziger, “Differences in water sorption and proton conductivity between Nafion and SPEEK,” *J Polym Sci B Polym Phys*, vol. 49, no. 20, pp. 1437–1445, Oct. 2011.

[98] X. Wu, G. He, L. Yu, and X. Li, “Electrochemical hydrogen pump with speek/CrPSSA semi-interpenetrating polymer network proton exchange membrane for H2/CO2 separation,” *ACS Sustain Chem Eng*, vol. 2, no. 1, pp. 75–79, Jan. 2014.

[99] A. Rico-Zavala *et al.*, “Synthesis and characterization of composite membranes modified with Halloysite nanotubes and phosphotungstic acid for electrochemical hydrogen pumps,” *Renew Energy*, vol. 122, pp. 163–172, Jul. 2018.

[100] R. E. Rosli *et al.*, “A review of high-temperature proton exchange membrane fuel cell (HT-PEMFC) system,” *Int J Hydrogen Energy*, vol. 42, no. 14, pp. 9293–9314, Apr. 2017.

[101] Q. Li, J. O. Jensen, R. F. Savinell, and N. J. Bjerrum, “High temperature proton exchange membranes based on polybenzimidazoles for fuel cells,” *Progress in Polymer Science (Oxford)*, vol. 34, no. 5. pp. 449–477, May 2009.

[102] R. Tanaka, H. Yamamoto, A. Shono, K. Kubo, and M. Sakurai, “Proton conducting behavior in non-crosslinked and crosslinked polyethylenimine with excess phosphoric acid,” *Electrochimica Acta*, vol. 45, pp. 1385-1389, 2000.

[103] G. P. Pandey, S. A. Hashmi, and R. C. Agrawal, “Hot-press synthesized polyethylene oxide based proton conducting nanocomposite polymer electrolyte dispersed with SiO2 nanoparticles,” *Solid State Ion*, vol. 179, no. 15–16, pp. 543–549, Jun. 2008.

[104] D. Rodriguez, C. Jegat, O. Trinquet, J. Grondin, and J. C. Lassègues, “Proton conduction in poly (acrylamide)-acid blends,” *Solid State lonics*, pp. 195–202, 1993.

[105] L. Xiao, H. Zhang, E. Scanlon, L. Ramanathan, E-W. Choe, D. Rogers, T. Apple, and B.C. Benicewicz, “High-Temperature Polybenzimidazole Fuel Cell Membranes via a Sol-Gel Process,” *Chem. Mater*, vol. 17, no. 21, pp. 5328–5333, Sep. 2005.

[106] T.-S. Chung, “A Critical Review of Polybenzimidazoles,” *Polymer Reviews*, vol. 37, no. 2, pp. 277–301, May 1997.

[107] Q. Li, R. He, J. O. Jensen, and N. J. Bjerrum, “PBI-based polymer membranes for high temperature fuel cells - Preparation, characterization and fuel cell demonstration,” *Fuel Cells*, vol. 4, no. 3. pp. 147–159, Aug. 2004.

[108] J. S. Wainright, J. -T. Wang, D. Weng, R. F. Savinell, and M. Litt, “Acid-Doped Polybenzimidazoles: A New Polymer Electrolyte,” *J Electrochem Soc*, vol. 142, no. 7, pp. L121–L123, Jul. 1995.

[109] C. Gao, M. Hu, L. Wang, and L. Wang, “Synthesis and properties of phosphoric-acid-doped polybenzimidazole with hyperbranched cross-linkers decorated with imidazolium groups as high-temperature proton exchange membranes,” *Polymers (Basel)*, vol. 12, no. 3, Mar. 2020.

[110] J. F. McElroy and D. S. Sokoloski, “High-temperature low-hydration ion exchange membrane electrochemical cell US 2003/0196893 A1,” 2003 Accessed: Dec. 25, 2023. [Online]. Available: https://patents.google.com/patent/US20030196893A1/en

[111] F. Huang, A. T. Pingitore, and B. C. Benicewicz, “Electrochemical Hydrogen Separation from Reformate Using High-Temperature Polybenzimidazole (PBI) Membranes: The Role of Chemistry,” *ACS Sustain Chem Eng*, vol. 8, no. 16, pp. 6234–6242, Apr. 2020.

[112] S. Bose, T. Kuila, T. X. H. Nguyen, N. H. Kim, K. T. Lau, and J. H. Lee, “Polymer membranes for high temperature proton exchange membrane fuel cell: Recent advances and challenges,” *Progress in Polymer Science (Oxford)*, vol. 36, no. 6, pp. 813–843, 2011.

[113] J. Kerres *et al.*, “Partially fluoridated arylene polyethers and their ternary blend membranes with PBI and H3PO4. Part I. Synthesis and characterisation of polymers and binary blend membranes,” in *Fuel Cells*, pp. 175–187, Jul. 2008.

[114] U. Sen, A. Bozkurt, and A. Ata, “Nafion/poly(1-vinyl-1,2,4-triazole) blends as proton conducting membranes for polymer electrolyte membrane fuel cells,” in *Journal of Power Sources*, pp. 7720–7726, Dec. 2010.

[115] C. G. Cho, S. H. Kim, Y. C. Park, H. Kim, and J. W. Park, “Fuel cell membranes based on blends of PPO with poly(styrene-b-vinylbenzylphosphonic acid) copolymers,” *J Memb Sci*, vol. 308, no. 1–2, pp. 96–106, Feb. 2008.

[116] Y. Si, H. R. Kunz, and J. M. Fenton, “Nafion-Teflon-Zr(HPO4)2 Composite Membranes for High-Temperature PEMFCs,” *J Electrochem Soc*, vol. 151, no. 4, p. A623, 2004.

[117] S. Wen, C. Gong, W. C. Tsen, Y. C. Shu, and F. C. Tsai, “Sulfonated poly(ether sulfone) (SPES)/boron phosphate (BPO4) composite membranes for high-temperature proton-exchange membrane fuel cells,” *Int J Hydrogen Energy*, vol. 34, no. 21, pp. 8982–8991, Nov. 2009.

[118] M. Amjadi, S. Rowshanzamir, S. J. Peighambardoust, M. G. Hosseini, and M. H. Eikani, “Investigation of physical properties and cell performance of Nafion/TiO2 nanocomposite membranes for high temperature PEM fuel cells,” in *International Journal of Hydrogen Energy*, pp. 9252–9260, Sep. 2010.

[119] W. A. Meulenberg, M. E. Ivanova, J. M. Serra, and S. Roitsch, “Proton-conducting ceramic membranes for solid oxide fuel cells and hydrogen (H2) processing,” in *Advanced Membrane Science and Technology for Sustainable Energy and Environmental Applications*, pp. 541–567, 2011.

[120] T. Sakai *et al.*, "Electrochemical hydrogen pumps using Ba doped LaYbO3 type proton conducting electrolyte," *Int J Hydrogen Energy*, vol. 38, no. 16, pp. 6842–6847, May 2013.

[121] A. Kalathil, A. Raghavan, and B. Kandasubramanian, "Polymer Fuel Cell Based on Polybenzimidazole Membrane: A Review," *Polymer-Plastics Technology and Engineering*, vol. 58, no. 5, pp. 465–497, Mar. 24, 2018.

[122] M. T. Nguyen, S. A. Grigoriev, A. A. Kalinnikov, A. A. Filippov, P. Millet, and V. N. Fateev, "Characterisation of a electrochemical hydrogen pump using electrochemical impedance spectroscopy," in *Journal of Applied Electrochemistry*, pp. 1033–1042, 2011.

[123] H. Uchida, K. Izumi, and M. Watanabe, "Temperature dependence of CO-tolerant hydrogen oxidation reaction activity at Pt, Pt-Co, and Pt-Ru electrodes," *Journal of Physical Chemistry B*, vol. 110, no. 43, pp. 21924–21930, Nov. 2006.

[124] C. L. Gardner and M. Ternan, "Electrochemical separation of hydrogen from reformate using PEM fuel cell technology," *J Power Sources*, vol. 171, no. 2, pp. 835–841, Sep. 2007.

[125] S. J. Kim *et al.*, "Highly active and CO2 tolerant Ir nanocatalysts for H2/CO2 separation in electrochemical hydrogen pumps," *Appl Catal B*, vol. 158–159, pp. 348–354, 2014.

[126] X. Wu, J. Benziger, and G. He, "Comparison of Pt and Pd catalysts for hydrogen pump separation from reformate," *J Power Sources*, vol. 218, pp. 424–434, Nov. 2012.

[127] S. J. Kim *et al.*, "Characterizations of polybenzimidazole based electrochemical hydrogen pumps with various Pt loadings for H2/CO2 gas separation," *Int J Hydrogen Energy*, vol. 38, no. 34, pp. 14816–14823, Nov. 2013.

[128] P. Pei, M. Wang, D. Chen, P. Ren, and L. Zhang, "Key technologies for polymer electrolyte membrane fuel cell systems fueled impure hydrogen," *Progress in Natural Science: Materials International*, vol. 30, no. 6, pp. 751–763, Dec. 01, 2020.

[129] Z. Liu, L. Ma, J. Zhang, K. Hongsirikarn, and J. G. Goodwin, “Pt alloy electrocatalysts for proton exchange membrane fuel cells: A review,” *Catalysis Reviews - Science and Engineering*, vol. 55, no. 3. pp. 255–288, Jul. 03, 2013.

[130] S. M. Brković, V. M. Nikolić, M. P. Marčeta Kaninski, and I. A. Pašti, “Pt/C catalyst impregnated with tungsten-oxide – Hydrogen oxidation reaction vs. CO tolerance,” *Int J Hydrogen Energy*, vol. 44, no. 26, pp. 13364–13372, May 2019.

[131] A. Pozio, L. Giorgi, E. Antolini, and E. Passalacqua, “Electroxidation of H2 on Pt/C Pt-Ru/C and Pt-Mo/C anodes for polymer electrolyte fuel cell,” *Electrochimica Acta*, vol. 46, pp. 555-561, 2000.

[132] H. Oetjen, V. M. Schmidt, U. Stimming, and F. Trila, “Performance Data of a Proton Exchange Membrane Fuel Cell Using H2 /CO as Fuel Gas,” *J. Electrochem. Soc.*, vol. 143, no. 12, Dec. 1996.

[133] B. Ibeh, C. Gardner, and M. Ternan, “Separation of hydrogen from a hydrogen/methane mixture using a PEM fuel cell,” *Int J Hydrogen Energy*, vol. 32, no. 7, pp. 908–914, May 2007.

[134] A. Tokarev and D. G. Bessarabov, “Modeling of bimetallic Pt-based electrocatalyst on extended-surface support for advanced hydrogen compression and separation,” *Int J Hydrogen Energy*, vol. 39, no. 15, pp. 7805–7810, May 2014.

[135] C. Jackson, L. F. J. M. Raymakers, M. J. J. Mulder, and A. R. J. Kucernak, “Assessing electrocatalyst hydrogen activity and CO tolerance: Comparison of performance obtained using the high mass transport ‘floating electrode’ technique and in electrochemical hydrogen pumps,” *Appl Catal B*, vol. 268, Jul. 2020.

[136] Y. Aykut and A. Bayrakçeken Yurtcan, “Catalyst development for viability of electrochemical hydrogen purifier and compressor (EHPC) technology,” *Int J Hydrogen Energy*, vol. 47, no. 45, pp. 19619–19632, May 2022.

[137] L. Vermaak, H. W. J. P. Neomagus, and D. G. Bessarabov, “Hydrogen Separation and Purification from Various Gas Mixtures by Means of

Electrochemical Membrane Technology in the Temperature Range 100–160 ◦C," *Membranes (Basel)*, vol. 11, no. 4, p. 282, 2021.

[138] S. Sharma and B. G. Pollet, "Support materials for PEMFC and DMFC electrocatalysts - A review," *Journal of Power Sources*, vol. 208. pp. 96–119, Jun. 15, 2012.

[139] Y. Shao, J. Liu, Y. Wang, and Y. Lin, "Novel catalyst support materials for PEM fuel cells: Current status and future prospects," *J Mater Chem*, vol. 19, no. 1, pp. 46–59, 2009.

[140] Y. Shao *et al.*, "Highly durable graphene nanoplatelets supported Pt nanocatalysts for oxygen reduction," *J Power Sources*, vol. 195, no. 15, pp. 4600–4605, Aug. 2010.

[141] G. Xia, C. Huang, and Y. Wang, "Highly uniform platinum nanoparticles supported on graphite nanoplatelets as a catalyst for proton exchange membrane fuel cells," *Int J Hydrogen Energy*, vol. 38, no. 31, pp. 13754–13761, Oct. 2013.

[142] M. González-Hernández, E. Antolini, and J. Perez, "CO tolerance and stability of PtRu and PtRuMo electrocatalysts supported on N-doped graphene nanoplatelets for polymer electrolyte membrane fuel cells," *Int J Hydrogen Energy*, vol. 45, no. 8, pp. 5276–5284, Feb. 2020.

[143] L. Cindrella *et al.*, "Gas diffusion layer for proton exchange membrane fuel cells-A review," *Journal of Power Sources*, vol. 194, no. 1. pp. 146–160, Oct. 20, 2009.

[144] P. C. Okonkwo and C. Otor, "A review of gas diffusion layer properties and water management in proton exchange membrane fuel cell system," *International Journal of Energy Research*, vol. 45, no. 3, pp. 3780–3800, Mar. 10, 2021.

[145] S. Park, J. W. Lee, and B. N. Popov, "A review of gas diffusion layer in PEM fuel cells: Materials and designs," *International Journal of Hydrogen Energy*, vol. 37, no. 7, pp. 5850–5865, 2012.

[146] W. Song, H. Yu, L. Hao, Z. Miao, B. Yi, and Z. Shao, “A new hydrophobic thin film catalyst layer for PEMFC,” *Solid State Ion*, vol. 181, no. 8–10, pp. 453–458, Mar. 2010.

[147] S. Toghyani, E. Afshari, and E. Baniasadi, “Parametric study of a proton exchange membrane compressor for electrochemical hydrogen storage using numerical assessment,” *J Energy Storage*, vol. 30, Aug. 2020.

[148] M. Lee and X. Huang, “Development of a hydrophobic coating for the porous gas diffusion layer in a PEM-based electrochemical hydrogen pump to mitigate anode flooding,” *Electrochem commun*, vol. 100, pp. 39–42, Mar. 2019.

[149] M. Lee and X. Huang, “An improved hydrophobic coating for the porous gas diffusion layer in a PEM-based electrochemical hydrogen pump to mitigate anode flooding,” *Electrochem commun*, vol. 117, Aug. 2020.

[150] F. Wu, B. Chen, Y. Yan, Y. Chen, and M. Pan, “Degradation of silicone rubbers as sealing materials for proton exchange membrane fuel cells under temperature cycling,” *Polymers (Basel)*, vol. 10, no. 5, May 2018.

[151] D. Shi *et al.*, “Fabrication methods, structure design and durability analysis of advanced sealing materials in proton exchange membrane fuel cells,” *Chemical Engineering Journal*, vol. 454, Feb. 15, 2023.

[152] D. Qiu, P. Liang, L. Peng, P. Yi, X. Lai, and J. Ni, “Material behavior of rubber sealing for proton exchange membrane fuel cells,” *Int J Hydrogen Energy*, vol. 45, no. 8, pp. 5465–5473, Feb. 2020.

[153] Hammoud A. N.; Baumann E. D.; Overton E.; Myers I. T.; Suthar J. L.; Khachen W.; Laghari J. R. In High Temperature Dielectric Properties of Apical, Kapton, PEEK, Teflon AF, and Upilex Polymers, 1992 Annual Report, Conference on Electrical Insulation and Dielectric Phenomena, Victoria, BC, Canada, pp 549–554, 1992.

[154] S. J. Schowalter, C. B. Connolly, and J. M. Doyle, “Permeability of noble gases through Kapton, butyl, nylon, and ‘Silver Shield,’” *Nucl Instrum Methods Phys Res A*, vol. 615, no. 3, pp. 267–271, Apr. 2010.

[155] R. Taherian, “A review of composite and metallic bipolar plates in proton exchange membrane fuel cell: Materials, fabrication, and material selection,” *Journal of Power Sources*, vol. 265, pp. 370–390, Nov. 01, 2014.

[156] R. A. Antunes, M. C. L. Oliveira, G. Ett, and V. Ett, “Corrosion of metal bipolar plates for PEM fuel cells: A review,” *International Journal of Hydrogen Energy*, vol. 35, no. 8. pp. 3632–3647, Apr. 2010.

[157] A. Hermann, T. Chaudhuri, and P. Spagnol, “Bipolar plates for PEM fuel cells: A review,” in *International Journal of Hydrogen Energy*, pp. 1297–1302, Sep. 2005.

[158] R. F. Silva, D. Franchi, A. Leone, L. Pilloni, A. Masci, and A. Pozio, “Surface conductivity and stability of metallic bipolar plate materials for polymer electrolyte fuel cells,” *Electrochim Acta*, vol. 51, no. 17, pp. 3592–3598, Apr. 2006.

[159] K. Feng *et al.*, “Conductive amorphous carbon-coated 316L stainless steel as bipolar plates in polymer electrolyte membrane fuel cells,” *Int J Hydrogen Energy*, vol. 34, no. 16, pp. 6771–6777, Aug. 2009.

[160] L. gang Xia, A. ju Li, W. qiang Wang, Q. Yin, H. Lin, and Y. bo Zhao, “Effects of resin content and preparing conditions on the properties of polyphenylene sulfide resin/graphite composite for bipolar plate,” *J Power Sources*, vol. 178, no. 1, pp. 363–367, Mar. 2008.

[161] Y. Tang, W. Yuan, M. Pan, and Z. Wan, “Feasibility study of porous copper fiber sintered felt: A novel porous flow field in proton exchange membrane fuel cells,” *Int J Hydrogen Energy*, vol. 35, no. 18, pp. 9661–9677, Sep. 2010.

[162] S. Asghari, M. H. Shahsamandi, and M. R. Ashraf Khorasani, “Design and manufacturing of end plates of a 5 kW PEM fuel cell,” *International Journal of Hydrogen Energy*, pp. 9291–9297, Sep. 2010.

[163] N. U. Hassan, M. Kilic, E. Okumus, B. Tunaboylu, and A. M. Soydan, “Experimental determination of optimal clamping torque for ab-pem fuel cell,” *Journal of Electrochemical Science and Engineering*, vol. 6, no. 1, pp. 9–16, Apr. 2016.

[164] T. Dey, J. Deshpande, D. Singdeo, and P. C. Ghosh, “Study of PEM Fuel Cell End Plate Design by Structural Analysis Based on Contact Pressure,” *Journal of Energy*, vol. 2019, pp. 1–11, Jan. 2019.

[165] S. Karvonen, T. Hottinen, J. Ihonen, and H. Uusalo, “Modeling of polymer electrolyte membrane fuel cell stack end plates,” *J Fuel Cell Sci Technol*, vol. 5, no. 4, Nov. 2008.

[166] T. J. Petek, J. S. Wainright, and R. F. Savinell, “High Temperature Electrochemical Hydrogen Pump Cell Using a PBI Membrane at High Current Densities,” *ECS Trans*, vol. 50, no. 2, 2012.

[167] J. O. Jensen, H. A. Hjuler, D. Aili, and Q. Li, “Introduction,” in *High Temperature Polymer Electrolyte Membrane Fuel Cells*, Q. Li, D. Aili, H. A. Hjuler, and J. O. Jensen, Eds., Springer, Cham, pp. 1–4, 2016.

[168] C. Y. Chen, W. H. Lai, Y. K. Chen, and S. S. Su, “Characteristic studies of a PBI/H3PO4 high temperature membrane PEMFC under simulated reformate gases,” in *International Journal of Hydrogen Energy*, pp. 13757–13762, Aug. 2014.

[169] D. S. Maxwell *et al.*, “High Purity Hydrogen Separation with HT-PBI Based Electrochemical Pump Operation at 120 °C,” *J Electrochem Soc*, vol. 170, no. 3, p. 034510, Mar. 2023.

[170] H. J. R. Maget, “US3489670A Process for gas purification” Accessed: Apr. 19, 2024. [Online]. Available: https://patents.google.com/patent/US3489670A/en

[171] J. M. Sedlak, J. F. Austin, and A. B. Lacont, “HYDROGEN RECOVERY AND PURIFICATION USING THE SOLID POLYMER ELECTROLYTE ELECTROLYSIS CELL,” *Int. J. of Hydrogen Energy*, vol. 6, pp. 45-51, 1981.

[172] R. Doucet, C. L. Gardner, and M. Ternan, “Separation of hydrogen from hydrogen/ethylene mixtures using PEM fuel cell technology,” *Int J Hydrogen Energy*, vol. 34, no. 2, pp. 998–1007, Jan. 2009.

[173] K. Onda, T. Araki, K. Ichihara, and M. Nagahama, “Treatment of low concentration hydrogen by electrochemical pump or proton exchange membrane fuel cell,” *J Power Sources*, vol. 188, no. 1, pp. 1–7, Mar. 2009.

[174] M. Thomassen, E. Sheridan, and J. Kvello, “Electrochemical hydrogen separation and compression using polybenzimidazole (PBI) fuel cell technology,” *J Nat Gas Sci Eng*, vol. 2, no. 5, pp. 229–234, 2010.

[175] P. J. Bouwman, “Advances in Electrochemical Hydrogen Compression and Purification,” *ECS Trans*, vol. 75, no. 14, pp. 503–510, Aug. 2016.

[176] S. Huang *et al.*, “Coupling hydrogen separation with butanone hydrogenation in an electrochemical hydrogen pump with sulfonated poly (phthalazinone ether sulfone ketone) membrane,” *J Power Sources*, vol. 327, pp. 178–186, Sep. 2016.

[177] F. Yun Ru, N. Noramelya Zulkefli, N. Yusra Mt Yusuf, and M. Shahbudin Masdar, “Effect of Operating Parameter on H2/CO2 Gas Separation using Electrochemical Cell,” *International Journal of Applied Engineering Research*, vol. 13, no. 1, pp. 505-510, 2018.

[178] G. N. B. Durmuş, C. O. Colpan, and Y. Devrim, “Investigation of the performance of high-temperature electrochemical hydrogen purification from reformate gases,” *Int J Energy Res*, vol. 46, no. 8, pp. 11443–11455, Jun. 2022.

[179] G. Venugopalan *et al.*, “Electrochemical Pumping for Challenging Hydrogen Separations,” *ACS Energy Lett*, vol. 7, no. 4, pp. 1322–1329, Apr. 2022.

[180] S. A. Grigoriev, I. G. Shtatniy, P. Millet, V. I. Porembsky, and V. N. Fateev, “Description and characterization of an electrochemical hydrogen compressor/concentrator based on solid polymer electrolyte technology,” *Int J Hydrogen Energy*, vol. 36, no. 6, pp. 4148–4155, Mar. 2011.

[181] M. G. H. Al-Tememy and Y. Devrim, “Development of effective bimetallic catalyst for high-temperature PEM fuel cell to improve CO tolerance,” *Int J Energy Res*, vol. 45, no. 2, pp. 3343–3357, Feb. 2021.

[182] İ. B. Bal, G. N. Bulanık Durmuş, and Y. Devrim, “Fabrication and performance evaluation of graphene-supported PtRu electrocatalyst for high-temperature electrochemical hydrogen purification,” *Int J Hydrogen Energy*, vol. 48, no. 63, pp. 24369–24384, Jul. 2023.

[183] M. Sakthivel, A. Schlange, U. Kunz, and T. Turek, “Microwave assisted synthesis of surfactant stabilized platinum/carbon nanotube electrocatalysts for direct methanol fuel cell applications,” *J Power Sources*, vol. 195, no. 20, pp. 7083–7089, Oct. 2010.

[184] S. Karadeniz and N. Ayas, “Microwave-assisted synthesis of Pt/C catalyst at high temperatures for PEM fuel cells,” *Int J Hydrogen Energy*, vol. 52, pp. 1564–1576, Jan. 2024.

[185] F. Taufany *et al.*, “Relating the composition of PtxRu100-x/C nanoparticles to their structural aspects and electrocatalytic activities in the methanol oxidation reaction,” *Chemistry - A European Journal*, vol. 19, no. 3, pp. 905–915, Jan. 2013.

[186] J. A. Argüello, J. M. Rojo, and R. Moreno, “Electrophoretic deposition of manganese oxide and graphene nanoplatelets on graphite paper for the manufacture of supercapacitor electrodes,” *Electrochim Acta*, vol. 294, pp. 102–109, Jan. 2019.

[187] A. N. Popova, “Crystallographic analysis of graphite by X-Ray diffraction,” *Coke and Chemistry*, vol. 60, no. 9, pp. 361–365, Sep. 2017.

[188] Y. Devrim, E. D. Arıca, and A. Albostan, “Graphene based catalyst supports for high temperature PEM fuel cell application,” *Int J Hydrogen Energy*, vol. 43, no. 26, pp. 11820–11829, Jun. 2018.

[189] P. V. Shanahan, L. Xu, C. Liang, M. Waje, S. Dai, and Y. S. Yan, “Graphitic mesoporous carbon as a durable fuel cell catalyst support,” *J Power Sources*, vol. 185, no. 1, pp. 423–427, Oct. 2008.

[190] A. B. Kashyout, A. B. A. A. Nassr, L. Giorgi, T. Maiyalagan, and B. A. B. Youssef, “Electrooxidation of Methanol on Carbon Supported Pt-Ru Nanocatalysts Prepared by Ethanol Reduction Method,” *Int. J. Electrochem. Sci.*, vol. 6, pp. 379-393, 2011.

[191] J. W. Guo, T. S. Zhao, J. Prabhuram, R. Chen, and C. W. Wong, “Preparation and characterization of a PtRu/C nanocatalyst for direct methanol fuel cells,” *Electrochim Acta*, vol. 51, no. 4, pp. 754–763, Nov. 2005.

[192] E. Antolini and F. Cardellini, “Formation of carbon supported PtRu alloys: an XRD analysis,” *Journal of Alloys and Compounds*, vol. 315, pp. 118-122, 2001.

[193] M. Li, H. Zheng, G. Han, Y. Xiao, and Y. Li, “Facile synthesis of binary PtRu nanoflowers for advanced electrocatalysts toward methanol oxidation,” *Catal Commun*, vol. 92, pp. 95–99, 2017.

[194] F. I. Pires, P. G. Corradini, V. A. Paganin, E. Antolini, and J. Perez, “Effect of the degree of alloying of PtRu/C (1:1) catalysts on ethanol oxidation,” *Ionics (Kiel)*, vol. 19, no. 7, pp. 1037–1045, Jul. 2013.

[195] K. I. B. Eguiluz, G. R. Salazar-Banda, D. Miwa, S. A. S. Machado, and L. A. Avaca, “Effect of the catalyst composition in the Ptx(Ru-Ir)1-x/C system on the electro-oxidation of methanol in acid media,” *J Power Sources*, vol. 179, no. 1, pp. 42–49, Apr. 2008.

[196] H. Wang, H. Da, R. Wang, and S. Ji, “Beef-derived Mesoporous Carbon as Highly Efficient Support for PtRuIr Electrocatalysts and their High Activity for CO and Methanol Oxidation,” *South African Journal of Chemistry*, vol. 67, pp. 33-39, 2014.

[197] Z. B. Wang, G. P. Yin, and P. F. Shi, “Stable Pt–Ru⁄C Catalysts Prepared from New Precursors by Thermal Reduction for Direct Methanol Fuel Cell,” *J Electrochem Soc*, vol. 152, no. 12, p. A2406, 2005.

[198] J. Zhao, L. Zhang, H. Xue, Z. Wang, and H. Hu, “Methanol electrocatalytic oxidation on highly dispersed platinum-ruthenium/graphene catalysts prepared in supercritical carbon dioxide-methanol solution,” *RSC Adv*, vol. 2, no. 25, pp. 9651–9659, Oct. 2012.

[199] J. F. Moulder, W. F. Stickle, P. E. Sobol, K. D. Bomben, and J. Chastain, Handbook of X-ray Photoelectron Spectroscopy: A Reference Book of Standard Spectra for Identification and Interpretation of XPS Data. Eden Prairie, Minnesota, USA: Perkin-Elmer Corporation, 1992. [Online]. Available: https://data.bris.ac.uk/datasets/q5hfkppqacnh2wbxkpa5t5r51/Experimental/xps_handbook.pdf

[200] S. H. Cho, H. N. Yang, D. C. Lee, S. H. Park, and W. J. Kim, “Electrochemical properties of Pt/graphene intercalated by carbon black and its application in

polymer electrolyte membrane fuel cell," *J Power Sources*, vol. 225, pp. 200–206, Mar. 2013.

[201] E. Antolini, L. Giorgi, F. Cardellini, and E. Passalacqua, "Physical and morphological characteristics and electrochemical behaviour in PEM fuel cells of PtRu/C catalysts," *Journal of Solid State Electrochemistry*, vol. 5, no. 2, pp. 131–140, 2001.

[202] E. O. Eren, N. Özkan, and Y. Devrim, "Polybenzimidazole-modified carbon nanotubes as a support material for platinum-based high-temperature proton exchange membrane fuel cell electrocatalysts," *Int J Hydrogen Energy*, vol. 46, no. 57, pp. 29556–29567, Aug. 2021.

[203] H. P. Cong, X. C. Ren, and S. H. Yu, "Controlled Synthesis of PtRu/Graphene Nanocatalysts with Enhanced Methanol Oxidation Activity for Fuel Cells," *ChemCatChem*, vol. 4, no. 10, pp. 1555–1559, Oct. 2012.

[204] X. Li, S. Biswas, and L. T. Drzal, "High temperature vacuum annealing and hydrogenation modification of exfoliated graphite nanoplatelets," *Journal of Engineering (United Kingdom)*, vol. 2013, 2013.

[205] S. L. Knupp, W. Li, O. Paschos, T. M. Murray, J. Snyder, and P. Haldar, "The effect of experimental parameters on the synthesis of carbon nanotube/nanofiber supported platinum by polyol processing techniques," *Carbon N Y*, vol. 46, no. 10, pp. 1276–1284, Aug. 2008.

[206] K. Vaarmets, S. Sepp, J. Nerut, E. Härk, I. Tallo, and E. Lust, "Electrochemical and physical characterization of Pt–Ru alloy catalyst deposited onto microporous–mesoporous carbon support derived from Mo2C at 600 °C," *Journal of Solid State Electrochemistry*, vol. 17, no. 6, pp. 1729–1741, Jun. 2013.

[207] T. Vidaković, M. Christov, and K. Sundmacher, "The use of CO stripping for in situ fuel cell catalyst characterization," *Electrochim Acta*, vol. 52, no. 18, pp. 5606–5613, May 2007.

[208] Y. Bao, F. Wang, X. Gu, and L. Feng, "Core-shell structured PtRu nanoparticles@FeP promoter with an efficient nanointerface for alcohol fuel electrooxidation," *Nanoscale*, vol. 11, no. 40, pp. 18866–18873, Oct. 2019.

[209] T. Vidaković, M. Christov, and K. Sundmacher, “A method for rough estimation of the catalyst surface area in a fuel cell,” *J Appl Electrochem*, vol. 39, no. 2, pp. 213–225, Feb. 2009.

[210] C. Wei, S. Sun, D. Mandler, X. Wang, S. Z. Qiao, and Z. J. Xu, “Approaches for measuring the surface areas of metal oxide electrocatalysts for determining their intrinsic electrocatalytic activity,” *Chemical Society Reviews*, vol. 48, no. 9, pp. 2518–2534, May 07, 2019.

[211] M. Sun *et al.*, “CO-tolerant PtRu@h-BN/C core–shell electrocatalysts for proton exchange membrane fuel cells,” *Appl Surf Sci*, vol. 450, pp. 244–250, Aug. 2018.

[212] C. L. Green and A. Kucernak, “Determination of the platinum and ruthenium surface areas in platinum-ruthenium alloy electrocatalysts by underpotential deposition of Copper. I. Unsupported catalysts,” *Journal of Physical Chemistry B*, vol. 106, no. 5, pp. 1036–1047, Feb. 2002.

[213] N. Shroti and M. K. Daletou, “The Pt–Co alloying effect on the performance and stability of high temperature PEMFC cathodes,” *Int J Hydrogen Energy*, vol. 47, no. 36, pp. 16235–16248, Apr. 2022.

[214] Y. J. Zhang, A. Maroto-Valiente, I. Rodriguez-Ramos, Q. Xin, and A. Guerrero-Ruiz, “Synthesis and characterization of carbon black supported Pt-Ru alloy as a model catalyst for fuel cells,” in *Catalysis Today*, pp. 619–626, Sep. 2004.

[215] J. Lobato, P. Cañizares, M. A. Rodrigo, and J. J. Linares, “PBI-based polymer electrolyte membranes fuel cells. Temperature effects on cell performance and catalyst stability,” *Electrochim Acta*, vol. 52, no. 12, pp. 3910–3920, Mar. 2007.

[216] C. Y. Chen and W. H. Lai, “Effects of temperature and humidity on the cell performance and resistance of a phosphoric acid doped polybenzimidazole fuel cell,” *J Power Sources*, vol. 195, no. 21, pp. 7152–7159, Nov. 2010.

[217] P. N. Ross, K. Kinoshita, A. J. Scarpellino, and P. Stonehart, “Electrocatalysis on binary alloys: II. Oxidation of molecular hydrogen on supported Pt+Ru alloys,” *J. Electroanal. Chem.*, vol. 63, pp. 97-110, 1975.

[218] M. Watanabe, and S. Motoo, “ELECTROCATALYSIS BY AD-ATOMS: PART III. ENHANCEMENT OF THE OXIDATION OF CARBON MONOXIDE ON PLATINUM BY RUTHENIUM AD-ATOMS,” *Electroanalytical Chemistry and lnterfacial Electrochemistry*, vol. 60, pp. 275-283, 1975.

[219] Y. Ishikawa, M.-S. Liao, and C. R. Cabrera, “Energetics of H2O dissociation and COads + OHads reaction on a series of Pt-M mixed metal clusters: a relativistic density-functional study,” *Surface Science*, vol. 513, pp. 98-110, 2002.

[220] P. Liu, A. Logadottir, and J. K. Nørskov, “Modeling the electro-oxidation of CO and H2/CO on Pt, Ru, PtRu and Pt3Sn,” *Electrochimica Acta*, pp. 3731–3742, Nov. 2003.

[221] P. P. Lopes, K. S. Freitas, and E. A. Ticianelli, “CO Tolerance of PEMFC Anodes: Mechanisms and Electrode Designs,” *Electrocatalysis*, vol. 1, no. 4, pp. 200–212, 2010.

[222] A. Pitois, J. C. Davies, A. Pilenga, A. Pfrang, and G. Tsotridis, “Kinetic study of CO desorption from PtRu/C PEM fuel cell anodes: Temperature dependence and associated microstructural transformations,” *J Catal*, vol. 265, no. 2, pp. 199–208, Jul. 2009.

[223] H. Igarashi, T. Fujino, Y. Zhu, H. Uchida, and M. Watanabe, “CO tolerance of Pt alloy electrocatalysts for polymer electrolyte fuel cells and the detoxification mechanism,” in *Physical Chemistry Chemical Physics*, pp. 306–314, Feb. 2001.

[224] Y. Oono, T. Fukuda, A. Sounai, and M. Hori, “Influence of operating temperature on cell performance and endurance of high temperature proton exchange membrane fuel cells,” *J Power Sources*, vol. 195, no. 4, pp. 1007–1014, Feb. 2010.

[225] G. Postole and A. Auroux, “The poisoning level of Pt/C catalysts used in PEM fuel cells by the hydrogen feed gas impurities: The bonding strength,” *Int J Hydrogen Energy*, vol. 36, no. 11, pp. 6817–6825, May 2011.

[226] F. Zhou, S. J. Andreasen, S. K. Kær, and J. O. Park, “Experimental investigation of carbon monoxide poisoning effect on a PBI/H3PO4 high temperature polymer electrolyte membrane fuel cell: Influence of anode humidification and

carbon dioxide," *Int J Hydrogen Energy*, vol. 40, no. 43, pp. 14932–14941, Nov. 2015.

[227] J. Zhang, Y. Tang, C. Song, and J. Zhang, "Polybenzimidazole-membrane-based PEM fuel cell in the temperature range of 120-200 °C," *J Power Sources*, vol. 172, no. 1, pp. 163–171, Oct. 2007.

[228] M. Nordio, M. Eguaras Barain, L. Raymakers, M. Van Sint Annaland, M. Mulder, and F. Gallucci, "Effect of CO2 on the performance of an electrochemical hydrogen compressor," *Chemical Engineering Journal*, vol. 392, Jul. 2020.

[229] Q. Li, R. He, J.-A. Gao, J. O. Jensen, and Niels. J. Bjerrum, "The CO Poisoning Effect in PEMFCs Operational at Temperatures up to 200°C," *J Electrochem Soc*, vol. 150, no. 12, p. A1599, 2003.

[230] A. Abdulla, K. Laney, M. Padilla, S. Sundaresan, and J. Benziger, "Efficiency of hydrogen recovery from reformate with a polymer electrolyte hydrogen pump," *AIChE Journal*, vol. 57, no. 7, pp. 1767–1779, Jul. 2011.